Functional Characterisation of a Novel Microtubule-Actin Interacting Protein, GAS2-like 3

A thesis submitted to The University of Manchester for the Degree of Doctor of Philosophy in the Faculty of Life Sciences

2010

Matthew Stroud

List of Contents

Word Count: 36,284

List of Figures

List of Tables

List of Abbreviations

+TIP – Microtubule plus-end tracking protein

ABD – Actin Binding Domain

ACF7 – Actin microtubule crosslinking factor 7

BLAST – Basic Local Alignment Tool

bp – Base pairs

BPAG1 – Bullous pemphigoid antigen 1

cDNA – complementary DNA

CH – Calponin homology

C-terminal – Carboxy-terminal

Cy – Cyanine

DMEM – Dulbecco's modified eagle medium

DNA – Deoxyribonucleic acid

dNTP – Deoxyribonucleotide triphosphate

E. coli – Escherichia coli

F-actin – Filamentous actin

EB1 – End binding protein 1

EDTA – Ethylenediaminetetraacetic acid

FA – Focal adhesion

FBS – Foetal bovine serum

FRAP – Fluorescence Recovery After Photobleaching

G-actin – Globular actin

GAR – Growth Arrest Specific-2 Related

GAS2 – Growth Arrest Specific 2

G2L1 – GAS2-like 1

G2L2 – GAS2-like 2

G2L3 – GAS2-like 3

GDP – Guanosine diphosphate

GST – Glutathione S-Transferase

GTP – Guanosine triphosphate

MACF1 – Microtubule-actin crosslinking factor 1

mol – Mole

MTs – Microtubules

MTBD – Microtubule binding domain

MTOC – Microtubule organising center

mRNA – messenger RNA

N-terminal – Amino-terminal

PBS – Phosphate buffered saline

PCR – Polymerase chain reaction

Pigs – Pickled eggs

PVDF – Polyvinylidene Fluoride

RNA – Ribonucleic acid

RNAi – RNA interference

SDS-PAGE – Sodium dodecyl sulphate polyacrylamide gel electrophoresis

Shot – Short stop

SPBA – Solid phase binding assay

Tris – Tris (hydroxymethyl) methylamide

U – Units (enzyme activity)

v/v – Volume per volume

w/v – Weight per volume

Abstract

This abstract is for the thesis entitled 'The functional characterisation of a novel microtubule-actin interacting protein, GAS2-like 3' submitted for the Degree of Doctor of Philosophy to the Faculty of Life Sciences, University of Manchester by Matthew Stroud in 2010.

The microtubule (MT) and actin cytoskeletons are fundamental to cell integrity, as they control a host of cellular activities. Until recently, studies have investigated these cytoskeletal components as separate entities, however, it has become increasingly clear that the MT and actin cytoskeletons function in an interdependent way. Elucidating how the two components interact will be key to our further understanding of fundamental cellular processes such as cell division, growth, polarisation and migration.

This study focused on a newly identified and highly conserved protein, named GAS2-like 3, which contains a putative actin binding calponin homology (CH) domain and a putative MT binding GAS2-related (GAR) domain. GAS2-like 3 predominantly localised to both MT and actin cytoskeletons. By using a series of truncation mutants, the fundamental regions of GAS2-like 3 involved in mediating these interactions were dissected, both in cells and *in vitro*. Data from sedimentation assays revealed the CH domain binds directly to F-actin, and the C-terminus binds directly to MTs, whereas the GAR domain does not interact directly with MTs. In order to assess the dynamics of GAS2-like 3 and its mutants in cells, Fluorescence Recovery After Photobleaching experiments were performed to reveal that the GAR domain of GAS2-like 3 modulates the binding strength of GAS2-like 3 to MTs and actin. GAS2-like 3 localisation is dependent on both MT and actin cytoskeletons, although MTs have a greater influence on GAS2-like 3 localisation. Interestingly, tubulin acetylation enhanced GAS2-like 3 localisation to MTs.

This study also uncovered two binding motifs for the MT plus-end binding protein 1 (EB1). EB1 was characterised as a new interaction partner of GAS2-like 3, which directly interacted with the C-terminus of GAS2-like 3 *in vitro*. Furthermore, a molecular mechanism in which GAS2-like 3 was recruited to MTs via EB1 in cells was revealed. Interestingly, the interaction between EB1 and GAS2-like 3 required the complete C-terminus, rather than the specific EB1-binding motifs themselves.

Taken together, this study provides insights into the new protein, GAS2-like 3, which has the capacity to crosslink MTs and actin and provides a mechanistic insight into how GAS2-like 3 localisation is regulated in cells.

Lay abstract

Human beings are made up of many living cells. Living cells are comprised of many different molecules, which all must work together in order to maintain a healthy individual. One important group of these molecules, are called proteins. There are thousands of different proteins that can be found in cells, and they are often specific for a certain cell type, however, there are a number of proteins that are found in all cells. These include the proteins that make up a cellular scaffold, known as the cytoskeleton. The cytoskeleton is made up of two important components; the actin cytoskeleton, which governs cell shape, and the microtubule cytoskeleton, which controls cell division. It is crucial for these two cytoskeletons to communicate with one another in order to keep both the cell and the individual healthy. Defects in proteins that manage the communication between the cytoskeletons result in various diseases including neurodegeneration, severe skin blistering and cancer. Thus, it is essential for us to understand the underlying regulatory mechanisms behind these medical conditions.

Here, we have discovered a new protein, named GAS2-like 3, which mediates the communication between the two cytoskeletons. By conducting a series of experiments, we have demonstrated the association of GAS2-like 3 with both the actin cytoskeleton and the microtubule cytoskeleton. We also revealed that GAS2-like 3 interacts with another protein, called EB1, which governs where GAS2-like 3 is found in the cell. This interaction could dictate the role of GAS2-like 3 in cells. In addition, we discovered that when GAS2-like 3 was expressed in cells, it resulted in cell death. Many cancers arise as a result of cells being unable to kill themselves, possibly indicating that cells lacking GAS2-like 3 are more susceptible to cancer. Intriguingly, we found GAS2-like 3 on mitochondria, which are specific regions of the cell that instigate cell death. Thus, GAS2-like 3 is likely to perform the cross-communication between actin, microtubules and mitochondria. GAS2-like 3 could therefore be a key therapeutic target to alleviate medical disorders, which arise as a result of defective proteins that control the cytoskeleton.

Declaration

No portion of the work referred to in the thesis has been submitted in support of an application for another degree or qualification of this or any other University or other institute of learning.

Copyright statement

i. The author of this thesis (including any appendices and/or schedules to this thesis) owns certain copyright or related rights in it (the "Copyright") and s/he has given The University of Manchester certain rights to use such Copyright, including for administrative purposes.

ii. Copies of this thesis, either in full or in extracts and whether in hard or electronic copy, may be made **only** in accordance with the Copyright, Designs and Patents Act 1988 (as amended) and regulations issued under it or, where appropriate, in accordance with licensing agreements which the University has from time to time. This page must form part of any such copies made.

iii. The ownership of certain Copyright, patents, designs, trade marks and other intellectual property (the "Intellectual Property") and any reproductions of copyright works in the thesis, for example graphs and tables ("Reproductions"), which may be described in this thesis, may not be owned by the author and may be owned by third parties. Such Intellectual Property and Reproductions cannot and must not be made available for use without the prior written permission of the owner(s) of the relevant Intellectual Property and/or Reproductions.

iv. Further information on the conditions under which disclosure, publication and commercialisation of this thesis, the Copyright and any Intellectual Property and/or Reproductions described in it may take place is available from the Director of the Wellcome Trust Centre for Cell-Matrix Research and the Dean of the Faculty of Life Sciences.

Acknowledgements

The work presented here was funded by the Wellcome Trust.

Firstly I would like to thank my supervisors Christoph Ballestrem and Richard Kammerer for their guidance and support throughout my studies. I would also like to thank past and present members of the Kammerer and Ballestrem labs, with a special mention for Mohammed Tasab for his proofreading of this thesis. I would also like to thank Philip Macdonald for helping me with a particularly tricky piece of molecular biology, Barbara Ciani for her help with sequence alignments and all things biophysical. Christina Lambri for showing me the ropes with using cDNA panels, as well as Alex Carisey for his guidance on my shiny new Mac! I would like to thank Tom Owens for his useful insight into apoptosis, and Alengo Nyamay'antu and Aisha Payapilly for their great spirits in the lab.
I would also like to thank my fellow PhD student and good friend, Pawel Leznicki for his inspirational chats in the pub and in various curry houses. Also I would like to thank Sanjai Patel and Chris Bayley for their support during my PhD.

Last but definitely not least I would like to take this opportunity to thank my mum, dad, and sister for their continued love and support throughout my life and for putting me through a solid education. I would also like to thank Lucy Coker for supporting me through tight deadlines and helping me talk through grand theories!

Preface

Matthew Stroud was raised and educated in Oxford. After completing his A-levels, he went to the University of Bristol to read Biochemistry and graduated with an upper second-class honours degree in 2005. He then worked as a research assistant in the lab of Gillian Griffiths at the University of Oxford, and secured his Wellcome Trust Funded Four-Year PhD, at the University of Manchester.

Matthew Stroud is currently working as a research associate for his PhD co-supervisor, Christoph Ballestrem, after which he aims to secure his own funding in order to pursue a career in academia.

Layout and contributions

This thesis is presented in the alternative format, with each Results chapter (Chapters 3-5) written in the style of a scientific manuscript. The first results chapter is an extended methods paper entitiled 'Fluorescence Recovery After Photobleaching' and has been accepted for publication by the Methods in Molecular Biology Journal. Matthew Stroud, Alex Carisey and Ricky Tsang all contributed equally to the work, which was supervised by Christoph Ballesrem.

The second results chapter entitled 'GAS2-like 3 is a new microtubule-actin interacting protein related to the spectraplakins' has been submitted to the Journal of Cell Science. Individual contributions of the authors to this manuscript are as follows: Christoph Ballestrem and Richard Kammerer co-supervised the work. Matthew Stroud designed and performed all the experiments. Other contributions by non-authors include the cloning of the G2L3-CH domain into pHisTrx and expression by Karolina Zielinska.

The third results chapter entitiled: 'The functional characterisation of a novel binding partner, end-binding protein 1 (EB1) to GAS2-like 3' will be submitted to the Journal of Cell Science. Individual contributions of the authors of this work are as follows: Christoph Ballestrem and Richard Kammerer co-supervised the work. Matthew Stroud designed and performed all of the experiments.

Following the results chapter is a 'Final Discussion' that aims to tie the chapters together and explore avenues of future investigation. Since each results chapter has its own independent reference section, a 'General References' section is provided towards the end of the thesis, and contains references for all non-results chapters.

1) Introduction

The cytoskeleton is fundamental to cellular integrity, providing a molecular framework for both mechanical support and the intracellular transport infrastructure. All eukaryotes contain actin filaments and microtubules (MTs), whereas only some contain intermediate filaments (Figure 1.1). It has become increasingly clear that the actin and MT cytoskeletons are organised and function in an interdependent way (Karakesisoglou et al., 2000; Leung et al., 2002; Subramanian et al., 2003).

Cytoskeletal proteins are linked to many human pathological conditions, such as cancer, infection, and various cardiovascular diseases. Some of the most well characterised proteins involved in linking actin filaments to MTs belong to the spectraplakin family, for example Microtubule-Actin Crosslinking Factor 1 (MACF1) (Kodama et al., 2003; Lee and Kolodziej, 2002; Roper et al., 2002; Sun et al., 2001).

Dissecting the mechanisms behind MT-actin crosslinking in greater detail will be essential to understand the underlying disorders that arise as a consequence of mutations in the respective proteins.

1.1) The Microtubule and Actin Cytoskeletons

1.1.1) Microtubule cytoskeleton

MTs play key roles in processes that are fundamental to cell homeostasis, such as cell division and cell motility, thus they also have central roles in many physiological and disease processes. MTs provide polarised molecular tracks, which molecular motors move along, transporting a variety of cargo from the microtubule organising centre (MTOC) to the cell periphery and vice versa (Caviston and Holzbaur, 2006).

MTs are composed of stable α/β-tubulin heterodimers that are aligned in a polarised head to tail fashion which form protofilaments. These protofilaments are assembled to form a cylindrical and helical MT wall, typically comprising 13 parallel protofilaments *in vivo* (Figure 1.2). MTs can grow and shrink through

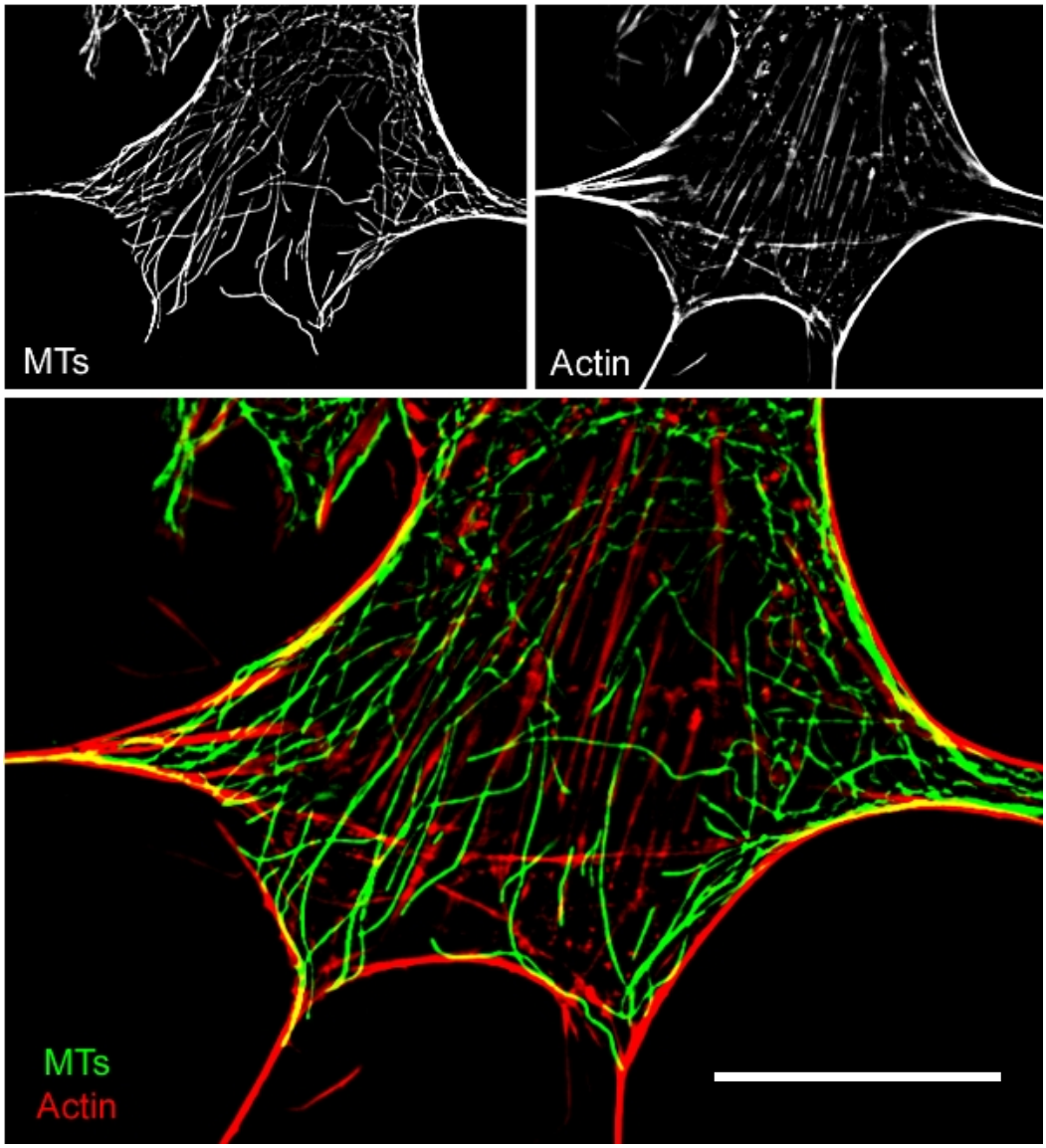

Figure 1.1: Localisation of microtubules (MTs) and actin cytoskeletons in NIH3T3 fibroblasts.

Above; NIH3T3 cells were fixed and stained for MTs using an antibody directed against α-tubulin, followed by a Cy5 conjugated secondary antibody. Actin was labelled using FITC-conjugated phalloidin. Below; merged image of MTs and actin. Scale bar = 10μm.

polymerisation and depolymerisation, respectively which is driven by the binding, exchange and hydrolysis of a guanine nucleotide on the β-tubulin monomer (Kirschner and Mitchison, 1986). Polymerisation is initiated from a pool of GTP-bound tubulin dimers, which are incorporated at the growing plus (+) end. Once incorporated into the MT lattice, GTP is hydrolysed and the inorganic phosphate is released. It has been postulated that GTP hydrolysis changes the conformation of the tubulin dimer from slightly curved to a profoundly curved conformation (Wang and Nogales, 2005). This nucleotide-dependent

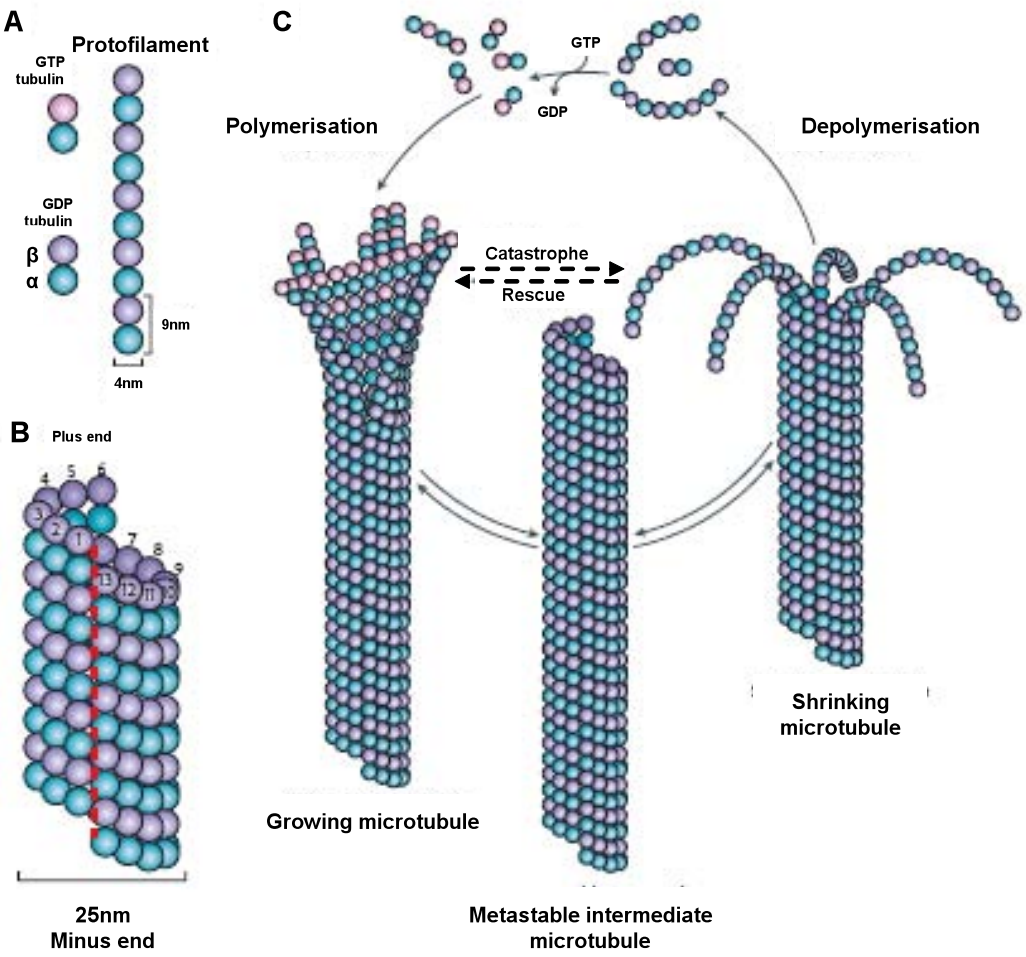

Figure 1.2: Microtubule structure and dynamic instability.

Adapted from (Akhmanova and Steinmetz, 2008). A: The stable α/β tubulin dimer with either GDP or GTP bound and assembled into protofilaments. B: The organisation of cylindrical and helical MT wall consists of 13 parallel protofilaments in vivo. C: The polymerisation/ depolymerisation cycle of MTs; MT polymerisation is driven from a pool of GTP-loaded tubulin. Once added to the growing MT end, the GTP is hydrolysed to release inorganic phosphate causing a conformational change in the tubulin dimer. This is thought to straighten the tubulin dimer once it is incorporated into the MT wall. Closure of the growing end results in a metastable intermediate MT, which may pause, grow (polymerisation) or shrink (depolymerisation) in a phenomenon known as 'dynamic instability'.

conformation change suggests that the curved tubulin-GDP is forced to remain straight once incorporated into the MT wall. The growing + end is thought to maintain a 'cap' of GTP-bound tubulin subunits to stabilise the straight tubulin conformation within the MT lattice. Closure of the MT end generates a metastable-intermediate structure, which can either pause, grow (termed rescue) or undergo depolymerisation (termed catastrophe). MTs undergoing catastrophe are characterised by a fountain-like array of ring and spiral protofilaments

structures (Figure 1.2). This is presumably directed by a conformational change in GDP-tubulin, resulting in the destabilisation of lateral contacts between adjacent protofilaments. The depolymerisation-polymerisation cycle is completed by the exchange of GDP for GTP on the β-tubulin subunit.

Whereas the β-tubulin subunit can exchange its GDP for GTP, the α-tubulin subunit can also undergo post-translational (PT) modification in an enzymatic detyrosination/ tyrosination cycle. The enzyme tubulin Tyrosine carboxypeptidase (TTCP) is used to repeatedly cleave the Tyrosine (Tyr) residue of the conserved EEY/F sequence motif, whereas the ATP-dependent tubulin Tyr ligase (TTL) repeatedly adds back a Tyr residue. TTCP preferentially acts on MTs and TTL can only act on free tubulin monomers. This means that longer living, more stable MTs accumulate Glutamate (Glu)-tubulin, whereas freshly polymerised MTs contain larger amounts of Tyr-tubulin. This cycle provides an explanation as to why MTs containing high proportions of Glu-tubulin are hypothesised to be more stable. In fibroblasts, Glu-MTs reorientate themselves to the leading edge of cells undergoing migration, thus they are thought to be important in cell polarisation (Li and Gundersen, 2008).

Another ubiquitous PT-modification of tubulin is the acetylation of α-tubulin on Lysine 40 (Edde et al., 1991). Similarly to detyrosination, acetylated MTs are also a hallmark of stabilised MTs. A prominent candidate to perform this role is histone deacetylase 6 (HDAC6), which belongs to the class II histone deacetylases (Boyault et al., 2007). HDAC6 can directly acetylate tubulin, and has been shown to regulate MT dynamics likely through an interaction with MT plus-end binding proteins or +TIPs (Zilberman et al., 2009). Whereas this evidence suggested that acetylation does not play a role in regulating MT dynamics, there is evidence to suggest tubulin acetylation does play a role in recruiting MT-associated proteins, such as the motor protein kinesin 1(Dompierre et al., 2007; Reed et al., 2006).

There are various other PT-modifications of tubulin which are beyond the scope of this study, such as the removal of the Glu-Tyr dipeptide from the C-terminus of α-tubulin, polyglutamylation and polyglycination of α and β-tubulins, and phosphorylation of some tubulins, which all occur at the acidic C-terminus of tubulin molecules.

1.1.2) Actin cytoskeleton

The actin cytoskeleton provides the cell with mechanical strength important for maintaining cellular integrity and for cell motility. Cellular actin comprises a pool of globular (G) actin monomers, which can polymerise to form filamentous (F) actin. In a similar fashion to MTs, F-actin fibres are polarised with the polymerising end (+ end equivalent) denoted as the 'barbed' end and the depolymerising end denoted as the 'pointed' end. G-actin in the cytoplasm is able to exchange ADP for ATP, which enables polymerisation to form F-actin. Once integrated at the barbed end, F-actin is able to hydrolyse ATP to ADP + Pi to form ADP-bound F-actin which eventually dissociates and returns to the ADP-bound G-actin state (Figure 1.3). In the steady state, actin is simultaneously undergoing both polymerisation and depolymerisation in a process known as 'treadmilling'. This enables the actin filament to move forward whilst remaining the same length, as well as generating a protruding force essential for many processes including cell migration.

Treadmilling of pure actin is often too slow for cell migration, hence various other proteins are used to regulate actin dynamics and nucleation. The respective proteins can bind to either the barbed or pointed ends of F-actin and prevent or promote the association and/ or dissociation of G- actin. Capping proteins bind to barbed ends with high affinity, preventing the addition of actin monomers, thereby increasing the local concentration of G-actin to enable rapid growth of adjacent noncapped filaments in a process called funnelling. The heterodimeric capping protein and gelsolin are implicated in cellular functions such as lamellipodium protrusion and cell migration, respectively (Le and Carlier, 2008).

Profilin also localises at the barbed ends, where it binds to G-actin and alters the conformation of G-actin to promote ATP/ADP exchange, which increases polymerisation. Cofilin localises throughout the lamellipodium and binds to the pointed ends of actin filaments to promote dissociation of G-actin, it can also inhibit ATP/ADP exchange to prevent actin polymerisation. Phosphorylation of cofilin results in dissociation from G-actin, this subsequently promotes ATP/ADP exchange and actin polymerisation.

As well as proteins which solely prevent or accelerate actin treadmilling, there are three major classes of proteins which are used to nucleate actin. The first of which is the Arp2/3 complex, which mediates simultaneous actin nucleation and

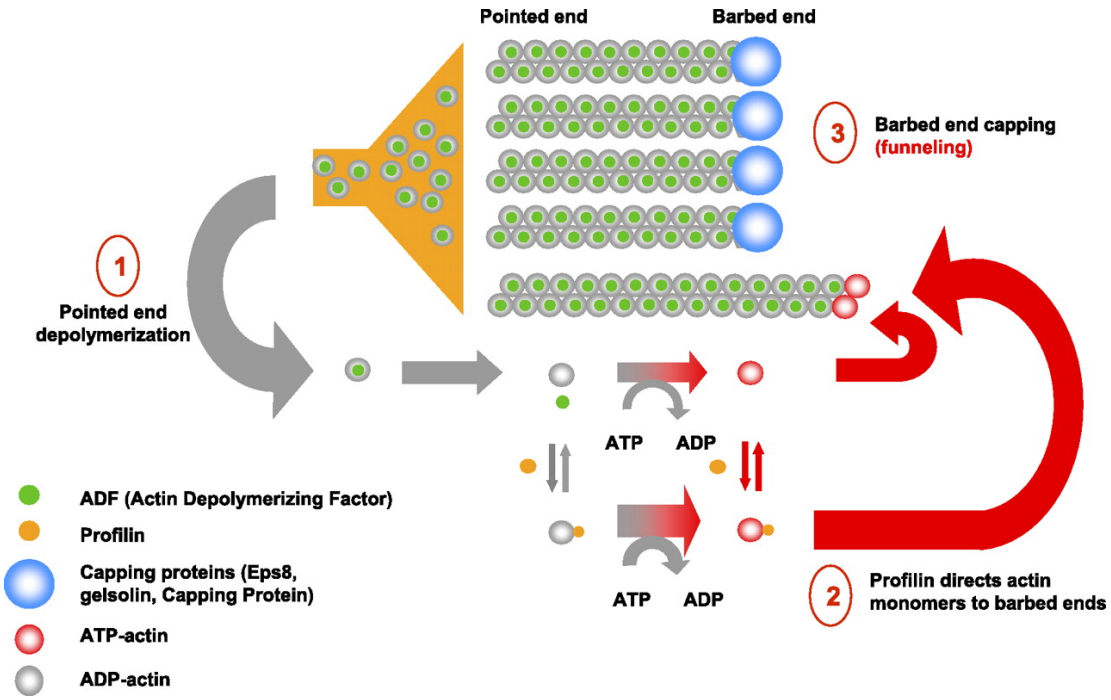

Figure 1.3: Regulation of actin treadmilling

Adapted from (Le and Carlier, 2008). 1) Cofilin (ADF) binds to ADP-actin filaments and promotes pointed end depolymerisation to increase the concentration of G-actin at steady state. 2) Profilin binds to the barbed end and promotes ATP/ADP exchange, to promote recycling of actin monomers. 3) Capping proteins at the barbed ends abrogate polymerisation of the actin filament by preventing the addition of G-actin. This enables 'funnelling' of G-actin to the noncapped filaments which accelerates their growth.

branching of F-actin at the pointed end and is important in lamellipodium formation (Arp2/3 complex) (Lai et al., 2008). Secondly, spire proteins nucleate actin to assemble unbranched filaments, and also bind to the pointed ends of F-actin. The third actin nucleation mechanism relies on the formin family of proteins, which nucleate parallel actin bundles such as those found in stress fibres (Romero et al., 2004). Generally, formins bind to the barbed ends and remain bound, adding G-actin to the growing end in a processive manner. The constant presence of formins at the barbed ends prevents capping proteins from binding, which aids filament growth. As well as their actin nucleating activity, formins are also able to stabilise MTs, which will be discussed later as they are potential MT- actin crosslinkers (see section 1.2.3) (Bartolini et al., 2008; Ishizaki et al., 2001; Palazzo et al., 2001).

1.2) Evidence of microtubules linking to the actin cytoskeleton

Several lines of evidence implicate the actin cytoskeleton in stabilising and guiding MTs from the MTOC to the cell periphery (Goode et al., 2000; Salmon et al., 2002; Schaefer et al., 2002). Dual-wavelength, fluorescent speckle microscopy reveals growth of MTs along F-actin bundles in epithelial cells (Salmon et al., 2002) and MTs in neuronal growth cones cease to grow in regions where the underlying actin network is perturbed (Schaefer et al., 2002).

Further evidence comes from studies of cell migration, during which cells must polarise, using their actin cytoskeleton to enable cell protrusion at the front and retraction at the rear of the cell (Vasiliev, 1991). In order to polarise, co-operation between the actin and MT cytoskeletons is required, as it is impaired or lost when MTs are disrupted (Ballestrem et al., 2000; Vasiliev et al., 1970). There is some evidence that the stability of MTs and/ or their coordinated movements with F-actin rely upon direct physical linkages of the two cytoskeletons (Kodama et al., 2003). The actin cytoskeleton is thought to provide a robust stabilising platform for MT capture, growth and/or guidance of MTs (Basu and Chang, 2007; Goode et al., 2000; Kaverina et al., 2002; Small and Kaverina, 2003; Wu et al., 2008). The molecular events regulating these processes are still unclear, although one can speculate that these events may use a combination of MT plus-end tracking proteins (+TIPS), spectraplakins, formins, and potentially the GAS2 family, amongst other proteins which are yet to be fully characterised.

1.2.1) Microtubule plus-end tracking proteins

MT dynamics are mostly regulated by tubulin-interacting proteins which can stabilise and maintain linear growth of MTs, promote instability, or capture MTs at specific cellular locations (Galjart and Perez, 2003). A collective group of proteins that mediate these roles are known as the +TIPS. These proteins bind to the distal ends of MTs and are thought to guide the MT +ends to the cell cortex, where the small Rho GTPases reside (Figure 1.4). Rho GTPases are molecular switches which play key roles in regulating the actin cytoskeleton, resulting in changes in cell polarity and microtubule dynamics amongst many others (Etienne-Manneville and Hall, 2003). For example, the Rho GTPase Cdc42 activates distinct MT tethering sites by promoting localised actin polymerisation (Etienne-Manneville and Hall, 2003). IQGAP1, which is an

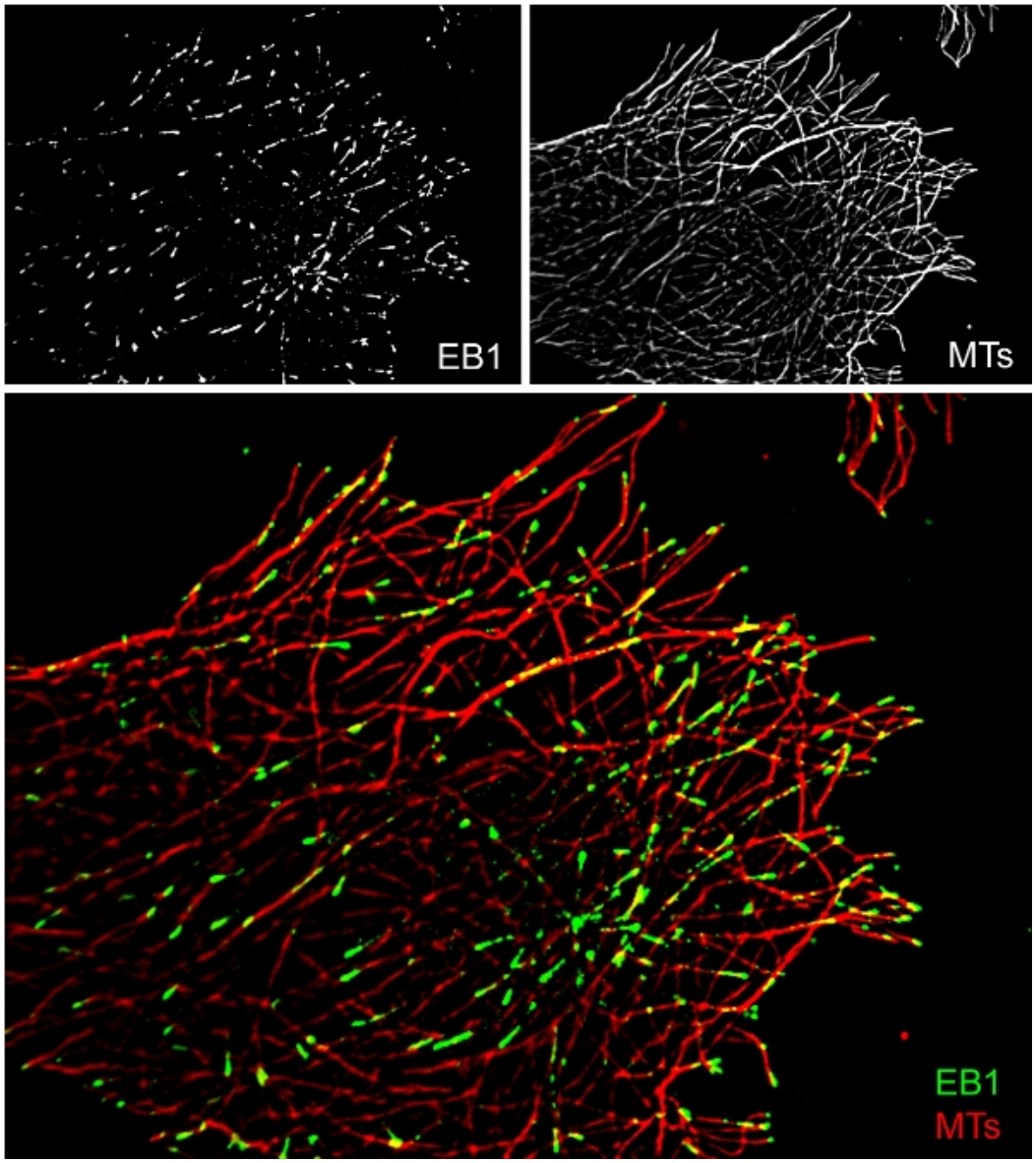

Figure 1.4: Localisation of EB1 to the plus-ends of MTs.
NIH 3T3 cells were transfected with EB1-GFP, fixed and stained using an antibody directed against α-tubulin followed by a Cy5-conjugated secondary antibody.

effector of Cdc42 and fellow Rho GTPases Rac1, has been shown to bind the +TIP CLIP-170 directly, providing a link between a polarised MT cytoskeleton and cell polarisation (see Figure 1.5). Several other links between activated Cdc42 binding proteins and +TIPS have been described (Etienne-Manneville and Hall, 2001; Fukata et al., 2002). Figure 1.5 shows the array of proteins which can bind to the +ends of MTs, and potential interacting proteins which could link MTs and F-actin. In addition to +TIP interactions with Rho family GTPases, there is also evidence suggesting that they interact with spectraplakins (as described in Section 1.2.2) (Applewhite et al., 2010; Wu et al., 2008).

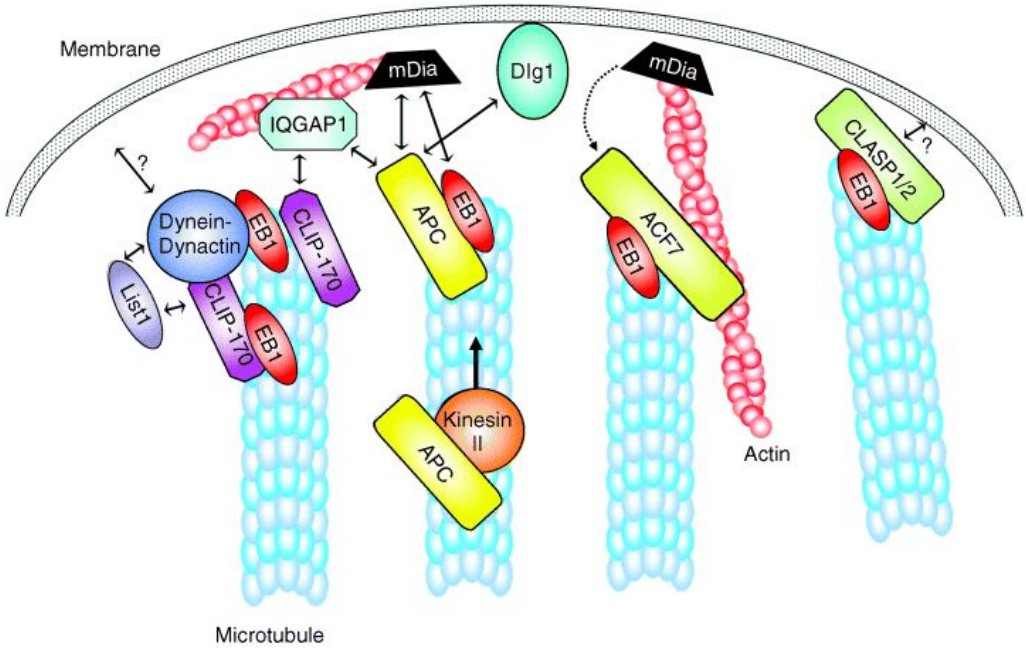

Figure 1.5: Organisation of MTs, F-actin bundles and various cytoskeleton associated proteins at the cell membrane.

Adapted from (Lansbergen and Akhmanova, 2006).The plus-ends of microtubules can bind to a variety of +TIP proteins, including APC, EB1 and CLIP-170. There are putative links between the MTs and actin bundles via the Rho effector, IQGAP and CLIP-170. Furthermore, the spectraplakin ACF7 can bind to both MT and actin cytoskeletons, implying it maybe involved in crosslinking the two.

In spite of recent advances, a lack of knockout mutations in most of these genes raises questions about their functional significance in multicellular organisms.

Are any of these links sufficient to tether and polarise MTs at activated cortical sites? Are additional proteins involved, if so, what are they and how are they involved? Most data suggest that cell polarisation is likely to involve coordinated integration of actin-MT dynamics, however little is known about the molecular integrators involved.

1.2.2) Spectraplakins

Other prominent candidate proteins for the role of microtubule guiding along F-actin belong to the spectraplakin family (Jefferson et al., 2004). Members of this family all have binding sites for both F-actin via their calponin homology (CH) domains and for MTs via the GAS2-related (GAR) domain and/ or GSR repeats as shown in Figure 1.6. The first members of this family were classified separately from the plakin

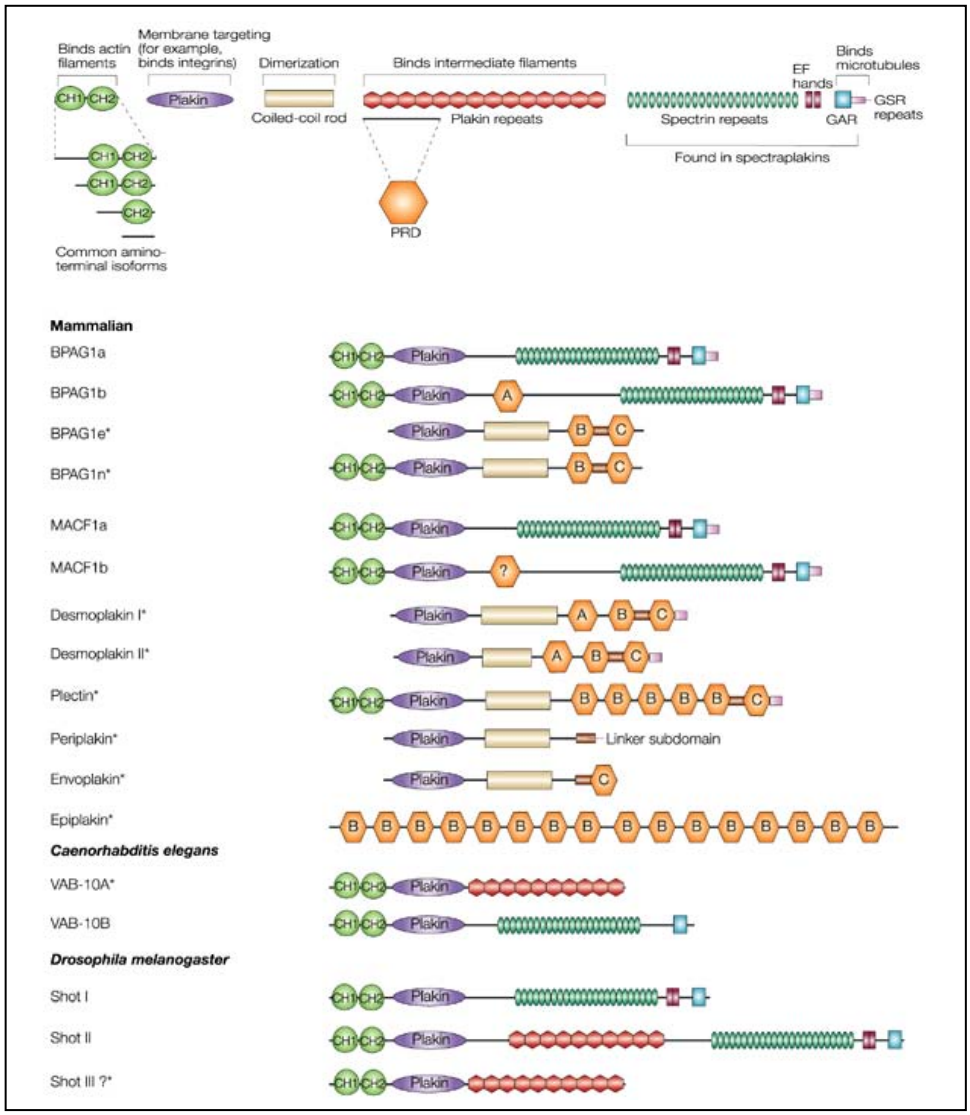

Figure 1.6: The domain organisation of the plakin family and the mammalian and invertebrate plakin isoforms.

Adapted from (Jefferson et al., 2004). All family members contain an actin binding domain (ABD) at their N-termini, which is conferred by tandem CH domains, and a MT binding domain (MTBD) at their C-termini conferred by the GAS2 domain and/ or GSR repeats.

superfamily (which connect adhesion receptors to intermediate filaments) and the spectrin superfamily (which bind and crosslink actin filaments and attach these to membrane receptors), as they can play these roles individually (Roper et al., 2002). Short-stop (Shot) in Drosophila and the dystonin/BPAG1 and MACF1 proteins in mammals were the first spectraplakins identified. More recently VAB-10 was identified in *C. Elegans* (Figure 1.6) (Bosher et al., 2003). The fact that their amino acid sequence is conserved and they are also found in lower organisms implies they have an important functional role.

Recent evidence regarding the mammalian spectraplakin MACF1 (Microtubule Actin Crosslinking Factor 1) uncovers roles for spectraplakins in MT dynamics, guidance, cortical tethering, stability and cellular polarisation (Kodama et al., 2003). It has been shown that the ablation of MACF1 in endodermal cells leads to the uncoupling of MT from microfilaments and a change in MT dynamics. Interestingly, MACF1 has also been shown to interact with the +TIP end-binding protein 1 (EB1) (Honnappa et al., 2009), implying that spectraplakins can also bind to the +ends of MTs, as well as to the MT lattice and F-actin.

In Drosophila S2 cells, the interaction with EB1 is hypothesised to be important when Shot is in its inactive form in the cell interior and the MT +ends are undergoing a 'search and capture' mechanism for an activation signal to engage with actin. Upon activation, Shot undergoes a conformational change to release EB1 and to engage with F-actin via its CH domains, and the MT lattice via its GAR domain. When engaged with both cytoskeletons, Shot stabilises MTs against lateral movements driven by motor proteins, and guides them along F-actin in the cell periphery (Applewhite et al., 2010). This study suggests that Shot only binds EB1 in the cell interior, however, another study suggests that the interaction between the mammalian spectraplakin, MACF1 and EB1 occurs throughout the cytoplasm from the cell interior to peripheral focal adhesions (FAs), and is necessary for the MT-actin crosslinking (Wu et al., 2008). In the latter study, an actin-dependent ATPase activity was identified in MACF1 and was found to be essential to recover defects in cell migration in MACF1 null cells. The ATPase activity of MACF1 is thought to be essential to target MTs to FAs for remodelling, which is fundamental for effective cell migration.

Mutations in spectraplakin genes result in the degeneration of cells that express them, and despite the large size of spectraplakins (>500kDa), rescue experiments using the actin and MT binding domains suggest that these domains are both necessary and sufficient to rescue defects in neurogenesis and cell polarisation (Kodama et al., 2003; Lee and Kolodziej, 2002).

Various medical conditions and developmental defects arise as a result of mutated spectraplakins, (Giorda et al., 2004; Leung et al., 2002; Sjoblom et al., 2006; Sonnenberg and Liem, 2007). The severe phenotypes observed illustrates the importance of proteins that link the actin and MT cytoskeletons. Further characterisation of these proteins will progress the understanding and importantly the alleviation of spectraplakin-associated pathological conditions.

1.2.3) Formins

Formins are a conserved family of proteins, containing a formin homology 2 (FH2) domain, which assembles unbranched actin filaments from the barbed end (Faix and Grosse, 2006). The diaphanous-related formins (DRFs) are a subfamily of formins characterised by domains that regulate their activation by the Rho family of small GTPases and their subcellular localisation. Binding of Rho-GTP to the GTPase Binding Domain (GBD) relieves the autoinhibitory conformation between the N-terminal diaphanous inhibitory domain (DID) and a short segment C-terminal to the FH2 domain termed the diaphanous autoregulatory domain (DAD) (Figure 1.7).

In terms of crosslinking MTs to F-actin, there is evidence to suggest that the MTs co-align with F-actin when a constitutively active version of mDia1 is expressed (Ishizaki et al., 2001). Ishizaki and colleagues propose that the FH2 domain is fundamental in this role, implying that other formins may also play a role in crosslinking the two cytoskeletons. To augment this data, similar observations were made using a constitutively active version of mDia2. However, from the mDia1 study no inferences were made as to the stability of MTs (as the orientation of stable MTs towards the leading edge is indicative of cell polarisation). When the stability of MTs was probed in a study on mDia2 (Palazzo et al., 2001), it was found that the MTs which co-aligned with F-actin were dynamic MTs, which are not indicative of cell polarisation as suggested by the mDia1 study. Palazzo and colleagues argue from this observation that mDia's ability to induce the formation and orientation of stable MTs is independent of its ability to co-align the MT and actin cytoskeletons. Nevertheless it is possible that dynamic MTs also crosslink with actin cytoskeletons, although crosslinking may decrease the dynamic instability of MTs.

For both the DRFs, murine Diaphenous1 (mDia1) and mDia2, the integrity of the FH1 and FH2 domains is vital for actin nucleation activity and MT stabilisation (Ishizaki et al., 2001;Palazzo et al., 2001;Bartolini et al., 2008).

A recent study using mDia2 implies that this protein can stabilise microtubules independently of its actin nucleation activity, as mutants defective at actin polymerisation were still able to stabilise MTs (Bartolini et al., 2008). Bartolini and coworkers conclude that the MT stabilisation effect could be via an

Figure 1.7: Schematic representation of the domain organisation of diaphanous-related formins (DRFs).

Adapted from (Faix and Grosse, 2006). The GTPase binding domain (GBD) enables partial activation of DRFs by Rho GTPase to relieve the autoinhibited hairpin conformation of the Diaphanous inhibitory domain (DID) interaction with the Diaphanous autoregulatory domain (DAD). Additional signals are required to fully activate DRFs.

interaction with the +TIPs, EB1 or APC. Interestingly, a 'knotted' MT phenotype, in which the stable MTs localised in a perinuclear distribution rather than a regular peripheral distribution was observed when the actin polymerisation defective mutants were expressed in cells. From this observation it is apparent that the actin nucleation driven by mDia2 plays a role in MT stabilisation albeit one that is not fundamental.

It remains unclear whether the FH2 domain plays a role in crosslinking MTs to actin in order to stabilise the MTs, or whether MT stabilisation by FH2 occurs independently of actin crosslinking. The FH1 domain has been implicated in playing a role in actin polymerisation, as it can bind to profilin (Ishizaki et al., 2001). It would be interesting to see whether mutations in this domain to abrogate actin binding affect MT co-alignment with actin.

It has been shown that the formation of stable MTs by mDia1 requires the +TIPS adenomatous polyposis coli (APC) and EB1, enabling capture at the cell cortex (Wen et al., 2004). From this study, it was concluded that EB1/ APC/ mDia1 may form a complex with EB1/ APC acting downstream of mDia1. Another link between MTs and F-actin could plausibly be formed between MT plus-end tracking proteins (+TIPS) and the small Rho GTPases.

1.3) Potential roles of members of the GAS2 family in MT-actin crosslinking

1.3.1) GAS2 family

Similar to the spectraplakins, members of the GAS2 family all contain a CH domain, a GAR domain and a non-conserved C-terminal domain, which varies in length between family members (Figure 1.8). The GAS2 protein family is little characterised and conserved among species ranging from C. elegans to H. sapiens, which implies an important functional role. Its constituent members are much smaller than the spectraplakins and currently include GAS2, GAR22 (GAS2-like 1), GAR17 (GAS2-like 2) (Brancolini et al., 1992; Goriounov et al., 2003; Schneider et al., 1988; Zucman-Rossi et al., 1996), and the new protein GAS2-like 3 (G2L3) (Stroud et al., 2010).

The first member of the GAS2 family was GAS2, which is shorter in length than GAS2-like proteins. GAS2 was described to be involved in growth arrest, apoptosis and may play a tumour suppressor role (Brancolini et al., 1995; Brancolini and Schneider, 1994; Lee et al., 1999). GAS2 is cleaved by caspases in cultured cells undergoing apoptosis, to produce an N-terminal fragment which contains the CH domain and dramatically reorganises the F-actin network of the cells collapsing it around the nucleus (Brancolini et al., 1995). This caspase-mediated cleavage of GAS2 is hypothesised to be necessary for the morphological changes observed in the cell during apoptosis. Further evidence of GAS2 playing a role in apoptosis is that GAS2 expression and cleavage are induced in interdigital tissues of mouse embryos between days 13.5 and 15.5, which are developmental stages characterised by extensive apoptosis (Lee et al., 1999). Nevertheless, it should be noted that GAS2 was undetectable in other regions, which are known to undergo extensive apoptosis, such as the heart. Whereas the literature supports the argument that GAS2 is involved in apoptosis, there is no evidence to suggest this for its related family members (Goriounov et al., 2003). For example, the cleaved form of GAS2-like1 was not found in a variety of cell lines treated with apoptotic signals. Full length GAS2-like1 isoforms or versions encoding the N-terminus which were transfected into COS7 cells resulted in no change in cell morphology, as was observed with the equivalent GAS2 construct. Similarly to GAS2, GAS2-like 1 expression increased during growth arrest, however, GAS2-like 1 is highly phosphorylated on serine

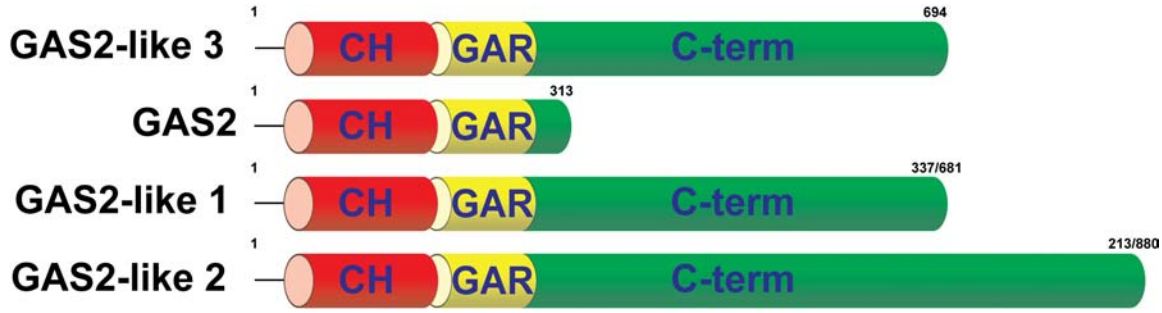

Figure 1.8: The constituent members of the GAS2 family and their domain organisations. All members contain a Calponin Homology (CH) and GAS2-Related domain (GAR), GAS2 contains a short C-terminal extension (C-term) in comparison to the GAS2-like proteins. GAS2-like 1 and GAS2-like 2 can be alternatively spliced to produce proteins 337 or 681 aas in length and 213 or 880 aas in length respectively (as indicated in the figure).

and threonine residues in quiescent cells. This is in contrast to GAS2, which is specifically phosphorylated on serine residues in cells undergoing the transition from quiescence (G0 phase) to the G1 phase (Brancolini and Schneider, 1994). Active GAS2 is thought to inhibit the G0 to G1 transition, and phosphorylation is thought to downegulate GAS2 activity, thus allowing cells to reenter the cell cycle. These results imply that GAS2 has different *in vivo* functions to its related family members. Indeed there is some evidence to suggest that GAS2-like 1 and GAS2-like 2 are able to crosslink F-actin and MTs in cells (Goriounov et al., 2003) through their CH and GAR domains, respectively (Sun et al., 2001). This finding suggests that their physiological functions may involve the integration of these two components of the cytoskeleton. Despite the apparent differences in function, it is likely that the GAS2 family members play tissue specific roles. For example, GAS2 is predominantly found in lung tissue, GAS2-like 1 in brain and testis, and GAS2-like 2 in skeletal muscle.

1.3.2) GAS2 Family Domains

1.3.2.1) Calponin Homology Domain

The CH domain was first identified at the N-terminus of calponin, which binds actin and plays a key role in regulating muscle contraction (Gimona et al., 2002;Korenbaum and Rivero, 2002). CH domains are found in a variety of proteins such as IQGAP, which is involved in signalling, and the spectraplakins, which bind actin filaments. They are categorised by sequence similarity into three classes; CH1, CH2 and CH3 (Gimona et al., 2002). CH1 and CH2 domains

are able to combine and form actin-binding domains (ABDs) with CH3 domains often found alone at the N-terminus. GAS2 family members contain a CH3 class domain, which is a putative ABD. It appears that the avidity of a protein for actin increases with the number of CH domains. The CH3 domain found in calponin appears not to bind to F-actin (Fu et al., 2000;Gimona and Mital, 1998), however there is well-founded evidence that the CH3 domain found in the GAS2 family appears to bind both *in vivo* and *in vitro* to F-actin (Goriounov et al., 2003;Brancolini et al., 1995;Brancolini et al., 1992). CH domain-containing proteins can also bind to MTs, for example it is speculated that EB1 can bind to tubulin (Gimona et al., 2002).

1.3.2.2) GAS2-Related Domain

The GAS2-Related (GAR) domain was originally identified in GAS2 and is a putative MTBD that is highly conserved during evolution (Sun et al., 2001). Sequence analysis revealed that the GAR domain also exists in spectraplakins, where, in concert with the C-terminus, it binds to MTs and partially stabilises them from the MT-depolymerising agent, nocodazole. The GAR domains contained in the GAS2 family members GAS2-like 1 and GAS2-like 2, weakly bind to the MTs, and shows some evidence of colocalisation to them (Goriounov et al., 2003).

1.3.2.3) C-terminus

The GAS2-like members of the GAS2 family contain extended C-termini, in which we have identified putative EB1 binding sites, also referred to as MT-tip localisation signals (MtLSs) (Honnappa et al., 2009). GAS2 itself contains only a short C-terminus of 40 amino acids (AAs), without any MtLSs, whereas its fellow family members have C-termini ranging from 60 to 600 AAs. GAS2-like1 and GAS2-like3 both contain two MtLSs, whereas GAS2-like2 contains four MtLSs. The lack of an extended C-terminus may explain the slightly different proposed functions of GAS2.

The CH and GAS2 domains make up only 30-40% of the total amino acid sequence of GAS2 proteins, raising the question of the possible functions of the remaining regions. It is likely that the uncharacterised regions of the GAS2 family play a role in the recruitment of proteins which regulate actin and MT dynamics.

Indeed preliminary evidence suggests that the +TIP protein EB1 may recruit GAS2-like 3 to microtubules (unpublished observation M. Stroud). This interaction alone could potentially create a plethora of interactions and further analysis of the C-terminus should enable identification of other important binding domains.

1.4) Aims and Objectives

The MT and actin cytoskeletons are fundamental to cell integrity, as they control a host of cellular activities including cell division, growth, polarisation and migration.

We have identified a new protein, called GAS2-like 3, which is a new member of the GAS2 family and has the potential to interact with both MT and actin cytoskeletons. The GAS2 family comprises the proteins GAS2, GAS2-like 1, GAS2-like 2 and GAS2-like 3. Currently, there are only a handful of papers describing the functions of the GAS2 family members, which include roles in apoptosis and in mediating the communication between MTs and actin. Despite these functions, very little is known about the molecular mechanisms underlying them. Thus, the overall aim of this study is to functionally characterise GAS2-like 3, and to gain insights into the molecular mechanisms underlying its function.

1.4.1) Elucidating the cell and tissue distribution of GAS2-like 3

Fellow members of the GAS2 family are expressed in various different tissues, suggesting they may play tissue-specific roles. As GAS2-like 3 is a new protein, nothing is currently known about its tissue and cell distribution. Without an antibody directed against GAS2-like 3 to detect it at the protein level, PCRs will be performed on cDNA libraries generated from different human tissues and cell lines. This analysis will reveal where GAS2-like 3 is expressed at the mRNA level and give an indication as to where the protein is expressed.

1.4.2) Determining the sub-cellular localisation and binding strengths of GAS2-like 3 to the MT and actin cytoskeletons

To gain insights into the function of GAS2-like 3, and the molecular mechanisms underlying this role, its sub-cellular localisation will be determined.

GAS2-like 3 contains a putative actin-binding CH domain, and a putative MT-binding GAR domain, suggesting it may localise to both MT and actin cytoskeletons. In order to establish where the full-length protein localises, fluorescent proteins will be conjugated to GAS2-like 3, and expressed in cells.

The roles of each domain in the potential localisation and binding to the cytoskeletons will be characterised by generating a series of truncation mutants. The localisation and binding to the cytoskeletons of the mutants will be

determined using both immunofluorescence and biochemistry-based approaches, respectively. This will provide insight into the function of the domains of GAS2-like 3, and whether they are able to recruit GAS2-like 3 to different places in the cell where it may exert its various functions.

To gain estimates of the binding strength of the various domains of GAS2-like 3 involved in linking GAS2-like 3 to the cytoskeleton or to other structures, live-cell imaging combined with Fluorescence Recovery After Photobleaching (FRAP) will be used. This will provide new information on the dynamics of GAS2-like 3 in live cells and will be used to confirm the fixed-cell imaging and biochemical sedimentation assays.

1.4.3) Identifying potential regulatory mechanisms which affect GAS2-like 3 localisation

Various post-translational modifications of tubulin are known to change MT dynamics, MT stability and the ability of MTs to recruit other proteins (Westermann and Weber, 2003). For example, acetylated and detyrosinated MTs are able to recruit MT-interacting proteins, such as the motor protein kinesin-1 and the MT-end binding protein, CLIP-170, respectively (Dompierre et al., 2007; Mishima et al., 2007). The question I aim to address is whether certain modifications of tubulin affect GAS2-like 3 localisation, and thus function.

Given the potential for GAS2-like 3 to interact with MTs, various drugs will be used to assess whether modifying the stability of MTs or whether post-translational modifications of tubulin affect GAS2-like 3 localisation.

1.4.4) Categorising the preliminary binding partners of GAS2-like 3

Insights into GAS2-like 3 function may be gained by identifying potential binding partners.

Preliminary sequence analysis has revealed that GAS2-like 3 contains two putative EB1-binding MtLSs at its C-terminus. There is also evidence to suggest that related sequences are used by EB1 to bind spectraplakins (Applewhite et al., 2010; Honnappa et al., 2009; Wu et al., 2008). In order to establish whether GAS2-like 3 interacts with EB1 *in vitro,* a combination of biochemical assays will be performed. Following which, full-length GAS2-like 3 and its C-terminus will be co-expressed with EB1 to determine whether their localisation is effected. If EB1

does bind GAS2-like 3 *in vitro* and affects GAS2-like 3 localisation in cells, a series of mutants of the GAS2-like 3 C-terminus will be created to dissect the key residues necessary for this interaction. By elucidating the key residues for GAS2-like 3 to bind to EB1, it may enable the prediction of fellow EB1 binding proteins in the GAS2 family and provide insight into the molecular mechanism underlying their function.

1.4.6) Functional characterisation of GAS2-like 3

As mentioned previously in this chapter, GAS2 has been implicated in apoptosis and growth arrest (Benetti et al., 2005; Benetti et al., 2001; Brancolini et al., 1995; Lee et al., 1999). There is a lack of knowledge as to how GAS2 induces apoptosis, and whether it can link to the key apoptotic machinery. There is little evidence to suggest the GAS2-like members of the GAS2 family play any role in apoptosis (Goriounov et al., 2003). Thus, it is unclear as to whether the GAS2 family plays a role in apoptosis. One of the main aims of this study is to characterise the function of GAS2-like 3 and increase the understanding of the GAS2 family.

By taking into consideration that GAS2-like 3 shares the highest degree of amino acid identity to GAS2, it is likely to play a similar, albeit separate function. Using immunofluorescence, the role of GAS2-like 3 will be assessed in cells by investigating whether it can instigate apoptosis. If GAS2-like 3 expression results in apoptosis, its localisation in cells will be further probed to investigate if there is evidence of localisation to mitochondria, which host the apoptotic machinery (Karbowski and Youle, 2003; Taylor et al., 2008).

The GAS2 family is related to the spectraplakins, which are implicated in diseases such as neurodegeneration and cancer (Giorda et al., 2004; Leung et al., 2002; Sjoblom et al., 2006; Sonnenberg and Liem, 2007). However, the precise cellular role of spectraplakins in these diseases is unclear. Neurodegeneration is often one of the consequences of defects in proteins that mediate mitochondrial dynamics (Lin and Beal, 2006), thus GAS2-like 3 is a potential candidate that links apoptosis and mitochondrial dynamics to cancer and neurodegeneration, respectively.

2) Materials and Methods

2.1) Materials

See Appendix 2

2.1.1) Vector Maps

See Appendix 3

2.1.2) Bacterial Strains

JM109 and JM109 (DE3) cells purchased from Novagen, UK.

BL21 CodonPlus (DE3) cells were purchased from Stratagene, UK

2.2) Methods

2.2.1) Cell Culture

All mammalian cells were grown in DMEM (Sigma Aldrich, Dorset, UK) supplemented with 10% FBS, 1% penicillin/ streptomycin, and 1% glutamine in a 5% CO2 in a humidified incubator, and passaged in a 1:10 dilution every 3 days.

2.2.2) Transfections

For transfections, cells were plated in 6-well dishes (for immunofluorescence) or 10cm petri dishes (for large scale) a day before transfections. For small and large-scale transient transfections, 1-1.5µg or 8µg of DNA respectively, was transfected into cells using Lipofectamine Plus (Invitrogen, Paisley, UK) in accordance with manufacturer's instructions. For immunofluorescence, cells were replated after 3-4 hours in glass-bottomed dishes (MatTek Corporation, Ashland, USA) coated with 10 µg/mL bovine fibronectin (pFN; Sigma). For drug treatment, cells were incubated for 30 mins with either nocodazole (10µM), cytochalasin D (2µM), trichostatin A (5µM), or paclitaxel (taxol, 10µM) (all from Sigma). For pulldown experiments, cells were washed thrice in PBS, and once in complete DMEM (as above), and left overnight before lysis the following day.

2.2.3) Fixed immunofluorescence Imaging

Cells were fixed and permeabilised with 3% paraformaldehyde (Sigma) containing 0.25% Triton X-100 (Sigma) and 0.05% glutaraldehyde (Sigma) for 15 mins, before being washed in PBS (Lonza, Verviers, Belgium). Autofluorescence from reactive amine groups was quenched using 0.01% sodium tetrahydroborate

(Sigma) in PBS for 15 mins before being washed in PBS. Subsequently cells were incubated for 45 mins with anti-α tubulin (DM1A) or anti-acetylated tubulin (6-11B-1) antibody, both at 1:500 dilution (both from Sigma), followed by three washes with PBS. Secondary antibodies conjugated to either Cy2, 3 or 5 (Jackson ImmunoResearch Laboratories, Suffolk, UK) were then applied for 30 mins. In the case of colabelling for actin, Texas Red or FITC-labelled phalloidin (Invitrogen) was added together with the secondary antibody). Cells were then washed three times in PBS before being imaged using an oil-immersed 100X objective, with 1.35 numerical aperture on an inverted microscope (IX71; Olympus) controlled by a Deltavision system (Applied Precision, Washington, USA). Images were captured using a Coolsnap HQ CCD camera (Princeton Instruments, Lurgan, UK).

2.2.4) Live-cell Imaging

Cells were washed thrice in PBS, and DMEM was replaced with pre-warmed Ham's F12 medium supplemented with 25mM HEPES, 1% L-glutamine, 1% penicillin/ streptomycin and the pH was adjusted to 7.3 with NaOH. Ham's F12 is preferred to DMEM for live imaging as it contains a very low amount of riboflavin, which exhibits a high autofluorescence in the excitation range of 450-490 nm and emssion range of 500-560 nm. Cells were placed in a pre-warmed microscope chamber at least an hour prior to the experiment and then imaged using an oil-immersed 100X objective, with 1.35 numerical aperture (NA) on an inverted microscope (IX71; Olympus) controlled by a Deltavision system (Applied Precision, Washington, USA). Movies were captured using a Coolsnap HQ CCD camera (Princeton Instruments, Lurgan, UK). For longer-term and real-time drug treatments, cells were imaged using an oil-immersed 100X objective, with 1.49 NA on an inverted microscope (Nikon TE2000E) with laser-based perfect focus system. Movies were captured using a Roper Cascade II EM CCD camera (Photometrics, AZ, USA), controlled by MetaMorph image acquisition software (Molecular Devices, PA, USA). For drug treatments, cells were incubated with 2μm cytochalasin D or 10μm nocodazole for 10 minutes, followed by washout using three washes in pre-warmed Ham's F12 media.

Antibody	Generated In	Directed Against	IF	WB	SPBA
DM1A (Sigma)	Mouse	α tubulin	1:500	1:5000	-
FITC-conjugated DM1A (Sigma)	Mouse	α tubulin	1:500	-	-
6-11B-1 (Sigma)	Mouse	Acetylated tubulin	1:500	-	-
GST (GE Healthcare)	Mouse	Glutathione-S Transferase	-	1:200	1:200
GFP (Roche)	Mouse	Green Fluorescent Protein	-	1:1000	-
Cy2, Cy3, Cy5 conjugated anti-mouse (Jackson Immunoresearch)	Goat	Mouse IgG	1:500	-	-
Cy2, Cy3, conjugated anti-rabbit (Jackson Immunoresearch)	Goat	Rabbit IgG	1:500	-	-
HRP-conjugated anti-mouse (Jackson Immunoresearch)	Goat	Mouse IgG	-	1:5000	1:5000
HRP-conjugated anti-rabbit (Jackson Immunoresearch)	Goat	Rabbit IgG	-	1:5000	-

Table 2.1: List of antibodies used for immunofluorescence (IF), Western Blotting (WB) and Solid Phase Binding Assays (SPBA).

Primary antibodies are in red, secondary antibodies are in blue.

2.2.5) Image Processing

Images were processed using ImageJ version 1.38X. For colocalisation studies and calculation of the ratio of G2L3 (or variation) / MTs, images were background subtracted using a 2D-bandpass filter, and overlay images were created. From these a threshold was set to restrict analyses to MTs, and the outline of the cell was drawn followed by measuring the percentage area of positive pixels (see Figure 2.1). This was repeated for full-length G2L3, its C-terminus, and for G2L3 after drug treatment and divided by the value given for MTs to give a ratio theoretically between zero and one. Adobe Photoshop CS4™ was used in the preparation of figures for this manuscript.

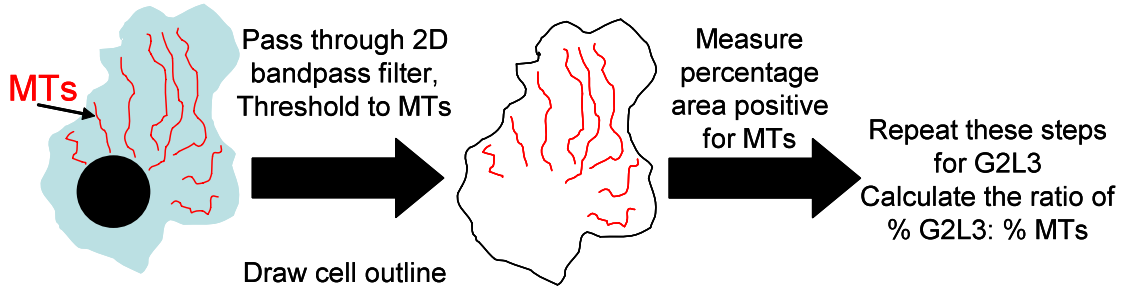

Figure 2.1: Image processing applied to cells.

Initially, images were taken and were background subtracted using a 2D bandpass filter. A threshold was set to restrict analysis to MTs, and an outline drawn around the cell. Following which, the percentage area of positive pixels were taken and the ratio of % G2L3: % MTs was calculated.

2.2.6) Statistical methods

Using the ratios obtained from the image processing, a Student's t-test was performed using Microsoft Excel to compare the ratios of GAS2-like 3 expressing control cells, taxol treated GAS2-like 3 expressing cells, and EB1 with GAS2-like 3 coexpressing cells. Student's t-test was also performed before and after drug treatments to determine if there was a significant shift of localisation.

It was also used to compare the % area of MTs for each condition.

2.2.7) Glutathione S-Transferase pull-down assay from cell lysates

Following overnight expression in 100mm petri dishes, COS cells were washed with PBS and trypsinised. They were subsequently centrifuged and lysed in 500µL ice cold lysis buffer (1% NP40, 50mM Tris pH7.4, 120mM NaCl, 2.5mM EGTA pH 7.4, 10mM MgCl, supplemented with 2X protease inhibitor cocktail solution). Lysates were passed 10X through a 27G needle, and centrifuged in a precooled centrifuge at 4°C for 15mins at 800g in order to remove the insoluble fraction. An aliquot of the supernatant was taken and placed in SDS-loading buffer as the total cell lysate, the remaining supernatant was precleared with Glutathione-coated Sepharose beads (GE Healthcare) for one hour at 4°C, followed by centrifugation at 2000g and aspiration of the supernatant. During preclearing, washed Glutathione-coated Sepharose beads were incubated with either Glutathione S-Transferase (GST) conjugated-EB1 or GST alone (control) in order to attach the bait protein to the bead. After preclearing, the EB1-GST or GST coated beads were washed thrice in PBS containing 0.01% Tween 20

(PBS-T), and were resuspended in the precleared lysate, and rotated for an hour at 4°C. The samples were centrifuged at 2000g, and an aliquot of the unbound fraction was taken. The beads were subsequently washed 4 times in PBS-T and the bound proteins were eluted from the beads in 2X SDS-loading buffer at 100°C for 10 mins. The individual fractions were then separated by SDS-PAGE and analysed by immunoblotting, using an anti-GFP antibody (See Table 2.1)

2.2.8) Glutathione S-Transferase pull-down assay using recombinant proteins

The C-terminus of G2L3 was incubated in a 1.5X molar excess with human EB1-GST for an hour at 4ºC in PBS containing 40mM EDTA. Before resuspending the beads, a fraction of the incubation mixture was taken for the prebound fraction. An excess of Glutathione-coated Sepharose beads (GE Healthcare) were washed five times in PBS before being resuspended with PBS containing EB1-GST, C-terminus or their respective combination. These were incubated on a rotator for an hour at 4ºC, after which an unbound fraction was taken. The beads were washed five times in PBS, with aliquots of supernatant aspirated after each wash (wash fractions). After the final wash, an aliquot of beads (resin fraction) was taken and boiled in 2X SDS-loading buffer for 10 mins along with the previously collected fractions. These were then analysed on a 15% SDS-PAGE gel.

2.2.9) Solid Phase Binding Assay

Wells of Costar high binding microtitre plates (Corning Costar, UK) were coated with 100µL aliquots of purified Thioredoxin-6X-His Tag- C-terminus G2L3 at 10µg/mL diluted in PBS overnight at 4ºC. Wells were blocked for 2-3 hours at room temperature with 200µL of blocking buffer [5% BSA (w/v) in PBS], followed by 3 washes with 200 µL washing buffer [0.1% BSA (w/v) in PBS]. Wells were incubated at the indicated concentrations of EB1-GST or GST (control) in a total of 100µL wash buffer for 2-3hrs, 37 ºC and washed 3X with 200 µL washing buffer. Mouse-α-GST antibodies (500ng/mL) were added to wells in 50µL wash buffer for 1 hour at 37 ºC followed by 3 further washes using 200 µL washing buffer. GST-binding proteins were detected using horseradish peroxidase (HRP)-conjugated anti-mouse antibody diluted 1:5000 in wash buffer incubated for 30mins at 37 ºC. Wells were washed 4 times with 200µL before the addition of 100µL ABTS substrate [0.55mg/mL 2,2'-azino-bis(3-ethylbenzthiazoline-6-

sulfonic acid), 0.0026% (v/v) H_2O_2 , 0.1M sodium acetate and 50mM NaH_2PO_4, pH5.0] at room temperature. Absorbance readings at 405nm were measured using a Powerwave 340 multiscan plate reader (Biotek, USA). Each experimental condition was assayed in at least three replicate wells and background attachment to BSA-blocked wells subtracted from all measurements. Means and standard error of the means were calculated for each experimental condition using Microsoft Excel 2003 (Microsoft, USA).

2.2.10) Molecular Biology Methods

2.2.10.1) Polymerase chain reaction (PCR)

2.2.10.1a) **cDNA panels**

To identify expression levels in tissues, a “master mix” containing forward and reverse primers, dNTPs, reaction buffer and Taq polymerase was made for Clontech cDNA panels as indicated in Table 2.2. PCR primers were designed to span exons 2-6 of GAS2-like 3, to avoid amplifying genomic DNA. A “master mix” was also made to identify expression in the following cell lines: HeLa, Human Foreskin Fibroblast (HFFs), HT1080, Human Embryonic Kidney 293T and murine NIH 3T3. The total reaction volume for each reaction was 25µL, they were incubated at 94ºC for 1 minute, followed by 35 cycles of 30 seconds at 94 ºC (denaturation), 30 seconds at 55 ºC (annealing) and 60 seconds at 72 ºC (extension). The reaction products were subsequently run on a 1% agarose (w/v) gel for an hour at 120V.

2.2.10.1b) **Sub-cloning**

G2L3 truncation products were produced as indicated in Figure 2.2, using the primers listed in Table 2.3. All reaction mixtures were made up to 50µL with ddH_2O, except from the production of the G2L3-ΔGAR construct, which was made up to 100µL. They were incubated at 94ºC for 1 minute, followed by 35 cycles of 30 seconds at 94 ºC (denaturation), 30 seconds at 50 ºC (annealing) and 2 minutes at 72 ºC (extension). The reaction products were subsequently run on a 1% agarose gel containing 0.005% (v/v) ethidium bromide (Sigma, Poole, UK), excised and purified using a QIAquick Gel Extraction kit (Qiagen, Crawley, UK).

"Master mix" Component	Volumes for Clontech Panel (µL)	Cell line cDNA library (µL)
cDNA	3	5
10X PCR buffer	28	44
dNTPs (2.5mM)	28	35
5' primer (10pmol/µL) 5' CACGGACCAGGATTGGCTAATG 3'	9	5
3' primer (10pmol/µL) 5' TGTAGCTCTTCATGCCGACAGC 3'	9	5
ddH_2O	180	330
Taq polymerase	1	1

Table 2.2: Showing the reaction volumes used to screen cDNA panels or cDNA libraries from different cell lines.

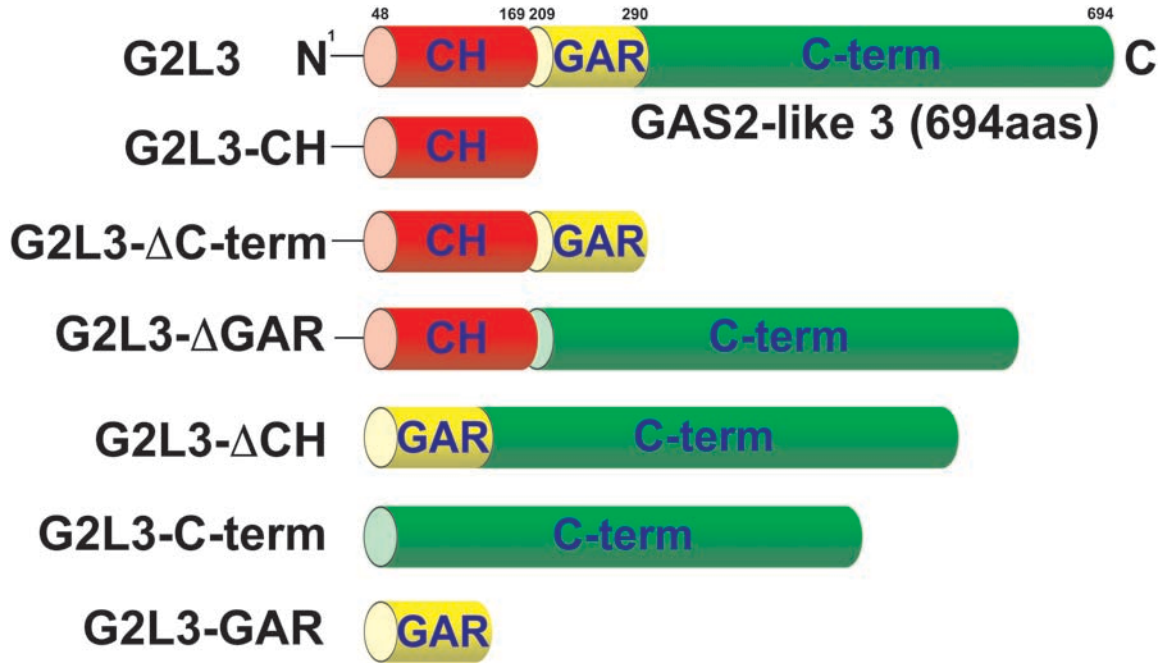

Figure 2.2: Showing the various constructs used for this study.

The truncations were cloned into eGFP-N1, mCherry-N1 or eGFP-C1 vectors for immunofluorescence. For recombinant expression, G2L3-CH and G2L3-C-term were cloned into pHisTrx and G2L3-GAR was cloned into pHisNusA.

Reaction Product	Primers Used	Template	dNTPs (uL)	PCR buffer (uL)	Taq
G2L3-ΔCH for eGFP-N1 or mCherry-N1	**Forward**: 5' CTGGTCGCTAGCATG**GGGCCTGAAGATTCCATCAG** -3' **(586-606bp)** **Reverse**: 5'-CTGGTCAAGCTT**TTTTCTAGGTTTCTTACTTCCAG** -3' **(2061-2094bp)**	300ng mCherryN1-G2L3	4	5	2.5 U
G2L3-ΔC-term for eGFP-N1 or mCherry-N1	**Forward**: 5'-CTGGTCGCTAGCATG**CAGCCTGCAATTCAAGTATG** -3' **(1-26bp)** **Reverse**: 5'-CTGGTCAAGCTT**TCGACAGGGGTCATATTTAAGC** -3' **(821-843bp)**	300ng mCherryN1-G2L3	4	5	2.5 U
G2L3-C-term for eGFP-N1 or mCherry-N1	**Forward**: 5'-CTGGTCGCTAGCATG**CGAATATTACAGTTTGCCACAC** -3' **(841-863bp)** **Reverse**: 5'-CTGGTCAAGCTT**TTTTCTAGGTTTCTTACTTCCAG** -3' **(2061-2094bp)**	300ng mCherryN1-G2L3	4	5	2.5 U
G2L3-CH for eGFP-N1 or mCherry-N1	**Forward**: 5'-CTGGTCGCTAGCATG**CAGCCTGCAATTCAAGTATG** -3' **(1-26bp)** **Reverse**: 5'-CTGGTCAAGCTT**TTTTCTAGGTTTCTTACTTCCAG** -3' **(565-588bp)**	300ng mCherryN1-G2L3	4	5	2.5U
G2L3-GAR for eGFP-N1 or mCherry-N1	**Forward**: 5'-CTGGTCGCTAGCATG**GAGCTACATGAAGCTGTTAAAC** -3' **(634-656bp)** **Reverse**: 5'-CTGGTCAAGCTT**TCGACAGGGGTCATATTTAAGC** -3' **(821-843bp)**	300ng mCherryN1-G2L3	4	5	2.5U

G2L3-ΔGAR for eGFP-N1 or mCherry-N1	**Forward**: 5'-CTGGTCGCTAGCATG**CAGCCTGCAATTCAAGTATG** -3' **(1-26bp)** **+** 5'-**GCTGTCGGCATGAACGAATATTACAGTTTGCCACAC** -3' **(597-633bp)** **Reverse**: 5'-CTGGTCAAGCTT**TTTTCTAGGTTTCTTACTTCCAG** -3' **(2061-2094bp) +** 5'- **CTGTAATATTCGTTCATGCCGACAGCATGATTTTG** -3' **(841-860bp)**	300ng mCherryN1-G2L3	8	10	2.5U
G2L3-CH for pHisTrx	**Forward:** 5' CTGGTCGGATCCATG**CAGCCTGCAATTCAAGTATG** -3' **(1-26bp)** **Reverse**: 5'-CTGGTCGAATTC**TTTTCTAGGTTTCTTACTTCCAG** -3' **(565-588bp)**	300ng mCherryN1-G2L3	4	5	2.5U
G2L3-GAR for pHisNusA and for pEGFP-C1	**Forward:** 5' CTGGTCGAATTC**GAGCTACATGAAGCTGTTAAAC** -3' **Reverse:** 5' CTGGTCGGATCC**TCGACAGGGGTCATATTTAAGC** -3'	300ng mCherryN1-G2L3	4	5	2.5U

G2L3-C-term for pHisTrx	**Forward:** 5’ CTGGTCGGATCC**CGAATA TTACAGTTTGCCACAC** -3’ **(841-863bp)** **Reverse:** 5’- CTGGTCGGATCC**TTTTCT AGGTTTCTTACTTCCAG** -3’ **(2061-2094bp)**	300ng mCherryN1-G2L3	4	5	2.5U
G2L3 for pEGFP-C1	**Forward**: 5’ CTCGTCTCCGGA**ATGCAGCCT GCAATTCAAGTATG** -3’ **Reverse**: 5’ CTCGTCGGATCC**TTATTTTCTA GGTTTCTTACTTCC** -3’	300ng mCherryN1-G2L3	4	5	2.5U
G2L3-C-term for pEGFP-C1	**Forward**: 5’ CTCGTCGGATCC**CGAATATTA CAGTTTGCCACAC** -3’ **Reverse**: 5’ CTCGTCGGATCCTTA**TTTTCTA GGTTTCTTACTTCCAG** -3’	300ng mCherryN1-G2L3	4	5	2.5U
G2L3-myc-GAR for pEGFP-C1	**Forward**: 5’ CTGGTCGAATTCATGGAGCAG AAACTCATCTCTGAAGAGGAT CTG **CGGCATGAAGAGCTACATGA AG**-3’ **Reverse**: 5’ CTGGTCTTATTAGCGGCCGC**T TGTTCTAGTGTGGCAAACTG**-3’	300ng mCherryN1-G2L3	4	5	2.5U
G2L3-CT1 for pEGFP-C1	**Forward**: 5’ CTCGTCTCCGGA**CGAATATTA CAGTTTGCCACAC** -3’ **Reverse**: 5’ CTCGTCGGATCCTTA**AGCTAA GTGAGATACTGCATTATC** -3’	300ng mCherryN1-G2L3	4	5	2.5U

G2L3-CT2 for pEGFP-C1	**Forward**: 5' CTCGTCTCCGGA**GCACATTCA AATTCATCCTCAAAA** -3' **Reverse**: 5' CTCGTCGGATCCTTA**TTTTCTA GGTTTCTTACTTCCAG** -3'	300ng mCherryN1-G2L3	4	5	2.5U
Primers to screen cDNA libraries	Forward: 5' **CACGGACCAGGATTGGCTAA TG** -3' Reverse: 5' **TGTAGCTCTTCATGCCGACAG C** -3'	cDNA libraries	2	2.5	1.25 U

Table 2.3: Primers used in PCRs for this study.

Blue= ATG start codon. Red = Incorporated restriction enzyme sites. Bold = DNA sequence corresponding to the published human G2L3 sequence. Green = Overlapping regions to produce ΔGAR construct. Brackets = Corresponding DNA base pair region of human G2L3 chain fragments.

Construct	Restriction endonucleases used
G2L3-CH, G2L3-ΔCH, G2L3-GAR, G2L3-ΔGAR, G2L3-C-term, G2L3-ΔC-term in pEGFP-N1 or pmCherry-N1	NheI and HindIII
G2L3-CH in pHisTrx	BamHI and EcoRI
G2L3-C-term in pHisTrx	BamHI
G2L3-GAR in pHisNusA	BamHI and EcoRI
G2L3 in pEGFP-C1	BspE1 and BamHI
G2L3-C-term in pEGFP-C1	BamHI
G2L3-myc-GAR in pEGFP-N1	BamHI and NotI
G2L3-CT1 and CT2 in pEGFP-C1	BspEI and BamHI

Table 2.4: List of restriction endonucleases used to prepare the G2L3 constructs.

2.2.10.2) Restriction Endonuclease Digestion, Cloning and Ligations

The pEGFP-N1, pmCherry-N1, and pEGFP-C1 vectors (Clontech) and pHisTrx and pHisNusA vectors as well as the reaction products designed for these vectors were restricted at 37ºC for 3 hours using the restriction enzymes listed in Table 2.4. They were subsequently run on a 1% agarose gel containing 0.005% (v/v) ethidium bromide, excised and purified using a QIAquick Gel Extraction kit.

For ligations, a 4:1 molar ratio of insert : plasmid, together with 2 µL 5X Ligate IT buffer (USB), 0.5 µL T4 DNA ligase (Roche) and ddH_2O were used to make up the reaction mixture to 10 µL. The ligation mixture was incubated at room temperature for 15 minutes, followed by a 1 hour incubation on ice with the E. coli strain JM109. After which cells were heat shocked at 42ºC for 45s (kanamycin vector) or 90s (ampicillin vector) and immediately cooled on ice for 2min, before being grown in 400µL LB broth [0.17M NaCl, 0.8% (w/v) tryptone, 1% (w/v) yeast extract] for an hour at 37ºC. They were subsequently plated and grown on LB agar plates containing 40 µg/mL kanamycin for eGFP-N1 and mCherry-N1 vectors or 50 µg/mL ampicillin for pHisTrx.

Three colonies were picked from each plate and then incubated overnight at 37ºC in 5mL LB media containing either 30 µg/mL kanamycin or 50 µg/mL ampicillin depending on the resistance conferred by the vector.

The insert sequences of each construct were confirmed by DNA sequencing with an ABI 377 automated sequencer (PE Applied Biosystems).

2.2.10.3) cDNA synthesis from Cell Lines

cDNA libraries were synthesised from various cell lines using the ‘Absolutely RNA Microprep Kit’ followed by the Stratascript QPCR cDNA Synthesis Kit (Stratagene, Stockport, UK). Briefly, cell pellets from 10cm petri dishes were snap frozen in liquid nitrogen. They were subsequently thawed and resuspended in lysis buffer (Absolutely RNA Microprep Kit, Stratagene), containing a strong protein denaturant guanidium thiocyanate to prevent ribonuclease degradation of the RNA. The lysate was treated with DNase I to degrade DNA, washed to remove contaminants and eluted into 30µL. 7µL of this eluate containing RNA, was added to 10 µL cDNA synthesis master mix (2X), with either 2 µL of random or oligo (dT) primers and 1 µL of StrataScript RT-RNase Block enzyme mixture. This was incubated at 25ºC for 5 minutes (annealing), followed by 42 ºC for 90

minutes (cDNA synthesis) and 95 ºC for 5 minutes to terminate the cDNA synthesis reaction.

2.2.11) Protein expression, purification and analysis

2.2.11.1) Protein Expression

300ng of DNA for each construct was used to transform the E. coli strain JM109 (DE3) using the same protocol as for the JM109 strain. Colonies were picked and grown over the day in 5ml LB containing 100µg/mL ampicillin. The cultures were then transferred to 500mL conical flasks containing 495mL auto-induction media (as prepared in (Studier, 2005), and incubated overnight at 37 ºC, with shaking at 225rpm.

2.2.11.2) Sonication and Metal Chelation Chromatography

Cells were spun down and pellets resuspended in 30mL 1X binding [40mM Imidazole (Sigma), 4M NaCl, 160mM Tris, pH7.9] and sonicated 6 times for 30 seconds at 20% amplitude. Cellular debris was pelleted by centrifugation at 18,000rpm for 20 minutes at 4ºC, and the crude cell lysate was retained on ice. A further 20mL 1X binding buffer was added to the pellet, sonicated and centrifuged as described above. The resulting supernatant was pooled with the original lysate. The protein was purified by exploiting the N-terminal 6X histidine tag, using a Chelating Sepharose Fast-Flow Column (GE Healthcare, Bucks, UK) charged with nickel ions, according to the manufacturer's protocol. All fractions were collected, with the protein content of each fraction analysed on a 15% SDS-PAGE gel. The cleanest collection fraction was dialysed at least twice into thrombin cleavage buffer (20mM TRIS, 150mM NaCl, 2M urea, pH 8.4) in preparation for thrombin cleavage.

2.2.11.3) Removal of 6x His tag

For test digestions, reaction mixtures were made up to 100µL with 0.1U thrombin (high activity thrombin from human plasma (Calbiochem, Beeston, UK) and 2.5mM $CaCl_2$. 20 µL aliquots were removed during the time course, and analysed using a 15% SDS-PAGE gel. From this, the optimal digestion conditions were determined and scaled up to digest the remainder of the eluates.

The digested protein was loaded onto the Chelating Sepharose Fast-Flow Column (GE Healthcare) purified as described earlier. Each fraction was collected and analysed using a Tricine-SDS-PAGE gel. Appropriate fractions that contained the digested target protein were pooled and dialysed into PBS.
Determination of protein concentration was achieved by analysis of tryptophan and tyrosine residues at 280nm.

2.2.11.4) SDS-Polyacrylamide (SDS-PAGE) gels

Samples were boiled at 95ºC in 2X SDS sample buffer (30% glycerol, 4% SDS, 0.125M Tris, 5% β mercaptoethanol, dH_2O, bromophenol blue at pH 6.8) and separated on 15% SDS-PAGE gels, run at 150V for 80 minutes. Gels were stained using either Instant Blue (Novexin, Cambridge, UK) or stained with Coomassie stain (0.25% Coomassie BB, 7.5% CH_3COOH, 50% methanol), and destained with destaining solution (45% methanol, 50% dH_2O, 5% CH_3COOH). Images were captured using an HP Scanjet 4600, with HP Photo and Imaging Gallery Version 1.1 (HP, Bracknell, UK).

2.2.11.5) Immunoblotting

Following SDS-PAGE, gels were transferred to PVDF membrane by creating a sandwich comprising of Whatman Paper, SDS-PAGE Gel, and PVDF membrane, which had been presoaked in methanol. The transfer was performed in Transfer Buffer (10mM Sodium Tetraborate) for 1hr at 250mA, followed by blocking in PBS-T supplemented with 5% Milk Powder (Marvel, London, UK) for an hour at room temperature or overnight at 4°C, to minimise cross-reactivity of primary antibodies. Primary antibodies were either incubated with membranes for an hour at room temperature or overnight at 4°C in PBS-T containing 2% milk. The membrane was washed thrice in PBS-T to remove unbound primary antibody and incubated with the appropriate HRP-conjugated secondary antibody (Jackson Laboratories) for 30mins at room temperature. The membrane was washed again 3X and incubated with ECL reagent (Cheshire Sciences, Cheshire, UK). The membrane was then exposed to Kodak MR photographic film (Sigma).

2.2.11.6) Tricine-SDS-PAGE gels

Samples were prepared as for SDS-PAGE gels. The gel contained a 1-70kDa separating gel (16.5% T/ 3%C), spacer gel (10% T / 3% C) and stacking gel (4% T / 3% C), and was run at 15mA overnight.

3) Results Chapter 1

Fluorescence Recovery After Photobleaching

Matthew Stroud, Alex Carisey, Ricky Tsang and Christoph Ballestrem

Wellcome Trust Centre for Cell-Matrix Research, Faculty of Life Sciences, University of Manchester, M13 9PT. UK

Correspondence should be addressed to Christoph Ballestrem
Wellcome Trust Centre for Cell Matrix Research
Faculty of Life Sciences, University of Manchester
Michael Smith Building, Oxford Road
Manchester, M13 9PT, United Kingdom
Phone: +44 (0) 161-275-1708
Fax: +44 (0) 161-275-1505
Email: christoph.ballestrem@manchester.ac.uk

Summary

This chapter describes the use of microscope-based Fluorescence Recovery After Photobleaching. To qualify the dynamics of proteins within a subcellular compartment, we first outline the general aspects of FRAP experiments and then provide a detailed protocol of how to measure and analyse the most important parameters of FRAP experiments such as mobile fraction and half-time of recovery.

Keywords

Fluorescence Recovery After Photobleaching; fluorescence microscopy; green fluorescent protein; half-time of recovery; mobile fraction; diffusion; binding reaction kinetics; focal adhesions.

1. Introduction

1.1. Principles of FRAP

Fluorescence Recovery After Photobleaching (FRAP) is a powerful, microscopy based methodology for investigating molecular dynamics within living cells. Whereas traditional fluorescence microscopy yields information in a qualitative 'yes or no' manner as to the localisation of molecules in cells, FRAP allows us to elucidate the dynamics of the protein of interest. In order to perform FRAP, this protein of interest must be tagged to a fluorophore. Green fluorescent protein (GFP) is a well-characterised fusion tag widely used for protein labelling in live cells. It was originally discovered in the jellyfish, *Aequorea victoria*, and has been subsequently modified to produce brighter and more photostable variants (Tsien, 1998). In FRAP, fluorescent molecules that localise to a region of interest (ROI) are irreversibly bleached using a high power laser illumination (see Figure 1A). The fluorescence recovery over time within the ROI provides details about the dynamics of the protein of interest (Axelrod et al., 1976) (see Figures 1A and 1B). The rate of fluorescence recovery is governed by two major events (Sprague and McNally, 2005). The first is the diffusion of the fluorescently tagged protein within the localised environment, a fast process occurring over a few milliseconds. The second event is the binding between the fluorescently tagged

protein and potential binding partners within the ROI. Most proteins in a cell undergo continuous turnover within complexes allowing bleached fluorescent proteins to be replaced by newly recruited fluorescent proteins, thus leading to the recovery of fluorescence (see Figure 1A). Such recovery can be quantified by plotting the intensity of the fluorescence over time within the defined ROI, before, during and after the bleaching event (see Figure 1B). Further mathematical analysis including curve fitting then allows a detailed assessment of the behaviour of a fluorescently tagged protein within live cells.

This protocol will focus on FRAP as a method to assess the mobility of fluorescently labelled proteins within focal adhesions of a live cell (see Figure 1C). We describe here the acquisition of time-lapse images, the bleaching and recovery of fluorescence with an emphasis on the compulsory controls, and cover some aspects of data processing. A complete methodology detailing the processing of raw data from FRAP experiments is described in (Sprague et al., 2006; Sprague et al., 2004).

1.2. Readouts of FRAP experiments

Analysis of the FRAP experiments yields information about the mobility of the fluorescently tagged protein. Two main parameters can be readily assessed, namely the mobile fraction and the half time of recovery.

The mobile fraction (F_M) is the proportion of bleached proteins that are replaced by unbleached proteins during the monitoring of the recovery event. Thus, mobile fraction can be determined by calculating the ratio of fluorescence intensity between the end of the time-lapse recordings (F_∞) and the initial intensity before the bleaching event ($F_{initial}$) corrected by the experimental bleach value (F_0) (Axelrod et al., 1976) (see Figure 1B). This ratio results in values between 0 and 1, or when expressed as a percentage, between 0 % and 100 %. Due to binding reactions within the ROI, the theoretical value of 100 % of recovery is rarely achieved in practice. Therefore, the recovery reaches a plateau below this value by the end of the time-lapse (see Figure 1A). Moreover, unintentional bleaching and dynamics of the overall structure during recovery limit the length of the time lapse recording. In general, proteins that bind strongly to fixed components will have lower mobile fractions than those that interact

weakly. Proteins that can freely diffuse show a maximal mobile fraction of 100 % as they don't interact with any partner.

The second parameter, the half-time of recovery, is the time it takes for the fluorescence to reach half of its maximal recovery intensity (termed $t_{1/2}$) (see Figure 1B). The rate of the recovery depends on the size of the complexes and the stability of the interaction with large or fixed proteins (Lippincott-Schwartz et al., 2001). Under some circumstances, the recovery may exceed 100% of the initial fluorescence value. This observation indicates that the bleached structure undergoes a formation or growth phase during the timeframe of the experiment.

The precise determination of F_M and $t_{1/2}$ is only possible in biological systems that have reached equilibrium before photobleaching, so that the total amounts of both fluorescent protein and its binding sites remain constant over the course of the experiment. In this case, the only parameter changing after photobleaching is the equilibrium between the bleached and the unbleached molecules and the return to equilibrium provides the readout of the recovery curve. Finally, reliable measurements will only be obtained for proteins that are part of an immobile complex during the length of the monitored recovery.

1.3. Requirements of the fluorescent label

To study the dynamics of a protein in FRAP experiments, the protein of interest must be fused to a fluorophore suitable for expression and monitoring in live cells. To avoid artefacts this fluorophore should have the following characteristics:

1. It should be bright enough to obtain a high signal-to-noise ratio.
2. It should be photostable to prevent excessive bleaching during time-lapse recordings however, it should not resist bleaching with the high power laser.
3. It should not be prone to photoreversible bleaching, an event whereby a proportion of the fluorophore is able to revert back to its original fluorescent state (see Note 1). Such an event can be tested to a certain extent by performing FRAP on fixed cells (see section 3.2).
4. It should be monomeric to avoid any irrelevant association between the tagged proteins.

The monomeric enhanced GFP (mEGFP) is usually a good choice, since it has

all these properties, to a greater extent than the original GFP and many other GFP derivatives. In addition, most confocal microscopes will be equipped with an argon laser line at 488 nm, which enables high power photobleaching and low power monitoring. The use of dyes emitting in the red spectrum is not preferred, as bleaching is less efficient with these lasers (see Note 2).

Independently of the chosen tag, the fused protein should carry out the same function as the endogenous protein. It is therefore crucial to choose wisely where the fluorescent tag is placed in order to avoid artefactual readouts (see Note 3).

1.4. Use of the correct microscope

FRAP experiments can be carried out on both confocal and wide-field microscopes equipped with the necessary laser, but one should be aware of the strengths and weaknesses of the respective systems.

Because of their design, wide-field microscopes capture the light emitted by the fluorescent molecules within a thicker optical section of the sample. On one hand this allows the measurement of low fluorescent intensities that would otherwise be below the threshold for a confocal microscope. Such systems can be fitted with electron multiplying-charge-coupled device (EM-CCD) cameras that have a higher sensitivity, a larger dynamic range and a faster acquisition rate than most conventional confocal scanning heads. On the other hand, FRAP experiments should be performed on the assumption that the movement of fluorescently labelled proteins is restricted to a two-dimensional plane (Sprague et al., 2006; Sprague et al., 2004). To a certain extent, it is possible to overcome this problem on a wide-field system by the use of background subtraction methods. However, since confocal microscopes monitor a precise optical section of a defined thickness, in many cases this type of microscope can deliver more accurate results.

In our hands, results of FRAP experiments on adherent cells expressing vinculin-mEGFP (see Figure 1C) are not significantly different when performed on a Leica SP5 confocal microscope or on a DeltaVision QLM wide-field microscope using the integrated analysis software.

1.5. Validation of measurements and data fitting

When performing FRAP experiments on proteins expressed transiently, the variability of the expression levels of the fluorescent protein can lead to misinterpretation of the results. The level of expression dictates the proportion between the pool of proteins interacting with other molecules and the pool of freely diffusing proteins in the immediate environment. Thus, it is important to determine whether there is a dependence between the FRAP coefficients and the protein expression levels. FRAP coefficients over a wide range of expression levels must be calculated and plotted against the overall cell fluorescence intensity; the slope of the regression line through the data points should not be statistically different from 0, with 95 % confidence (see Section 3.3.3).

Correct data fitting is essential for the interpretation of the results. There are many software packages available but we recommend using MATLAB in order to process large amounts of data. MATLAB allows easy automation of the analysis by fitting the recovery curve and extracting the FRAP coefficients such as F_M and $t_{1/2}$.

The fitting parameters depend on several factors, which have been outlined in great detail in (Sprague et al., 2004). Two major processes can influence the kinetics of the recovery: the diffusion of the fluorescent protein and the binding to its partners. Most of the FRAP protocols used by biologists assume that the binding reaction is dominant in their system, however this should be determined empirically on a protein-by-protein basis. To test whether the binding reaction is dominant, it is important to compare the different fluorescence recovery curves obtained by changing diameter of the region bleached by the FRAP laser. If the fluorescence recovery curves are similar and give the same rates of recovery independently of the diameter of the bleached spot, then diffusion is negligible.

This is referred to as a ‘reaction dominant model’ (Sprague et al., 2004) in which diffusion occurs a lot faster than the binding reaction. Therefore, the recovery of fluorescence is driven by the following binding equation:

$$F + S \underset{k_{off}}{\overset{k_{on}}{\rightleftharpoons}} FS$$

Where F represents free proteins, S represents unoccupied binding sites for the tagged protein and FS represents the bound complex. In this case of a single binding state, the predicted FRAP recovery curve is the inverse of an exponential

decay. The FRAP data can then be fitted with the following equation to obtain the off-rate constant of binding (k_{off}):

$$F(t) = 1 - A\, e^{-koff\, t}$$

The parameter A can be used to calculate the association rate (k_{on}), using:

$$A = k_{on} / (k_{on} + k_{off})$$

The mobile fraction is given directly by:

$$F_M = F_\infty - F_0 / F_{initial} - F_0$$

The half-time of recovery can be determined from the curve fitting equation with $F(t_{1/2})=(F_\infty - F_0) / 2$:

$$t_{1/2} = \ln 2 / k_{off}$$

2. Materials

2.1. Cell culture and transfection: equipment and reagents

1. Laminar flow, tissue culture cabinet.
2. Temperature-regulated, humidified incubator set at 37°C and 5 % CO_2 gas for the maintenance of mammalian cells.
3. Cell culture medium (Dulbecco's modified Eagle's medium, DMEM) supplemented with 10% foetal calf serum (FCS), glutamine, and antibiotics.
4. Trypsin–ethylene diamine tetraacetic acid (EDTA) dissociation solution.
5. Sterile phosphate-buffered saline (PBS^-) without Mg^{2+} and Ca^{2+}.
6. Cultured adherent cells (e.g. NIH 3T3 mouse fibroblasts) expressing the protein of interest as a fusion protein with mEGFP (see Note 4).
7. Flasks or Petri dishes treated for cell culture.
8. Six-well tissue culture plates.
9. Transfection kit suitable for the cell type used. We use Lipofectamine Plus reagent (Invitrogen Corporation).
10. mEGFP expression vectors (Clontech).

2.2. Microscope setup and reagents for imaging

The microscope setup described here is currently used in our laboratory; however, any laser scanning confocal microscope with an equivalent setup is suitable.

1. Leica TCS SP5 AOBS inverted laser scanning confocal microscope (Leica microsystems) (see Notes 5 and 6).
2. Leica HCX PL Apo 63x (lambda blue and NA iris corrected) objective (NA = 1.4) or another high numerical aperture oil immersion objective.
3. An argon 488 nm laser line (see Note 6).
4. Leica LAS AF software for image acquisition and FRAP procedure (supplied with the microscope) or another image acquisition software package.
5. Heated chamber enclosing the microscope stage (see Note 7).
6. Glass-bottom sterile culture containers (e.g., glass bottom dishes from MatTek or CellView from Greiner BioOne) for live imaging of cells (see Note 8).
7. Fibronectin from bovine plasma (see Note 9).
8. Ham's F12 medium supplemented with a final concentration of 25 mM HEPES and pH adjusted to 7.3 using a 1 M NaOH solution. After sterile filtration, supplement with glutamine and antibiotics (see Notes 7 and 10).
9. 4% paraformaldehyde (PFA) solution in PBS (w/v) (see Note 11)

2.3. Software for analysis

1. Software to extract the fluorescence measurements from the time-lapse images generated by the microscope system. Many software suites controlling microscopes are more or less suitable to perform the complete analysis through simplified wizards (e.g. Leica LAS AF software from Leica Microsystems, softWoRx Suite from Applied Precision). For a better controlled and a more accurate analysis, we prefer to use an open-source image-processing program such as ImageJ (NIH, freely available at http://rsbweb.nih.gov/ij/).
2. Software to perform the data analysis. Any basic spreadsheet software is suitable, however, we recommend the use of a more advanced software package such as MATLAB (The MathWorks), enabling rapid automation in the analysis of large datasets (see Note 12).

3. Methods

3.1. Transfection and preparation of cells

This protocol is based on conditions optimised for our measurements of FRAP coefficients of focal adhesion plaque and cytoskeleton associated proteins.

1. Prepare the mEGFP fusion proteins using standard molecular biology techniques.
2. Transfect cells with either the construct encoding the fusion protein in a 6 well plate using Lipofectamine Plus reagent according to the manufacturer's instructions (see Note 2).
3. Coat the glass-bottom dishes for 1 h at room temperature with 10 µg/mL of fibronectin (see Note 10).
4. After 4 hours of incubation, wash the cells twice with sterile PBS^-.
5. Trypsinise the cells and wash them twice in DMEM supplemented with FCS and plate $5x10^4$ cells per 35-mm glass bottom dish (see Note 9).
6. Incubate the cells for 12 to 48 hours in an incubator until the expression of the transfected plasmid reaches its maximum (see Note 13).
7. Replace the DMEM with pre-warmed Ham's F12 medium (see Note 11).
8. Place the dish in the pre-warmed microscope chamber at least 1 hour prior to the FRAP experiment to allow the medium to equilibrate (see Notes 8 and 14).

3.2. Data acquisition

3.2.1. Protocol

Three separate phases of the experiment can be distinguished. Firstly, the ROI must be defined and the fluorescence intensity of the GFP fusion protein within this ROI monitored using low-power laser settings. Secondly, a high intensity laser pulse is emitted to irradiate the ROI and eliminate the fluorescence within this region. Thirdly, immediately after bleaching, the sample is monitored using the same low-intensity imaging settings as before the bleach. Images are collected at regular time intervals until the intensity in the bleached ROI reaches a plateau (see Note 15). To facilitate the acquisition of in-focus images over a long time period, the microscope can be fitted with a real-time autofocusing

system (see Note 16).

1. Select cells expressing a reasonable level of fluorescent protein in the appropriate cellular compartment using the eyepiece of the microscope (see Note 5).
2. Set the parameters following the guidelines provided for monitoring the fluorescence. The individual parameters must be adjusted empirically to obtain high quality data while achieving three objectives: [1] obtaining an almost complete bleach in the specified ROI, [2] monitoring over a sufficient period of time until the fluorescence recovery becomes stable, and [3] keeping the photobleaching and phototoxicity to a minimum (see Note 17). Additionally, the intensity measured must always be confined to the dynamic range of the scan head (see Note 18).
The settings we use on the confocal microscope are:

- Confocal scan head settings: scan rate of 400 Hz for an intermediate size image of 512x512 pixels, using bi-directional scanning (see Note 19).
- Laser power of the 488 nm argon laser line is set to 20 % and the transmission of the AOBS to 20 % during the monitoring. For the bleaching pulse, the AOBS setting is increased to 100 % (see Note 6).
- Pinhole setting: 1 Airy Unit (see Note 20).
- Zoom factor: set between 1.6 and 2 to fit the ROI for the bleaching event only.
- Gain adjustment: 900 V (see Note 21).
- Offset value: -1 (as close to zero as possible until a few zero intensity pixels appears on screen).
- Beam size (or ROI radius): set to 0.5 mm of radius (see Note 22).
- Iterations: 3-5 iterations to achieve full bleach (see Note 17).
- Time lapse (see Notes 15, 17 and 22):
    - 1 frame every 10 seconds for 3 frames before bleach.
    - 1 frame every 10 seconds for 10 minutes after bleach, starting straight after the bleaching event.

3. Adjust precisely the focus and select your desired ROI (see Note 24).
4. Start your time-lapse.
5. Proceed with another cell. Acquire multiple cells showing a broad range of expression levels, as this will give useful information for the analysis (see

Section 1.5 and 3.3.3).

3.2.2. Controls

Using this detailed protocol and the same settings as for the biological samples, several controls must be performed at the same time to accurately interpret the results of a FRAP experiment:

1. Carry out initial experiments to optimise the ideal time course and image acquisition number to ensure that the recovery of fluorescence is complete and photoreversible bleaching is minimised.
2. Bleach several ROI with different spot sizes to test whether diffusion has a major role in the fluorescence recovery. This will allow the user to apply the appropriate mathematical model for determining the protein dynamics according to (Sprague et al., 2004).
3. Ensure that the overall fluorescence intensity of the entire cell is not significantly different before and after photobleaching. Bleached spots must comprise a relatively small proportion of the cellular pool of fluorescent proteins. To do this, one should perform several FRAP experiments with increasing size and/or number of bleached ROI to determine the limit for the bleach area. Slower recovery curves in experiments with a larger bleach spot size indicate that recovery of fluorescence is affected by a depletion of the pool of fluorescently labelled proteins.

3.3. FRAP data analysis

3.3.1. Intensity measurements

1. Collect a complete set of FRAP experiments (20 to 30 cells per condition) and transfer the images to the analysis workstation.
2. Correct any noticeable stage drift by realigning the individual images, e.g. ImageJ plug-in StackReg (Thevenaz et al., 1998) (see Note 25).
3. Redraw the boundaries of the bleached ROI using the circular selection tool (see Note 22). The ROI position and diameter are likely to be found in the metadata recorded by the microscope software during acquisition.
4. Extract the fluorescence intensity values for:
    - The bleached ROI

- Unbleached areas representative of the background fluorescence
- Unbleached structures similar to the bleached target (see Note 26).

5. Label the data in a fully comprehensive manner and store them in a backed-up text file or spreadsheet.

3.3.2. Normalisation and curve fitting

Several calculations must be carried out to allow the comparison of the FRAP readouts between different biological samples or FRAP experiments.

1. Plot all the raw data from each ROI separately to validate the integrity of the measurements (see Figure 2A and Note 27).
2. Obtain the background value ($F_{bgd}[t]$) by averaging the fluorescence intensity from unbleached areas representative of the background and subtract this background value from each measurement of a photobleached ROI ($F_{bleach}[t]$):

$$F[t] = (F_{bleach}[t] - F_{bgd}[t])$$

4. Obtain the control value ($F_{ctr}[t]$) by averaging the fluorescence intensity from several unbleached structures similar to the bleached target (see Note 26) in order to compensate for the overall loss of fluorescence.
5. Correct each measurement with the background subtracted control value from an unbleached ROI to obtain the experimental recovery ($R_{norm}[t]$) as follows:

$$R_{norm}[t] = F[t] / (F_{ctr}[t] - F_{bgd}[t])$$

6. Correct the experimental recovery with the first postbleach fluorescence intensity set to zero (F_0) to obtain the fractional recovery measurement ($R_{frac}[t]$):

$$R_{frac}[t] = (R_{norm}[t] - F_0) / (1 - F_0)$$

7. Average the multiple $R_{frac}[t]$ obtained within the same cell and over the same time course.
8. Plot the average fractional fluorescence recovery curve ($R_{frac}[t]$) obtained (see

Figure 2B).

9. Superimpose multiple fractional fluorescence recovery curves obtained from different cells and use them to calculate the standard deviation (see Figure 2C).

10. The mobile fraction and the half-time of recovery can already be estimated from this curve but a more accurate approach requires curve fitting.

11. Export the data to MATLAB.

12. Fit the plotted data using the following equation with the ezyfit toolbox for MATLAB (see Note 28):

$$F(t) = 1 - A\, e^{-koff\, t}$$

13. Obtain the FRAP coefficients.

3.3.3. Evaluation of the relationship between expression level and FRAP coefficients

To assess any relationship between the expression level of the fluorescently tagged protein and the FRAP coefficients which could invalidate the results, a correlation study must be performed:

1. With the help of the selection tool in ImageJ, measure the intensity of the fluorescence in the cell before the bleaching event.

2. Plot the overall intensity value against its estimated mobile fraction in a scatter plot (see Figure 2D); in a second figure, plot the same value against the estimated half-time of recovery.

3. Calculate the slope of the regression line through the data points. It must not be statistically different from 0 with 95 % confidence.

4. Notes

1. Photoreversible bleaching can pose a problem during the quantitative analysis of FRAP data and lead to an artefactual measurement of protein dynamics. Furthermore, different fluorescent proteins show different rates of photoreversible bleaching; therefore comparisons between GFP variants within an experiment may give misleading results. Photoreversible bleaching can occur in the GFP species on a millisecond time scale (Dickson et al.,

1997). It is known that YFP species also exhibit photoreversible bleaching, which occurs in the timescale of seconds and is dependent on complex protonation reactions (McAnaney et al., 2005). The longer time scale associated with YFP may become apparent in experiments with short time intervals, therefore GFP is usually the preferred option.

2. Being able to completely bleach the fluorescence emitted by the tagged protein is crucial. Theoretically, bleaching using a high-power laser beam can be achieved on any fluorescent protein, depending on the availability of the appropriate laser line on the microscope system; this should match the excitation peak of the targeted molecule. For example, the red fluorescent protein (RFP) or its derivative, mCherry (Shaner et al., 2004) may also be used for FRAP, however the fluorescence quantum yield is significantly lower than that of EGFP and suitable lasers (like the Helium-Neon Orange 594 nm) are known to be weak and may not achieve full bleach, therefore the GFP variant is preferred.
3. Ideally, the fluorescent tag should be inserted in at least two different positions, for example on the N- and C-termini of the protein separately. The localisation of the overexpressed construct should be similar to that of the endogenous protein, and concerns about a potential perturbation of the function must rise if the FRAP coefficients obtained are significantly different between the constructs. Such control experiments can be easily done on paraformaldehyde-fixed cells (see Note 11).
4. In most cases, either transient or stable expression of the fusion protein in cells can be performed. Using a stable cell line for FRAP ensures that the measurements are more consistent by reducing the variability of expression levels (see also 3.3.3).
5. The Acousto-Optical Beam Splitter (AOBS) is a common feature on more recent confocal microscopes, allowing the physical separation of emission and excitation light paths with high transmission efficiency. An Acousto-Optical Tunable Filter (AOTF) allows the rapid alternation between switching the laser on and off, and the adjustment of laser lines and their respective intensities by modifying the transmission coefficient, as opposed to changing the power of the laser emission itself. This component is essential to perform automated monitoring and bleaching of the sample over time.
6. The use of laser-based microscopes is restricted to persons who have been

adequately trained and are familiar with the local safety regulations.

7. We use a temperature and CO_2 controlled chamber to provide the optimal conditions for live imaging. It is possible to avoid the need for CO_2 by using a CO_2 independent buffered system such as HEPES instead of bicarbonate buffer.
8. Plastic culture dishes and plates are poorly suited for fluorescence studies as they exhibit non-stable auto fluorescence (Piruska et al., 2005), therefore cells must be transferred to a glass-bottomed dish after transfection.
9. Other extracellular matrix proteins such as laminin, vitronectin or collagen may be required to ensure the spreading of some cell lines.
10. In order to reduce background fluorescence due to the medium, Ham's F12 medium is preferred to DMEM for live imaging as it contains low amount of riboflavin and less phenol red. Riboflavin exhibits high autofluorescence in the excitation range of 450-490 nm and emission range of 500-560 nm. Phenol red has a maximum excitation peak around 555 nm. To further minimise the autofluorescence, FRAP experiments are preferably performed in low serum or serum-free medium.
11. Paraformaldehyde (PFA) is a toxic powder that must be handled with care using gloves and a respiratory mask in an isolated environment. A 4 % PFA solution in PBS (w/v) will dissolve overnight with constant stirring at 50°C. The stock solution can be aliquoted and stored at -80°C for a year. Thawed aliquots must be kept at 4°C and used within a week. Fixation of cells is performed at room temperature for 15 minutes followed by 3 washes in PBS.
12. MATLAB can be linked to ImageJ through an additional Java package created by Daniel Sage and Dimiter Prodanov (Biomedical Imaging Group, Swiss Federal Institute of Technology, Lausanne, Switzerland, http://bigwww.epfl.ch/sage/soft/mij/)
13. The expression of the construct in a suitable cell line for the study must be monitored by fixing the cells in PFA (see Note 4) at various time points after transfection as the expression level and maturation speed of the fluorescently tagged protein vary considerably depending on the tag and the cell line. Moreover, the delivery of the overexpressed protein in the appropriate cellular compartment is another feature that varies, as it is dependant on the renewal rate of the endogenous protein.
14. To equilibrate the sample with the experimental conditions, it should be

placed on the microscope stage an hour before the beginning of the experiment.

15. The duration of the recorded recovery should be continued until the intensity of fluorescence within the ROI reaches a plateau value.
16. Real-time autofocus systems can help to compensate for focus drifts due to temperature variations for example.
17. Despite the fact that the parameters will be used to monitor living cells, it is more convenient to use a fixed sample (see Note 4) maintained in the same conditions as for the live cells. The laser settings for the bleaching event should be set to achieve a sufficient decrease in fluorescence within the ROI. As a guideline, we consider that the first reading after bleach should be less than 20 % of the measurement before the bleaching event. Although, this value is subject to discussion as the bleaching illumination must be kept as low as possible for two reasons: firstly, to avoid excessive phototoxicity and secondly, because the beginning of fluorescence recovery must not overlap with the last bleaching iteration. Indeed, the bleaching duration must be confined to a limited space (*i.e.* the ROI) and time (ideally instantaneous) to allow accurate measurement. Unfortunately, there is no general rule and it is more a case of a trial and error for the user to get the optimal bleaching and imaging parameters.
18. It is crucial to adjust the acquisition parameters of the photomultiplier tube (PMT) in order to remain in the dynamic range of intensity acquisition. Saturation of fluorescence intensity during the time-lapse will result in inaccurate measurements of FRAP coefficients.
19. On the majority of line scanning confocal microscopes, an option is available for bi-directional scanning. This allows the scan head to image the sample in both directions along the x-axis and inevitably increases the acquisition rate. Additionally, the frame averaging function should be avoided while doing live measurements as it leads to a loss of time resolution.
20. The pinhole value, determined by the numerical aperture of the objective and the light wavelength, should ideally be adjustable. For live cell work, the pinhole should be opened wide enough to get adequate signal intensity, while keeping the laser intensity low to minimise photobleaching and phototoxicity. Meanwhile, opening the pinhole affects the resolution by increasing the thickness of the optical section.

21. The PMT gain value should be around 900-1000 V. A value below 600 V means that the laser line intensity can be lowered; conversely it needs to be increased if the gain setting is above 1100 V.
22. If these experiments will be analysed according to the method detailed by Sprague et al. (Sprague et al., 2004), the ROI must be circular.
23. It is necessary to record 3 to 5 frames before the bleaching step to get the value of the initial maximum intensity within the ROI.
24. It is recommended to bleach multiple ROI of identical size for each time lapse. Recovery curves obtained from multiple ROI within the same cell should be averaged after normalisation to obtain smooth data (see Section 3.3.2 and Figure 2C). Pooling data is acceptable under these circumstances as the level of expressed fusion proteins (i.e. both fractions of bound and free molecules) is the same between the different ROI.
25. Plug-in created by Philippe Thévenaz (Biomedical Imaging Group, Swiss Federal Institute of Technology, Lausanne, Switzerland, http://bigwww.epfl.ch/thevenaz/stackreg/)
26. The data have to be corrected for unintentional bleaching that occurs during the monitoring phases. Two techniques can be used: the first consists of recording the fluorescence intensity within several unbleached regions to the one displayed in the bleached ROI. The second technique involves the recording of the averaged intensity of the cell.
27. Discard any sets of data that exhibit any of the following defects: inconsistent background fluorescence intensities, unstable prebleach intensities and recovery curve that does not exhibit a plateau.
28. Ezyfit toolbox for MATLAB created by Frederic Moisy, Laboratory FAST, University Paris Sud, Paris, France, http://www.fast.u-psud.fr/ezyfit/).

5. Acknowledgments

We would like to thank Dr. Janet Askari for critical reading of the manuscript. CB acknowledges BBSRC (BB/G004552/1). The Bioimaging Facility microscopes used in this study were purchased with grants from BBSRC, Wellcome Trust and the University of Manchester Strategic Fund.

6. References

Tsien, R. Y. (1998) The green fluorescent protein, *Annu Rev Biochem* ***67***, 509-544.

Axelrod, D., Koppel, D. E., Schlessinger, J., Elson, E., and Webb, W. W. (1976) Mobility measurement by analysis of fluorescence photobleaching recovery kinetics, *Biophys J* ***16***, 1055-1069.

Sprague, B. L., and McNally, J. G. (2005) FRAP analysis of binding: proper and fitting, *Trends Cell Biol* ***15***, 84-91.

Sprague, B. L., Muller, F., Pego, R. L., Bungay, P. M., Stavreva, D. A., and McNally, J. G. (2006) Analysis of binding at a single spatially localized cluster of binding sites by fluorescence recovery after photobleaching, *Biophys J* ***91***, 1169-1191.

Sprague, B. L., Pego, R. L., Stavreva, D. A., and McNally, J. G. (2004) Analysis of binding reactions by fluorescence recovery after photobleaching, *Biophys J* ***86***, 3473-3495.

Lippincott-Schwartz, J., Snapp, E., and Kenworthy, A. (2001) Studying protein dynamics in living cells, *Nat Rev Mol Cell Biol* ***2***, 444-456.

Thevenaz, P., Ruttimann, U. E., and Unser, M. (1998) A pyramid approach to subpixel registration based on intensity, *IEEE Trans Image Process* ***7***, 27-41.

Dickson, R. M., Cubitt, A. B., Tsien, R. Y., and Moerner, W. E. (1997) On/off blinking and switching behaviour of single molecules of green fluorescent protein, *Nature* ***388***, 355-358.

McAnaney, T. B., Zeng, W., Doe, C. F., Bhanji, N., Wakelin, S., Pearson, D. S., Abbyad, P., Shi, X., Boxer, S. G., and Bagshaw, C. R. (2005) Protonation, photobleaching, and photoactivation of yellow fluorescent protein (YFP 10C): a unifying mechanism, *Biochemistry* ***44***, 5510-5524.

Piruska, A., Nikcevic, I., Lee, S. H., Ahn, C., Heineman, W. R., Limbach, P. A., and Seliskar, C. J. (2005) The autofluorescence of plastic materials and chips measured under laser irradiation, *Lab Chip* ***5***, 1348-1354.

Shaner, N. C., Campbell, R. E., Steinbach, P. A., Giepmans, B. N. G., Palmer, A. E., and Tsien, R. Y. (2004) Improved monomeric red, orange and yellow fluorescent proteins derived from Discosoma sp. red fluorescent protein, *Nat Biotechnol* ***22***, 1567-1572.

7. Figure Legends

Figure 1: Principle of FRAP experiment and example.

A. Scheme depicting the photobleaching and fluorescence recovery of a region of interest (ROI) within a focal adhesion (FA) in a cell; Before the bleach event, the fluorescent proteins are uniformly distributed within the structure and are in dynamic equilibrium, immediately after photobleaching the equilibrium is lost and the fluorescence intensity recovers as fluorescent proteins move back into the ROI. This model represents a reaction-dominant recovery, in which diffusion is negligible. **B.** Fluorescence intensity is recorded as a function of time; this enables the half-time of recovery ($t_{1/2}$), and the mobile and immobile fractions (F_M and F_I respectively) to be measured. The fluorescence intensities before and immediately after bleaching, are indicated ($F_{initial}$ and F_0 respectively) as well as the intensity after recovery (F_∞). **C.** Example of a FRAP experiment on a focal adhesion plaque component; FRAP was performed on NIH 3T3 cells transiently expressing vinculin-mEGFP. Panels represent still frames taken at the indicated timepoints (in seconds), throughout the course of the experiment. Dashed circles indicate the bleach ROI, scale bar = 5μm.

Figure 2: Workflow of analysis of FRAP data

A. Fluorescence intensities extracted from the time-lapse images are individually plotted over time to visualise any abnormal behaviour. The intensity recorded within several bleached ROI are termed FRAP1, FRAP2 and FRAP3. The background readings are termed bgd1, bgd2 and bgd3; and finally, the recording for the unintentional bleaching are labelled as ctrl1 and ctrl2. **B.** After background subtraction and correction for the postbleach intensity, the fractional fluorescence recovery of the three bleached ROI are plotted over time. The intensity of the monitored fluorescence now varies between 1 (prebleached value) and 0 (immediatly after the bleach event). **C.** Multiple fractional fluorescence recovery curves acquired in the same cell are averaged and plotted with their standard deviation of the mean. The curve is the best fit obtained from the experimental data. The main parameters discussed in the text have been extracted for these data (see legend). **D.** A scatter plot is shown here to illustrate the absence of correlation between the intensity of fluorescence in the cell, *e.g.* the expression level of the tagged protein, and the mobile fraction over a 4.5 fold

range. A similar graph should be plotted with the half-time of recovery and the overall fluorescence intensity (see Section 3.3.3).

Figure 1

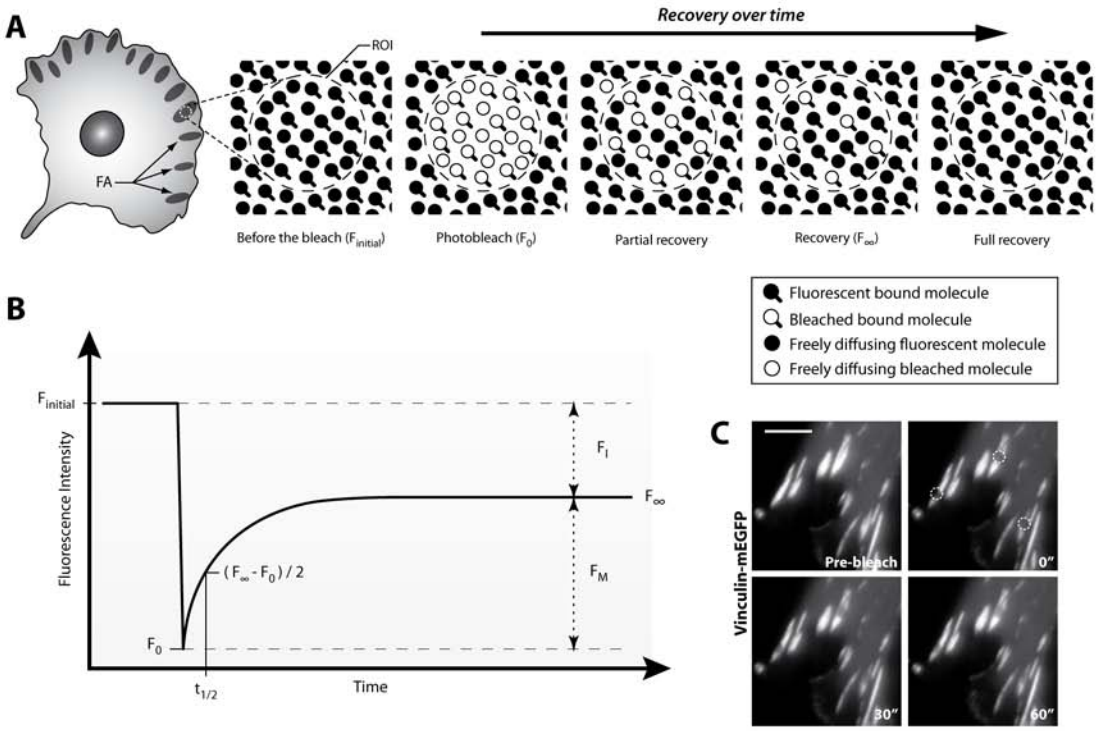

Figure 1: Principle of FRAP experiment and example.

Figure 2

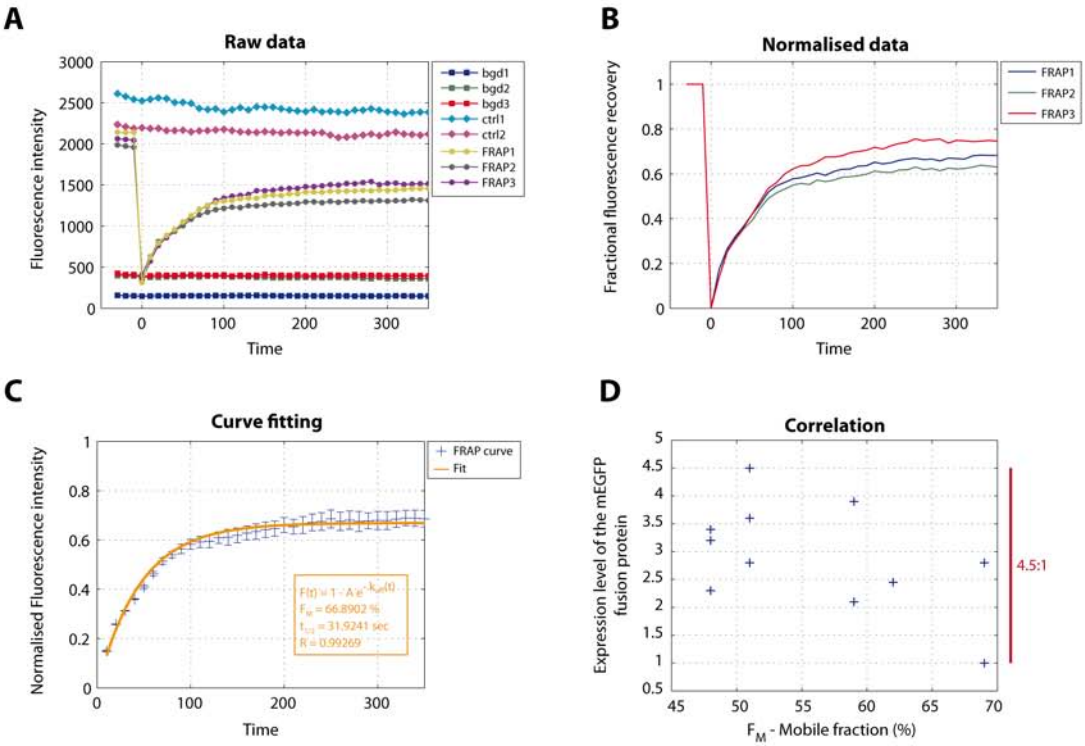

Figure 2: Workflow of analysis of FRAP data

4) Results chapter 2

GAS2-like 3 is a new microtubule-actin interacting protein related to the spectraplakins

Matthew J Stroud, Christoph Ballestrem, Richard Kammerer*

Wellcome Trust Centre for Cell-Matrix Research, Faculty of Life Sciences, University of Manchester, M13 9PT. UK

*** Correspondence should be addressed to Richard Kammerer**

Wellcome Trust Centre for Cell Matrix Research

Faculty of Life Sciences, University of Manchester

Michael Smith Building, Oxford Road

Manchester, M13 9PT, United Kingdom

Phone: +44 (0) 161-275-1708

Fax: +44 (0) 161-275-1505

Email: richard.kammerer@manchester.ac.uk

Abstract

The microtubule (MT) and actin cytoskeletons are fundamental to cell integrity, as they control a host of cellular activities. Until recently, studies have investigated these cytoskeletal components as separate entities, however, it has become increasingly clear that the MT and actin cytoskeletons function in an interdependent way. Elucidating how the two components interact will be key to our further understanding of fundamental cellular processes such as cell division, growth, polarisation and migration. Proteins involved in mediating the crosstalk between MT and actin cytoskeletons are fundamental to many cellular processes and play important physiological roles.

Here we describe a new member of the spectraplakin superfamily, GAS2-like 3. We show that GAS2-like 3 is widely conserved throughout evolution and is ubiquitously expressed in human tissues. GAS2-like 3 interacts with filamentous (F) actin and MTs via its single calponin homology type 3 (CH3) domain and C-terminus, respectively. Interestingly, the role of the putative MT-binding GAS2-related (GAR) domain is to modulate the binding of GAS2-like 3 to F-actin and MTs. This is in contrast to GAR domains found in related proteins, where it functions as a MT-binding domain. We find that both MTs and F-actin influence GAS2-like 3 localisation, although MTs have a greater influence on this localisation. Furthermore, we describe that GAS2-like 3 localisation to MTs can be enhanced by tubulin acetylation.

Introduction

The cytoskeleton is fundamental to cellular integrity, providing a molecular framework for both mechanical support and an intracellular transport infrastructure (Li and Gundersen, 2008). Until recently, the microtubule (MT) and actin cytoskeletons have been investigated as separate entities, however, it has become clear that the MT and actin cytoskeletons function in an interdependent way (Goriounov et al., 2003; Kodama et al., 2003). For example, there is evidence to suggest MTs use filamentous actin (F-actin) to guide them from the cell interior to focal adhesions at the cell periphery (Wu et al., 2008). Understanding how the two components interact will therefore be key to our further understanding of fundamental cellular processes, such as cell division, growth, polarisation and migration.

The spectraplakins are a well characterised example of a protein family which can crosslink MT and actin cytoskeletons (Jefferson et al., 2004). There are two members expressed in mammals, microtubule-actin crosslinking factor 1 (MACF1 or ACF7) and bullous pemphigoid antigen 1 (BPAG1), both of which are huge, multi-domain containing proteins (>500kDa in mass) with binding sites for both F-actin via their calponin homology (CH) domains and MTs via their GAS2-related (GAR) domain and/ or GSR repeats. Ablation of the ACF7 gene in mice results in embryonic lethality. However, ACF7 -/- cells can be derived from the embryo and display defects in MT dynamics, guidance, cortical tethering, stability and cellular polarisation (Kodama et al., 2003). Interestingly, the expression of a mini-version of ACF7 consisting of the CH and GAR domains is necessary and sufficient to rescue these perturbations in function, implying these are the key functional domains of spectraplakins. Accordingly, various medical conditions and developmental defects arise as a result of mutations in genes encoding spectraplakins, including mental retardation, cancer and chronic skin blistering (Sonnenberg and Liem, 2007), which shows the importance of proteins which link the actin and MT cytoskeletons.

Whereas the role of spectraplakins in crosslinking the MT and actin cytoskeletons is well established (Kodama et al., 2003; Sun et al., 2001; Wu et al., 2008), the functions of the related GAS2 family remain to be determined.

The GAS2 family can be thought of as mini-versions of spectraplakins, as they too contain a putative actin-binding CH domain and a putative MT-binding GAR domain. The first identified member of the GAS2 crosslinking family, termed GAS2, was originally identified in a screen looking for genes induced by growth arrest (Schneider et al., 1988). GAS2 localises along stress fibers (Brancolini et al., 1992) and it may also be involved in apoptosis and tumour suppression (Brancolini et al., 1995; Brancolini and Schneider, 1994; Lee et al., 1999). Two related family members were identified either in a search for putative tumour suppressors (human Gas2-related gene on chromosome 22 (hGAR22) or GAS2-like 1 (G2L1)) or by sequence similarity to hGAR22 (human Gas2-related gene on chromosome 17 (hGAR17) or GAS2-like 2 (G2L2)) (Goriounov et al., 2003; Zucman-Rossi et al., 1996). Both transcripts which code for the respective proteins are subject to alternative splicing, which result in proteins with different localisation and binding properties. The shorter isoforms termed, hG2L1α and hG2L2α, predominantly localise to the actin cytoskeleton, and interact with F-actin *in vitro*. Conversely, both of the longer isoforms, termed hG2L1β and hG2L2β, localise and bind to both F-actin and MTs (Goriounov et al., 2003), suggesting that they may play a role in mediating crosstalk between the cytoskeletal systems.

In the present study, we describe the characterisation of a new family member, GAS2-like 3 (G2L3), which has the potential to communicate between MTs and actin. G2L3 is widely conserved through evolution, and it is abundant in most human tissues, and the majority of cell lines we tested. Full-length G2L3 interacts with both F-actin and MTs in cells and *in vitro* via its CH domain and C-terminus, respectively. A third domain, termed the GAR domain, does not directly bind to F-actin or MTs, however is involved in modulating the binding strength of G2L3 to each cytoskeletal system. Interestingly, we found that acetylation of α-tubulin contributes to the recruitment of G2L3 to MTs.

Results

GAS2-like 3 is highly conserved amongst species and is widely expressed in human tissues

In order to identify potential actin and MT binding proteins, we performed a TBLASTN search for genes containing both CH and GAR domains using GAS2 as a template. As a proof of principle, we identified GAS2, G2L1, G2L2, MACF1, BPAG1, but also an uncharacterised gene, G2L3 (GenBank/ EMBL/DDJB accession No. AC_000144). It has an open reading frame of 2229 base pairs, spanning eight exons and encodes a putative protein of 694 amino acids with a deduced molecular mass of 75.2 kDa (Figure 1A). The protein sequence consists of a single CH3-class, CH domain comprising 122 amino acids at the amino terminus, with 24% amino acid identity to the CH domain identified in calponin. To the carboxy terminus of the CH domain is an 82 amino acid-long GAR domain, which is abutted to a stretch of 404 amino acids that is predicted to have little secondary structure. The domain organisation of G2L3 is the same as GAS2, G2L1 and G2L2, therefore classifying it as a new member of the GAS2 protein family.

We next examined how closely related the members of the human GAS2 family were. We discovered G2L3 shared the highest identity to GAS2 (60%), and the lowest identities with G2L1 and G2L2 at 30% and 36%, respectively (Figures 1B and 1C). In terms of domain sequence conservation, the CH and GAR domains of G2L3 are compared to the other members in Figure 1C.

In addition to comparing human GAS2 members, we investigated whether G2L3 homologues are conserved across different species. We found G2L3 homologues are present in all vertebrates; For example, there is 65% identity between the conserved CH and GAR domains belonging to the human G2L3 and the zebrafish G2L3 (see Supplementary Table 1). There is also evidence for the existence of genes with the same domain architectures in fruit flies, where it has been named ‘picked eggs’ (Pigs) (Accession number: NM_132103) (Pines et al., 2010). A similar protein is expressed in *Caenorhabditis elegans*, except the CH domain has been duplicated (Accession number: NM_069025). Taken together, we have discovered a new member of the GAS2 family by searching for genes

related to GAS2 that is highly conserved through evolution, which implies it plays an important function.

After confirming G2L3 is widely conserved amongst species, we next sought to determine the expression of G2L3 in human tissues and cell lines. Using cDNA libraries generated from different human tissues and cell lines, we performed PCRs to investigate the respective levels of G2L3 mRNA, and used this as an indication of G2L3 protein levels. G2L3 mRNA was widely expressed within the body, and was most prominently found in the pancreas, heart, skeletal muscle, liver, kidney, placenta and lung, whereas it was expressed at low levels in the brain (Figure 2A). As tissues contain many different cell types, we investigated whether G2L3 expression was confined to a particular one. We discovered G2L3 in a wide variety of cell lines, including HeLa, Human Foreskin Fibroblasts, Human Embryonic Kidney 293 cells, and we found the murine homologue in NIH3T3 cells. Conversely, it was not expressed in HT1080 cells, which are a highly transformed cell line (Figure 2B). These data suggest that G2L3 is abundantly expressed in many tissues and cell lines. Notably, it is absent in HT1080 cells, which may indicate a role in tumour suppression.

The calponin homology domain mediates localisation to actin stress fibres and the C-terminus recruits GAS2-like 3 to microtubules

In order to determine the subcellular localisation of G2L3 and to study the roles of its domains in this localisation, we expressed fluorophore-tagged versions of G2L3 and a series of G2L3 mutants in NIH3T3 cells. We found that full-length G2L3 localised to overlapping MTs and actin stress fibers in 70% of all tested cells and G2L3 localised only to MTs in the remaining 25% of cells (Figure 3A, Supplementary Movie 1). The localisation to actin was mediated by the CH domain, since expression of this domain alone (referred to as G2L3-CH) decorated actin stress fibers in all cells (Figures 3B and 3D). In contrast, a construct missing the CH domain (G2L3-ΔCH) localised predominantly to MTs, suggesting that the remaining sequence contained a MT binding site (Figures 3B and 3C). The localisation to MTs was mediated by the C-terminus, since expression of this domain (G2L3-C-term) localised exclusively to MTs (Figure 3C). Notably, the MTs appeared to be bundled in 82% of cells expressing G2L3-C-term. To investigate whether the GAR domain, a domain which has been

frequently implicated in MT binding in other proteins (Sun et al., 2001), played a role in localising G2L3 to either cytoskeleton, we generated mutants including and excluding this domain (G2L3-GAR and G2L3-ΔGAR, respectively). We found that G2L3-GAR localised diffusely in the cytoplasm in most cells and G2L3-ΔGAR localised along the MT lattice, implying that the GAR domain does not regulate G2L3 localisation to MTs or actin (Figure 3C). Interestingly, G2L3-ΔC-term, which lacks the C-terminus but contains both the CH and GAR domains localised predominantly to the actin cytoskeleton, albeit to different actin structures than G2L3-CH. Specifically, G2L3-ΔC-term localised to both lamellipodia and filopodia (Figure 3D and Supplementary Movie 2).

Taken together, these data indicate that the CH domain controls the localisation of G2L3 to actin and the C-terminus regulates its localisation to MTs. The GAR domain is not essential for localisation to MTs and the bundling of MTs by the C-terminus may imply that it has the ability to crosslink MTs.

GAS2-like 3 interacts directly with microtubules and filamentous actin

To determine whether the localisation of the individual domains of G2L3 is mediated by direct interactions with the different cytoskeletal systems, we performed *in vitro* co-sedimentation assays using recombinant purified domains. We found that purified G2L3-CH co-sedimented with F-actin after high-speed centrifugation, indicating they directly interact (Figure 3E). Conversely, G2L3-C-term remained in the supernatant, implying it fails to directly interact with actin (Figure 3E). As controls, the proteins were centrifuged in the absence of polymerised actin and both were found in the supernatant, showing they fail to sediment alone. A similar assay was performed with MTs, to reveal that G2L3-C-term interacts directly with MTs (Figure 3F). In contrast, neither G2L3-CH nor G2L3-GAR were found in the pellet fraction with MTs, implying neither interact directly with MTs (Figure 3F).

Overall, these data are consistent with the IF data, confirming that the CH domain binds to actin, and the C-terminus binds to MTs. These data suggest that the GAR domain does not interact with MTs directly *in vitro*.

The individual domains of GAS2-like 3 influence the binding strength to microtubules and F-actin

To study the influence of the different domains of G2L3 on its binding strength to F-actin or MTs, we performed Fluorescence Recovery After Photobleaching (FRAP) experiments on cells expressing different mutants (Figures 4A and 4B). In these experiments we determined the half-time ($t_{1/2}$) of recovery of the different mutants, and used it as an indicator of protein mobility (Humphries et al., 2007; Stroud et al., 2011). In comparison to the subpopulation of G2L3 which localised to actin, we observed a twofold increase in the $t_{1/2}$ of recovery of 28.5s for G2L3-CH, indicating that the turnover of the CH domain is slower than full-length G2L3 (Figure 4B). Conversely, G2L3-ΔC-term showed a sixfold decrease in $t_{1/2}$ of recovery of 2.5s compared to G2L3, implying the turnover of G2L3-ΔC-term is faster and has a weaker interaction with actin than G2L3. These data indicate that the removal of the GAR domain and C-terminus amplifies the binding strength of the CH domain for actin. Interestingly, the presence of the GAR domain alone is sufficient to destabilise the interaction of the CH domain with actin. We subsequently analysed the mobility of the various constructs which localised to MTs. We discovered that full-length G2L3 and the construct lacking the CH domain (G2L3-ΔCH) had the slowest turnovers with $t_{1/2}$s of recovery of 14.9s and 15.3s, respectively. In contrast, the $t_{1/2}$ of recovery of G2L3-C-term was reduced almost fourfold (3.9s) and the $t_{1/2}$ of recovery of G2L3-ΔGAR was more than halved (6s). These data indicate that the CH domain does not affect the interaction of G2L3 with MTs, conversely the simultaneous removal of both the CH and GAR domains destabilises the interaction of the C-terminus with MTs.

These data suggest a critical role for the GAR domain in modulating the binding to the different cytoskeletal systems, i.e. it strengthens the interaction with MTs, however weakens the interaction with F-actin.

GAS2-like 3 localisation is dependent on both microtubule and actin cytoskeletons

The presence of both MT and actin binding sites on G2L3 raises the question as to whether the binding of G2L3 to one of the cytoskeletons influences the binding to the other. To elucidate this, we analysed the localisation of G2L3 in the absence of either F-actin or MTs. In 70% of control cells, G2L3 localised to both

MTs and F-actin and in 25% of cells it localised exclusively to MTs. Disruption of the actin cytoskeleton using cytochalasin D resulted in G2L3 localising more to MTs (74% compared to 25% in untreated control cells) (Figures 5A and B). These data suggest that F-actin is not required for G2L3 localisation to MTs. After treatment of cells with nocodazole to ablate MTs, G2L3 localised diffusely in the cytoplasm (36% compared to 5% in control cells). More importantly, G2L3 localised to the actin cytoskeleton in a small percentage of cells treated with nocodazole (4%). Notably, G2L3 localisation was enhanced to nocodazole resistant MTs, in a subset of cells. These data imply that MTs aid G2L3 localisation to F-actin, however they are not fundamental for it.

In summary, these data suggest that G2L3 is able to localise to both F-actin and MTs irrespectively of one another, however the presence of MTs aids G2L3 localisation to F-actin.

Post-translational acetylation of tubulin enhances GAS2-like 3 localisation to MTs

The enhancement of localisation of G2L3 to remnant MTs after nocodazole treatment, suggests that G2L3 preferentially binds to stable MTs. One way MTs can be stabilised against nocodazole is through post-translational (PT) modifications of tubulin, such as acetylation (Gundersen et al., 1994). To examine this possibility, we treated G2L3-GFP expressing cells with the histone deacetylase 6 (HDAC6) inhibitor trichostatin A (TSA), which dramatically increases the amount of acetylated α-tubulin. This increase in tubulin acetylation lead to a significant 9% increase in G2L3 recruitment to MTs in comparison to DMSO treated control cells (Figures 6A and 6C). This increase was not due to the possible stabilisation of MTs by the inhibitor per se, since MTs stabilised by taxol were not found to increase G2L3 localisation (data not shown).

In summary, these data suggest that G2L3 localisation may be regulated by molecular mechanisms that lead to MT acetylation.

Discussion

Here, we have characterised a new member of the GAS2 family, G2L3, which is highly conserved and expressed in many tissues. G2L3 binds to both F-actin and MTs via its single CH domain and unstructured C-terminus, respectively. Moreover we have shown that the GAR domain can modulate the interaction strength of G2L3 with both actin and MTs, and that tubulin acetylation enhances G2L3 localisation to MTs.

A single type 3-calponin homology domain mediates actin binding

Actin-binding of many prominent proteins such as MACF1 and α-actinin is mediated very efficiently by tandem type 1 (CH1) and type 2 (CH2) CH domain repeats (Gimona et al., 2002; Roper et al., 2002). The importance of the tandem repeat has been highlighted, as the removal of the CH1 domain in MACF1, ablates its actin binding ability, despite the remaining CH2 domain (Lee and Kolodziej, 2002).

In contrast to the tandem CH1 and CH2 domain repeats, single CH3 domains such as the ones found in calponin and MT-end-binding proteins are considered to be inefficient actin binding domains (ABDs) (Gimona et al., 2002; Gimona and Mital, 1998). It is hypothesised that CH3 domains serve to locate canonical ABDs, for example the CH3 domain on calponin is thought to interact with the CH1 domain on α-actinin and bring it in proximity to actin (Galkin et al., 2006; Leinweber et al., 1999). Despite this evidence for other CH3 domains, we found that the single CH3 domain in G2L3 does indeed function as an ABD, an observation which is supported by the other GAS2 family members (Goriounov et al., 2003). Interestingly, full-length G2L3 only localises to actin stress fibers in a subset of cells, implying that the mechanism of CH3 domain binding to actin, in the context of the full-length protein, is tightly regulated. In support of this, our FRAP experiments show lower binding strength to actin when the CH domain is coupled with the GAR domain and may suggest that the latter domain contains a motif that can modulate actin binding. This is further substantiated by F-actin sedimentation assays of G2L2, in which actin was less able to sediment G2L2β, than the truncated splice-mutant encoding the single CH domain (G2L2α) (Goriounov et al., 2003).

The C-terminus is essential for efficient microtubule binding

We discovered that the C-terminus in G2L3 is fundamental for binding to the MT cytoskeleton. Given the high degree of similarity between the GAR domain in G2L3 and the published MT-binding GAR domains in GAS2 (63% identity) and MACF1 (38%), we predicted that the G2L3-GAR domain would interact with MTs. Conversely to our hypothesis, we found that the GAR domain in G2L3 localises very weakly to MTs in cells and is unable to bind to them *in vitro*. Our observations are similar to those described for G2L1 and G2L2 (Goriounov et al., 2003). This raises an important question as to how the other GAR domains mediate this interaction? Initial sequence analyses revealed that the other GAR domains have overall positive charges, ranging from +2 to +6, whereas the G2L3-GAR has a net charge of zero. As MTs have an overall negative charge, one likely possibility is that the GAR domains of other proteins interact electrostatically, as has been shown for cationic peptides (Wolff, 1998). Further examination of the other GAR domains used to characterise MT binding exposed a weakness in construct design. For example, the GAR domain in GAS2 appears to be missing a final methionine residue, which is predicted to form part of the ultimate alpha helix (Sun et al., 2001). Also, the GAR domain used in a recent study on the *Drosophila* spectraplakin, Shot (Applewhite et al., 2010), lacks the first four residues which form part of the initial alpha helix. This study showed that the GAR domain localised to MTs very strongly. Both of these published GAR domains are likely to fold incorrectly and may act similarly to the positively charged and unfolded C-terminus of G2L3. In spite of these observations, it appears that the G2L3-GAR domain contributes slightly to MT binding strength since our FRAP data suggest that the presence of the GAR domain increases the binding strength of G2L3 to MTs. We speculate that the GAR domain in G2L3, and indeed in other proteins, interact with MT-associated proteins, which modulate binding to the microtubular network.

Acetylation contributes to GAS2-like 3 recruitment to microtubules

It has been reported previously that detyrosination and acetylation of α-tubulin are hallmarks of MT stabilisation (Gundersen and Bulinski, 1988; Webster and Borisy, 1989). We discovered that G2L3 localisation to MTs is enhanced to acetylated MTs, which is similar to other MT-interacting proteins such as the motor protein, kinesin-1 (Dompierre et al., 2007; Reed et al., 2006). Although the

function of this regulation is unclear, parallels can be drawn to the function of tubulin detyrosination. Recently it has been shown that detyrosination of α-tubulin effects the recruitment of proteins which contain a cytoskeleton-associated protein glycine-rich (CAP-GLY) domain (Mishima et al., 2007). Proteins containing these domains include the MT plus-end binding proteins, CLIP-170 and $p150^{glued}$, which can regulate MT dynamics and targeting. Thus, it is possible that localised tubulin acetylation can drive recruitment of G2L3 to specific loci within the cell, where it then exerts its function.

The similarity to spectraplakins

Members of the GAS2 family and the spectraplakins have a similar domain organisation, they equally bind to MTs and actin, they both localise similarly in cells and they exhibit similar behaviour in response to cytoskeleton-disrupting drugs (Karakesisoglou et al., 2000). These findings strongly suggest they may have similar functions. ACF7 regulates MT growth as well as the dynamics of focal adhesions associated with F-actin (Wu et al., 2008). Targeting of focal adhesions by MTs is essential for focal adhesion turnover (Kaverina et al., 1999), and disrupting MTs leads to inhibition of cell migration (Ballestrem et al., 2000). MTs grow along F-actin and can thus be guided to adhesion sites ((Rodriguez et al., 2003); and our observation). In the absence of ACF7, MT growth is unlinked from F-actin in epidermal cells, leading to a diminished turnover rate of focal adhesions and proteins therein (Wu et al., 2008). Given the potential exciting roles the GAS2 family may play in cell motility, future experiments will be necessary to clarify whether G2L3 or other members of the GAS2 family exert a similar function. With the potential role of stable MTs in migration (Gundersen and Bulinski, 1988), one possible avenue of investigation will be into the role of tubulin acetylation, and the proteins which mediate this, as they may govern G2L3 function.

Materials and Methods

Cell Culture and Transfections

All cells were grown in DMEM (Sigma Aldrich, Dorset, UK) supplemented with 10% FBS, and 1% glutamine in a 5% CO2 in a humidified incubator, and passaged in a 1:10 dilution every 3 days. For transfections, cells were plated in 6-well dishes a day before transfections. For transient transfections, 1-1.5µg of DNA in total was transfected into cells using Lipofectamine Plus (Invitrogen, Paisley, UK) in accordance with manufacturer's instructions. Cells were replated after 3 hours in glass-bottomed dishes (MatTek Corporation, Ashland, USA) coated with 10 µg/mL bovine fibronectin (pFN; Sigma). For drug treatments, cells were incubated for 30mins with either nocodazole (10µM), cytochalasin D (2µM), or trichostatin A (TSA) (5µM), (all from Sigma).

Immunofluorescence Imaging

Cells were fixed and permeabilised with 3% paraformaldehyde (Sigma) containing 0.25% Triton X-100 (Sigma) and 0.05% glutaraldehyde (Sigma) for 15 mins, before being washed in PBS (Lonza, Verviers, Belgium). Autofluorescence from reactive amine groups was quenched using 0.01% sodium tetrahydroborate (Sigma) in PBS for 15 mins before being washed in PBS. Subsequently cells were incubated for 45 mins with anti-tubulin or anti-acetylated tubulin antibodies at 1:500 dilution (DM1A and 6-11B-1, respectively Sigma), followed by three washes with PBS. Secondary antibodies conjugated to either Cy2, 3 or 5 (Jackson ImmunoResearch Laboratories, Suffolk, UK) were then applied for 30 mins. In the case of colabelling for actin, Texas Red or FITC-labelled phalloidin (Invitrogen) was added together with the secondary antibody). Cells were then washed three more times in PBS before being imaged using an oil-immersed 100X objective, with 1.35 numerical aperture on an inverted microscope (IX71; Olympus) controlled by a Deltavision system (Applied Precision, Washington, USA). Images were captured using a Coolsnap HQ CCD camera (Princeton Instruments, Lurgan, UK).

Fluorescence Recovery After Photobleaching (FRAP)

An inverted microscope (IX70) equipped with a 488-nm laser lines (Olympus) under the control of software (DeltaVisionRT) were used for FRAP experiments. Cells plated on glass-bottom dishes and expressing indicated GFP-tagged

constructs were imaged at 37°C in Ham's F12 medium. 1.5-µm-diam regions of interest were selected. Half-times of recovery were calculated using softWoRx FRAP analysis software (see application notes at http://www.api.com/lifescience/dv-pubsandapps.html#appnotes).

Image Processing

Images were processed using ImageJ version 1.43R. For colocalisation studies and calculation of the ratio of GAS2-like 3 / MTs for TSA analysis, images were background subtracted using a 2D-bandpass filter, overlay images were created. From these a threshold was set to restrict analyses to MTs, and the outline of the cell was drawn followed by measuring the percentage area of positive pixels. This was repeated for GAS2-like 3 and divided by the value given for MTs to give a ratio theoretically between zero and one. Adobe Photoshop CS4 was used in the preparation of figures for this manuscript.

cDNA panels

To identify human tissue expression, a "master mix" containing forward and reverse primers, dNTPs, reaction buffer and Taq polymerase was made for cDNA panels (Clontech, CA, USA). cDNA libraries from various cell lines were made using the 'Absolutely RNA Microprep Kit' followed by the Stratascript QPCR cDNA Synthesis Kit (Stratagene, Cheshire, UK) according to the manufacturer's recommendations A "master mix" was also made to identify expression in the cell lines; HeLa, Human Foreskin Fibroblast (HFFs), HT1080, Human Embryonic Kidney 293T and murine NIH 3T3. The total reaction volume for each reaction was 25µL, they were incubated at 94ºC for 1 minute, followed by 35 cycles of 30 seconds at 94 ºC (denaturation), 30 seconds at 55 ºC (annealing) and 60 seconds at 72 ºC (extension). The reaction products were subsequently run on a 1% agarose (w/v) gel for an hour at 120V.

Sub-cloning

For immunofluorescence, the CH domain, ΔC-term, ΔGAR, and ΔCH constructs were cloned into pEGFP-N1 or mCherry-N1 vectors (Clontech) using the restriction endonucleases NheI and HindIII at the amino acids indicated in Figure 1A. The other constructs were all cloned into the pEGFP-C1 vector (Clontech) using the restriction endonucleases BspEI and BamH1 for GAS2-like 3, EcoR1 and BamHI for the GAR domain, and BamH1 for the C-terminus.

For recombinant expression in E. coli, the CH domain and C-terminus were cloned into the pHisTrx vector (Kammerer et al., 1998) using either the restriction endonucleases BamHI and EcoRI or BamHI, respectively. The GAR domain was cloned into pHisNusA vector using the same restriction sites as for immunofluorescence. All recombinant insert DNA was verified by DNA sequencing.

Protein expression and purification

The recombinant GAS2-like 3 constructs were expressed in E. coli JM109 (DE3) host strain (Merck Biosciences, Nottingham, UK) as previously described (Kammerer et al., 1995) using an autoinduction protocol (as described by (Studier, 2005)). The 6xHis-tagged proteins were purified by immobilised metal affinity chromatography on Ni2+-Sepharose (GE Healthcare, Bucks, UK). Purification was performed under denaturing condition using 8 M urea as described in the pET system manual (Merck Biosciences). Removal of the 6xHis tags by thrombin from the CH domain and C-terminus was performed as previously described (Kammerer et al., 1995). Determination of protein concentration was achieved by the absorbance of tryptophan and tyrosine residues at 280 nm (Edelhoch, 1967).

In-vitro sedimentation assays

Actin and MT-binding assays were performed using the Non-Muscle Actin Binding Protein Spin-Down Biochem Kit (Cytsokeleton, Inc., CO, USA) and the Microtubule Associated Protein Spin-Down Assay Kit (Cytoskeleton, Inc.) respectively, according to the manufacturer's recommendations. Briefly, the proteins were pre-spun before the experiment, they were then incubated with the polymerised forms of either F-actin or MTs, followed by a high-speed centrifugation step. The supernatents were aspirated and boiled in SDS sample buffer and the pellets resuspended in SDS sample buffer. Following which, the samples were analysed on 10% SDS-PAGE gels for the GAR domain and C-terminus and 15% SDS PAGE gels were used for the CH domain. All protein bands were visualised using Coomassie blue staining.

Sequence alignments

Sequence alignments were performed using the program Jalview (Clamp et al., 2004)

Statistical analysis

Using the ratios obtained from the image processing, Student's t-tests were performed using Microsoft Excel to compare the ratios of G2L3 expressing control cells and TSA treated G2L3 expressing cells.

References

Applewhite, D. A., Grode, K. D., Keller, D., Zadeh, A., Slep, K. C. and Rogers, S. L. (2010). The spectraplakin Short stop is an actin-microtubule cross-linker that contributes to organization of the microtubule network. *Mol Biol Cell* **21**, 1714-24.

Ballestrem, C., Wehrle-Haller, B., Hinz, B. and Imhof, B. A. (2000). Actin-dependent Lamellipodia Formation and Microtubule-dependent Tail Retraction Control-directed Cell Migration. *Mol Biol Cell* **11**, 2999-3012.

Blose, S. H., Meltzer, D. I. and Feramisco, J. R. (1984). 10-nm filaments are induced to collapse in living cells microinjected with monoclonal and polyclonal antibodies against tubulin. *J Cell Biol* **98**, 847-58.

Brancolini, C., Benedetti, M. and Schneider, C. (1995). Microfilament reorganization during apoptosis: the role of Gas2, a possible substrate for ICE-like proteases. *EMBO J* **14**, 5179-5190.

Brancolini, C., Bottega, S. and Schneider, C. (1992). Gas2, a growth arrest-specific protein, is a component of the microfilament network system. *J.Cell Biol.* **117**, 1251-1261.

Brancolini, C. and Schneider, C. (1994). Phosphorylation of the growth arrest-specific protein Gas2 is coupled to actin rearrangements during Go-->G1 transition in NIH 3T3 cells. *J Cell Biol.* **124**, 743-756.

Clamp, M., Cuff, J., Searle, S. M. and Barton, G. J. (2004). The Jalview Java alignment editor. *Bioinformatics* **20**, 426-427.

Dompierre, J. P., Godin, J. D., Charrin, B. C., Cordelieres, F. P., King, S. J., Humbert, S. and Saudou, F. (2007). Histone deacetylase 6 inhibition compensates for the transport deficit in Huntington's disease by increasing tubulin acetylation. *J Neurosci* **27**, 3571-83.

Edelhoch, H. (1967). Spectroscopic determination of tryptophan and tyrosine in proteins. *Biochemistry* **6**, 1948-54.

Galkin, V. E., Orlova, A., Fattoum, A., Walsh, M. P. and Egelman, E. H. (2006). The CH-domain of calponin does not determine the modes of calponin binding to F-actin. *J.Mol.Biol.* **359**, 478-485.

Gimona, M., Djinovic-Carugo, K., Kranewitter, W. J. and Winder, S. J. (2002). Functional plasticity of CH domains. *FEBS Letters* **513**, 98-106.

Gimona, M. and Mital, R. (1998). The single CH domain of calponin is neither sufficient nor necessary for F-actin binding. *Journal of Cell Science* **111**, 1813-1821.

Goriounov, D., Leung, C. L. and Liem, R. K. (2003). Protein products of human Gas2-related genes on chromosomes 17 and 22 (hGAR17 and hGAR22) associate with both microfilaments and microtubules. *J.Cell Sci.* **116**, 1045-1058.

Gundersen, G. G. and Bulinski, J. C. (1988). Selective stabilization of microtubules oriented toward the direction of cell migration. *Proc Natl Acad Sci U S A* **85**, 5946-50.

Gundersen, G. G., Kim, I. and Chapin, C. J. (1994). Induction of stable microtubules in 3T3 fibroblasts by TGF-beta and serum. *J Cell Sci* **107 (Pt 3)**, 645-59.

Humphries, J. D., Wang, P., Streuli, C., Geiger, B., Humphries, M. J. and Ballestrem, C. (2007). Vinculin controls focal adhesion formation by direct interactions with talin and actin. *J Cell Biol* **179**, 1043-57.

Jefferson, J. J., Leung, C. L. and Liem, R. K. (2004). Plakins: goliaths that link cell junctions and the cytoskeleton. *Nat.Rev.Mol.Cell Biol.* **5**, 542-553.

Kammerer, R. A., Antonsson, P., Schulthess, T., Fauser, C. and Engel, J. (1995). Selective chain recognition in the C-terminal alpha-helical coiled-coil region of laminin. *J Mol Biol* **250**, 64-73.

Kammerer, R. A., Schulthess, T., Landwehr, R., Lustig, A., Fischer, D. and Engel, J. (1998). Tenascin-C hexabrachion assembly is a sequential two-step process initiated by coiled-coil alpha-helices. *J.Biol.Chem.* **273**, 10602-10608.

Karakesisoglou, I., Yang, Y. and Fuchs, E. (2000). An epidermal plakin that integrates actin and microtubule networks at cellular junctions. *J Cell Biol.* **149**, 195-208.

Kaverina, I., Krylyshkina, O. and Small, J. V. (1999). Microtubule targeting of substrate contacts promotes their relaxation and dissociation. *J Cell Biol* **146**, 1033-44.

Kodama, A., Karakesisoglou, I., Wong, E., Vaezi, A. and Fuchs, E. (2003). ACF7: an essential integrator of microtubule dynamics. *Cell* **115**, 343-354.

LeDizet, M. and Piperno, G. (1991). Detection of acetylated alpha-tubulin by specific antibodies. *Methods Enzymol* **196**, 264-74.

Lee, K. K., Tang, M. K., Yew, D. T., Chow, P. H., Yee, S. P., Schneider, C. and Brancolini, C. (1999). gas2 is a multifunctional gene involved in the regulation of apoptosis and chondrogenesis in the developing mouse limb. *Dev.Biol.* **207**, 14-25.

Lee, S. and Kolodziej, P. A. (2002). Short Stop provides an essential link between F-actin and microtubules during axon extension. *Development* **129**, 1195-1204.

Leinweber, B. D., Leavis, P. C., Grabarek, Z., Wang, C. L. and Morgan, K. G. (1999). Extracellular regulated kinase (ERK) interaction with actin and the calponin homology (CH) domain of actin-binding proteins. *Biochem J* **344 Pt 1**, 117-23.

Li, R. and Gundersen, G. G. (2008). Beyond polymer polarity: how the cytoskeleton builds a polarized cell. *Nat.Rev.Mol.Cell Biol.* **9**, 860-873.

Mishima, M., Maesaki, R., Kasa, M., Watanabe, T., Fukata, M., Kaibuchi, K. and Hakoshima, T. (2007). Structural basis for tubulin recognition by cytoplasmic linker protein 170 and its autoinhibition. *Proc Natl Acad Sci U S A* **104**, 10346-51.

Reed, N. A., Cai, D., Blasius, T. L., Jih, G. T., Meyhofer, E., Gaertig, J. and Verhey, K. J. (2006). Microtubule acetylation promotes kinesin-1 binding and transport. *Curr Biol* **16**, 2166-72.

Rodriguez, O. C., Schaefer, A. W., Mandato, C. A., Forscher, P., Bement, W. M. and Waterman-Storer, C. M. (2003). Conserved microtubule-actin interactions in cell movement and morphogenesis. *Nat Cell Biol* **5**, 599-609.

Roper, K., Gregory, S. L. and Brown, N. H. (2002). The 'spectraplakins': cytoskeletal giants with characteristics of both spectrin and plakin families. *Journal of Cell Science* **115**, 4215-4225.

Schneider, C., King, R. M. and Philipson, L. (1988). Genes specifically expressed at growth arrest of mammalian cells. *Cell* **54**, 787-793.

Sonnenberg, A. and Liem, R. K. (2007). Plakins in development and disease. *Exp.Cell Res.* **313**, 2189-2203.

Stroud, M., Carisey, A., Tsang, R. and Ballestrem, C. (2011). Fluorescence Recovery After Photobleaching. *Manuscript accepted by Methods Mol.Biol.*

Studier, F. W. (2005). Protein production by auto-induction in high density shaking cultures. *Protein Expr.Purif.* **41**, 207-234.

Sun, D., Leung, C. L. and Liem, R. K. (2001). Characterization of the microtubule binding domain of microtubule actin crosslinking factor (MACF): identification of a novel group of microtubule associated proteins. *Journal of Cell Science* **114**, 161-172.

Webster, D. R. and Borisy, G. G. (1989). Microtubules are acetylated in domains that turn over slowly. *J Cell Sci* **92 (Pt 1)**, 57-65.

Wolff, J. (1998). Promotion of microtubule assembly by oligocations: cooperativity between charged groups. *Biochemistry* **37**, 10722-9.

Wu, X., Kodama, A. and Fuchs, E. (2008). ACF7 regulates cytoskeletal-focal adhesion dynamics and migration and has ATPase activity. *Cell* **135**, 137-148.

Zucman-Rossi, J., Legoix, P. and Thomas, G. (1996). Identification of new members of the Gas2 and Ras families in the 22q12 chromosome region. *Genomics* **38**, 247-254.

Figure Legends

Figure 1: Schematic representation of the intron-exon boundaries of the G2L3 gene and the sequence alignments of the human GAS2 protein family. **(A)** The G2L3 gene consists of eight exons interspersed by seven introns. The CH and GAR domains are depicted in red and yellow, respectively, and the C-terminus in green. **(B)** Sequence alignment of the GAS2 family, showing the conservation between the amino termini of the GAS2 family members. The beta isoforms of G2L1 and G2L2 are shown. Note the high degree of conservation between family members. **(C)** The percentage identities between G2L3 and the other GAS2 family members are indicated, as well as the percentage identities between the various domains.

Figure 2: G2L3 is expressed ubiquitously in human tissues and cell lines. **(A)** PCRs were performed on cDNA panels generated from different tissues, using primers specific for G2L3, which spanned exon 2 to exon 6. Primers designed specifically to recognise β-actin were used as loading controls. **(B)** PCRs were performed using cDNA libraries generated from different cell lines. The human tissues, human cell lines (HeLa, HT1080, HFF, HEK293) and mouse cell line (NIH 3T3) are indicated above each panel, the sizes of DNA are indicated on the left side of the panel in base pairs (bps), and the expected PCR product sizes are indicated by arrowheads. Note the low expession of G2L3 in brain tissue and its absence in the HT1080 cell line. Data are representative of three independent experiments.

Figure 3: G2L3 binds and localises to both MT and actin cytoskeletons. **(A,C,D)**, G2L3 constructs were transiently expressed in NIH3T3 cells, followed by fixation and staining using an antibody which recognises α-tubulin (DM1A; (Blose et al., 1984) and phalloidin to label actin. **(A)** G2L3 localises to both filamentous actin (white arrowheads) and MTs cytoskeletons (white arrows); **(B)** G2L3 constructs that were expressed as fusion constructs to GFP or mCherry (mCh) in NIH3T3 cells: **(C)** G2L3-CH (CH) and G2L3-ΔC-term (ΔC-term) localise to F-actin structures; **(D)** G2L3-ΔCH (ΔCH), G2L3-ΔGAR (ΔGAR) and G2L3-C-term (C-term) all localise to MTs and G2L3-GAR (GAR) localises diffusely in the cytoplasm. **(E)** Actin-binding assays were performed using recombinant versions of G2L3-CH (CH) and G2L3-C-term (C-term), showing that the CH domain directly binds F-actin, whereas the C-term does not. **(F)** MT-spin down assays were performed using G2L3-CH (CH) and G2L3-GAR (GAR) as well as G2L3-C-

term (C-term), showing that only G2L3-C-term directly interacts with MTs in vitro. Both immunofluorescence and binding assay data are representative of three independent experiments. Bars, 10μm.

Figure 4: The individual domains of G2L3 influence the binding strength to microtubules and actin. To assess the turnover of indicated proteins in NIH3T3 cells, circular areas of 1.5-μm diameter were bleached, and recovery was measured. **(A)** FRAP experiments performed on the actin localising constructs. Note the slower fluorescence recovery of bleached areas in G2L3-CH (CH) expressing cells and much faster recovery in G2L3-ΔC-term expressing cells compared to areas in G2L3 expressing cells. **(B)** FRAP experiments peformed on MT localising constructs. Note the similar fluorescence recovery of bleached areas in cells expressing G2L3 and G2L3-ΔCH. Conversely, the fluorescence recovers faster in the bleached areas in G2L3-ΔGAR and G2L3-C-term expressing cells. Either the prebleach (PRE) or the time in seconds is indicated in the bottom right hand corner of each image, and the encircled areas indicate the bleach regions. **(C)** The $t_{½}$s of recovery of the actin binding constructs are labelled in red, and the MT binding constructs in blue. Note the $t_{½}$ of recovery of G2L3-CH is almost double that of G2L3, and the $t_{½}$ of recovery of G2L3-ΔC-term is much faster than G2L3. In accordance with (B), the $t_{½}$ of recovery of G2L3-ΔCH is similar to G2L3, whereas G2L3-ΔGAR and G2L3-C-term have much faster $t_{½}$s of recovery. Data represent the results from more than n=20 bleach regions from n=10 cells.

Figure 5: The integrity of neither actin, nor MTs is a prerequisite for G2L3 localisation to MTs or actin cytoskeletons, respectively. **(A)** NIH3T3 cells expressing G2L3 were either treated with 10μM nocodazole (NOC) or 2μM cytochalasin D for 30 mins (CYTO D) to determine their effects on G2L3 localisation. Note that G2L3 can localise to stable MTs (white arrows) and actin filaments (white arrowheads) after NOC treatment. Whereas G2L3 predominantly localises to MTs (white arrows) after treatment of cells with CYTO D. **(B)** The sub-cellular localisation of G2L3 in cells was quantified after treatment with nocodazole or cytochalasin D. Note that G2L3 localises diffusely in a greater proportion of cells after NOC treatment, whereas G2L3 localises to MTs in more cells after CYTO D treatment. More than 50 cells were counted for each treatment.

Figure 6: Post-translational acetylation of tubulin enhances G2L3 localisation to MTs. **(A)** NIH3T3 cells expressing G2L3-GFP were treated with trichostatin A (TSA), and were fixed and costained using antibodies directed against α -tubulin (DM1A) and acetylated α -tubulin (6-11B-1, (LeDizet and Piperno, 1991)). **(B)** G2L3 and MT images were passed through a FFT-2D bandpass filter and background subtracted. The resulting image was thresholded to MTs, and the cell outline drawn. Following which, the area fraction for G2L3 positive pixels and MTs were recorded, and the ratio between G2L3: MTs was calculated. **(C)** The enhancement of G2L3 to MTs was quantified as in (B), to show that G2L3 localisation was enhanced to MTs after treatment of TSA. More than 50 cells were counted for each condition, ($p<0.01$, student's t-test).

Figure 1: Schematic representation of the intron-exon boundaries of the G2L3 gene and the sequence alignments of the human GAS2 protein family.

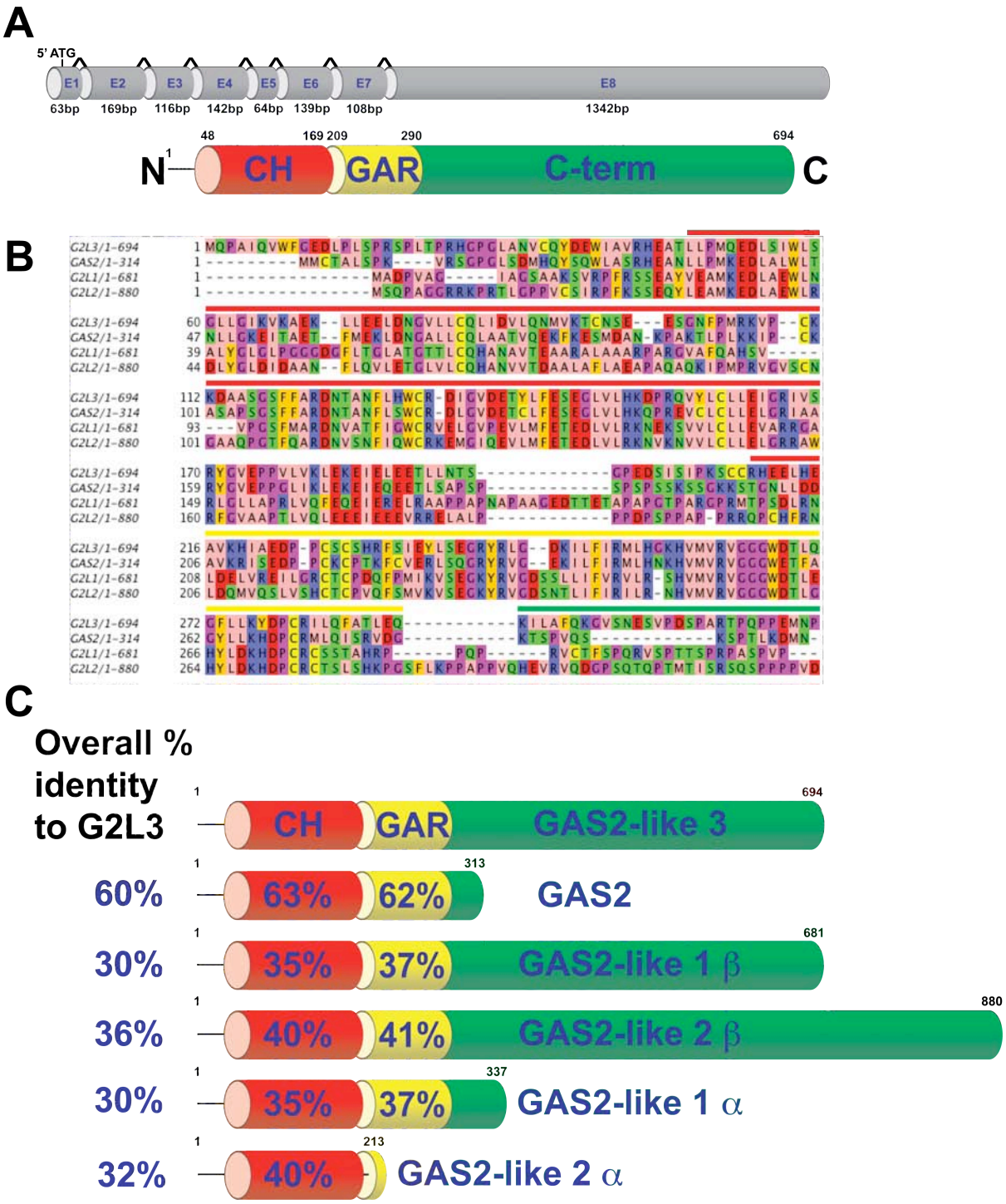

Figure 2: G2L3 is expressed ubiquitously in human tissues and cell lines.

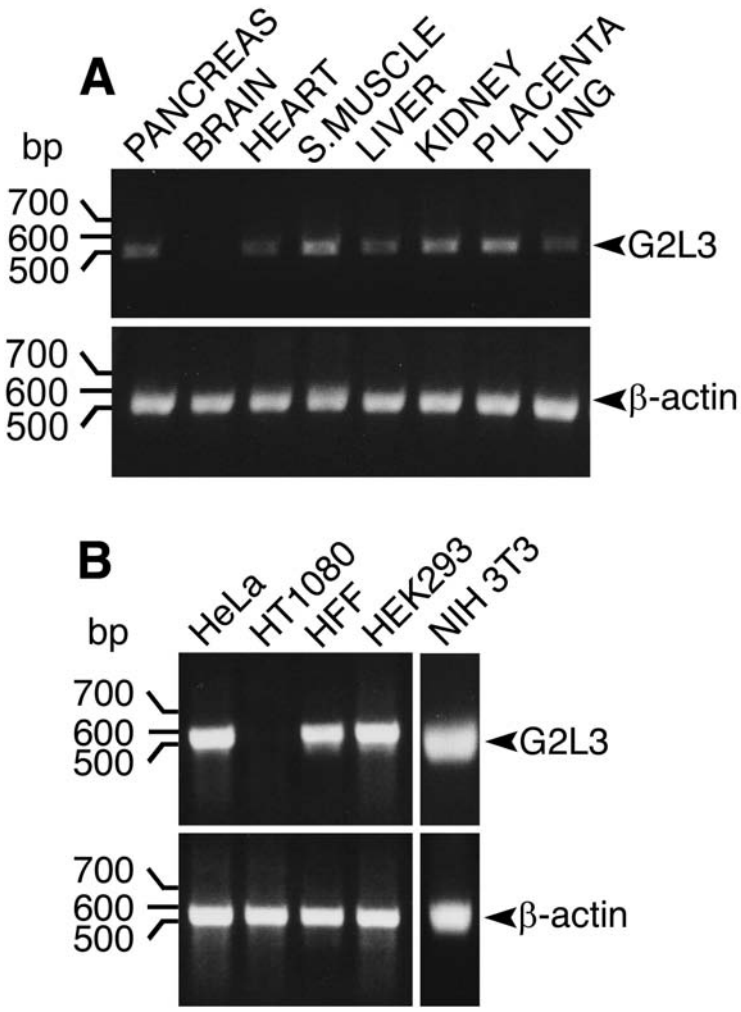

Figure 3: G2L3 binds and localises to both MT and actin cytoskeletons.

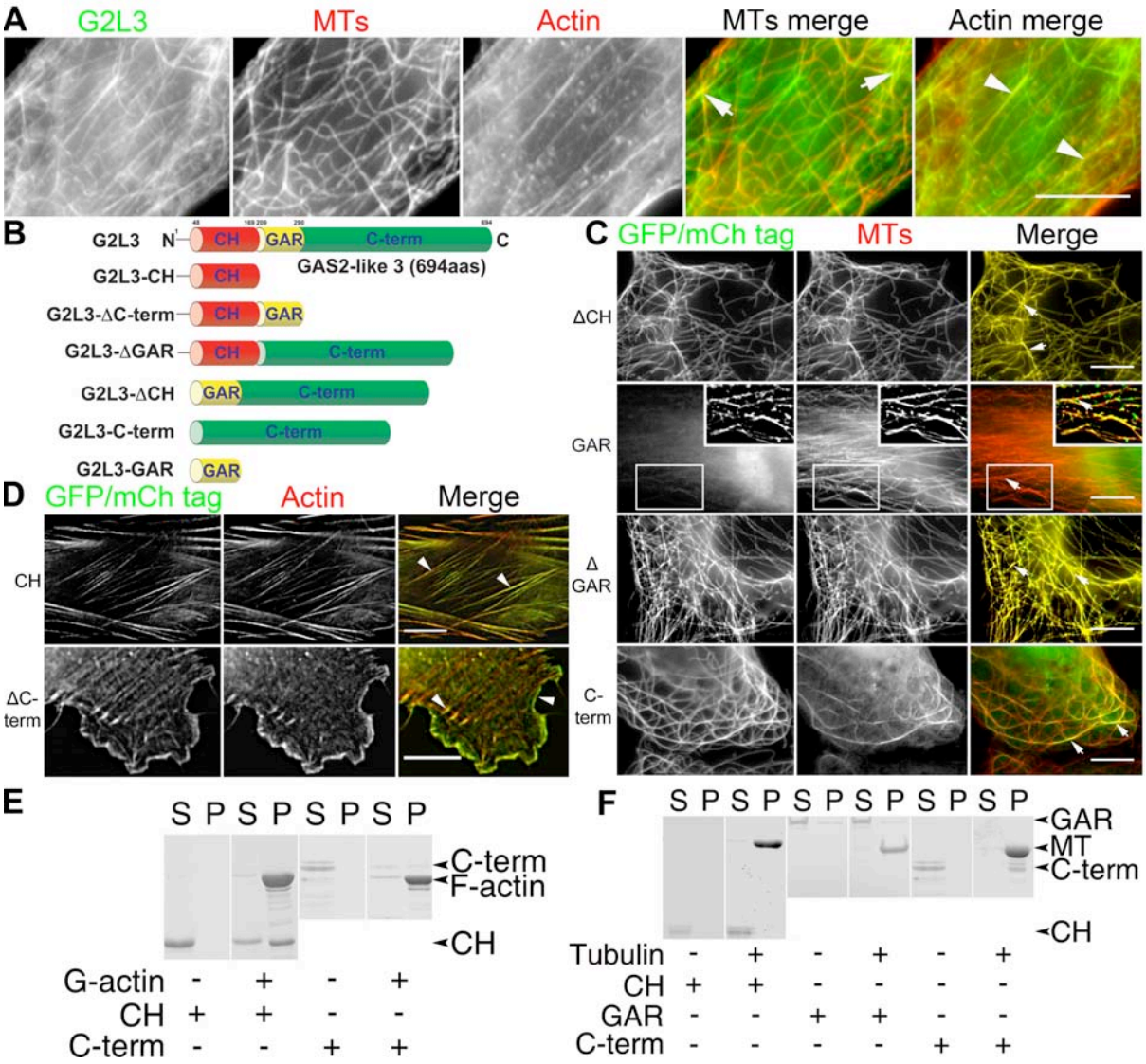

Figure 4: The individual domains of G2L3 influence the binding strength to MTs and actin

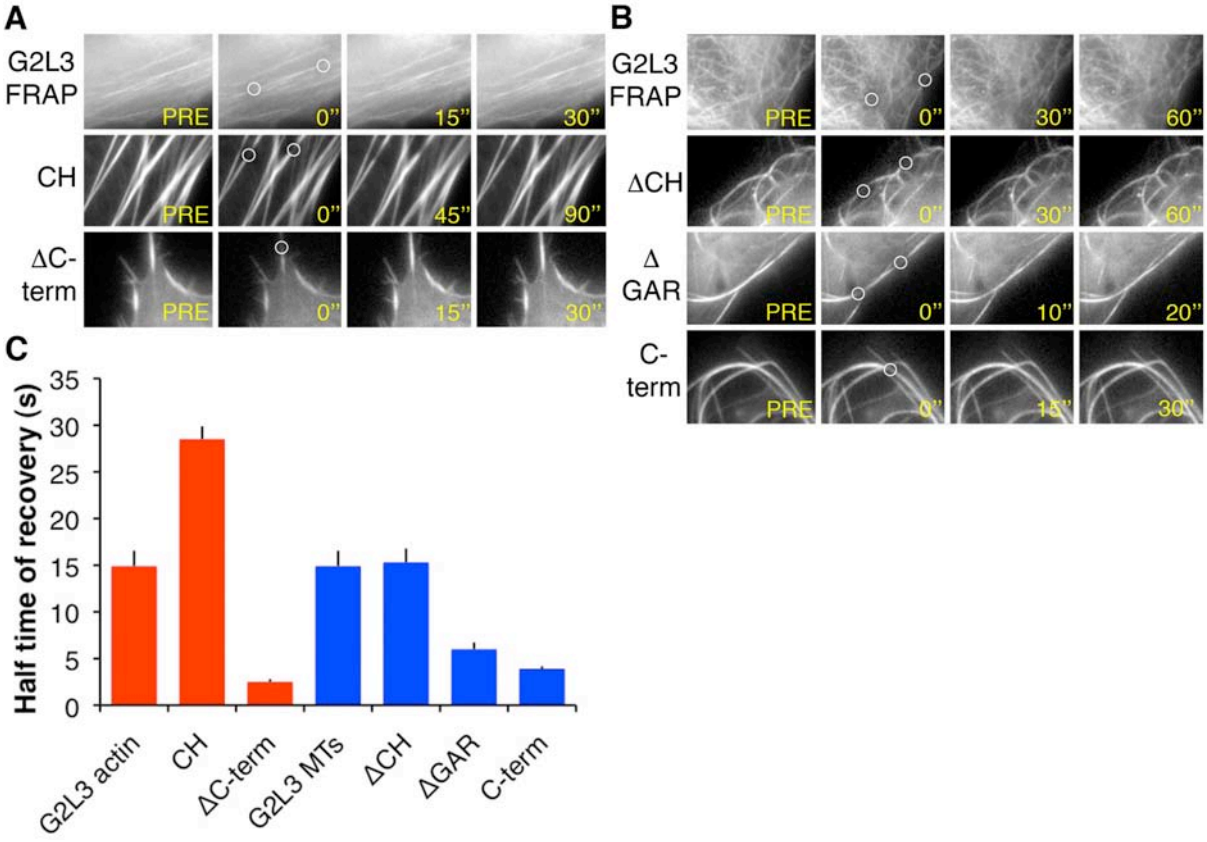

\

Figure 5: The integrity of neither actin, nor MTs is a prerequisite for G2L3 localisation to MTs or actin cytoskeletons, respectively.

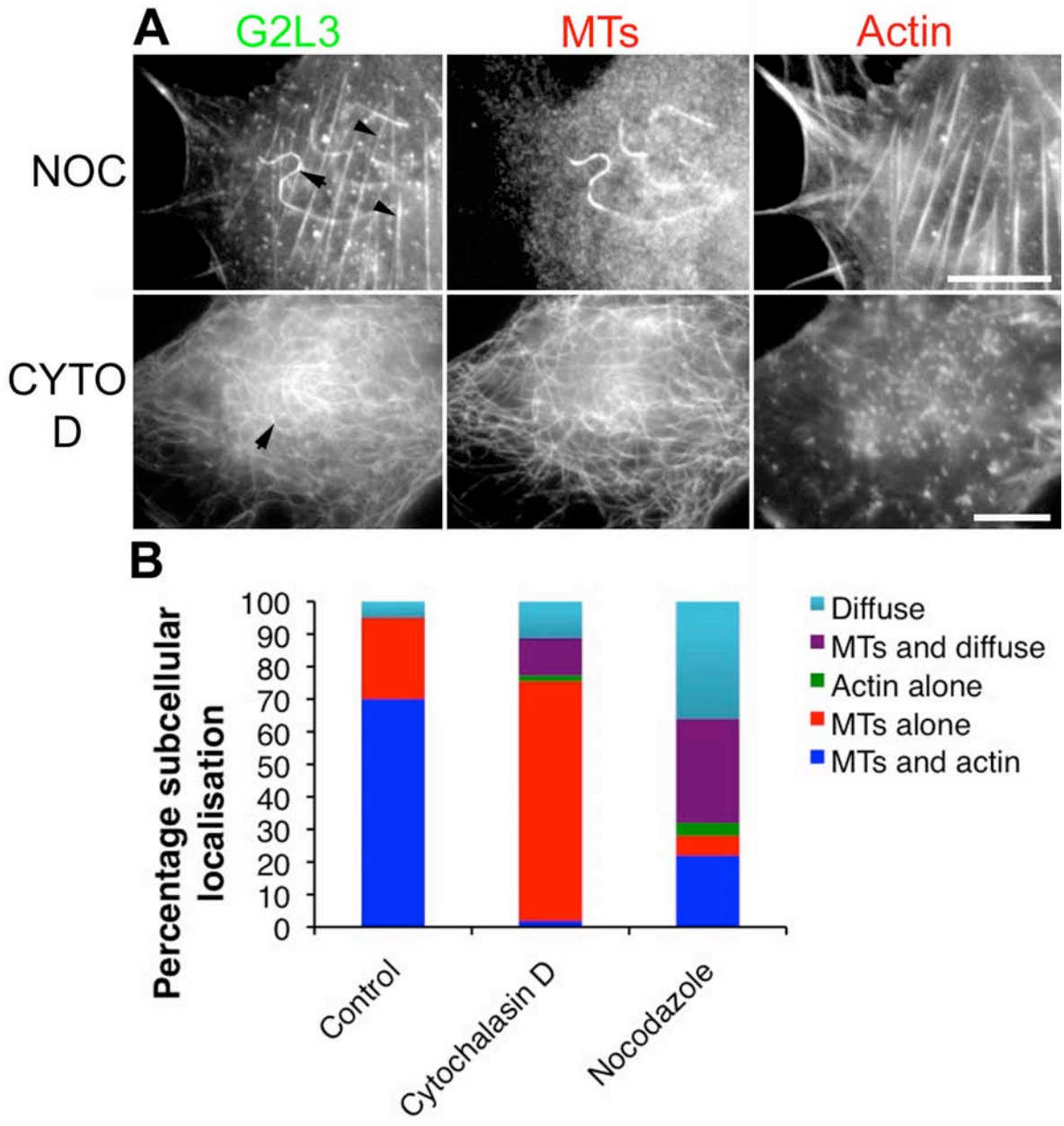

Figure 6: Post-translational acetylation of tubulin enhances G2L3 localisation to MTs.

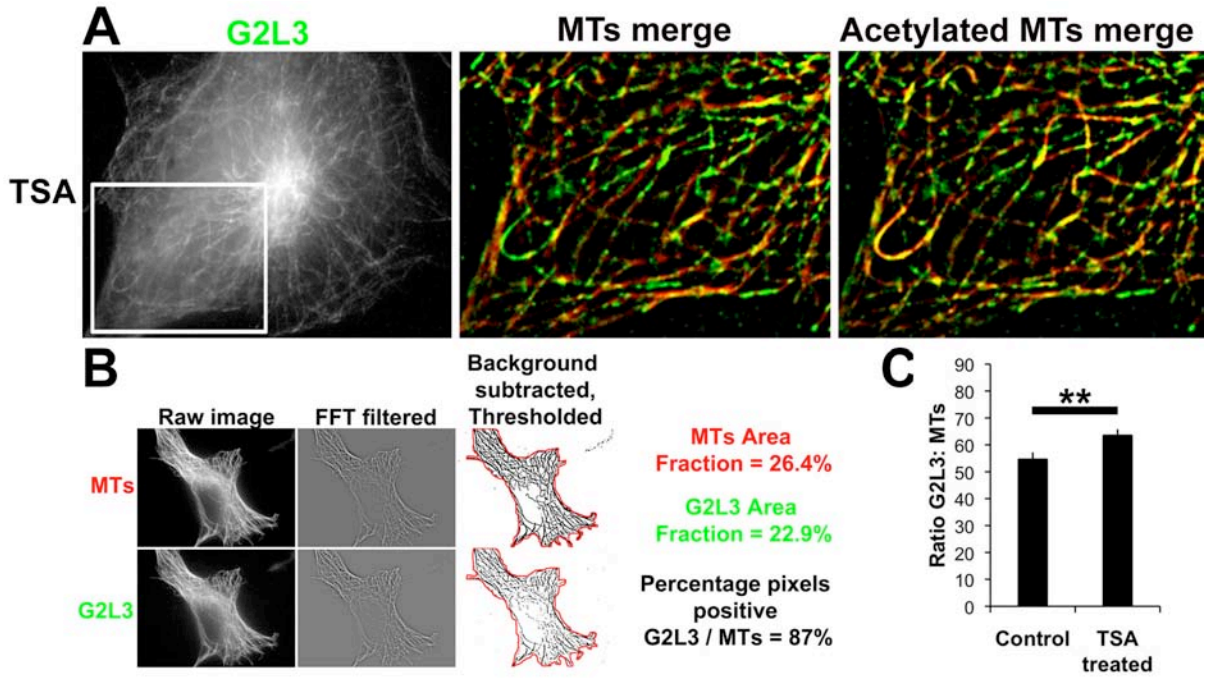

Supplementary Figure Legends:

Supplementary Figure 1: Percentage identities between other family members. The percentage identities between GAS2 and G2L1 and the other GAS2 family members are indicated, as well as the percentage identities between the various domains.

Supplementary Table 1: Listing the percentage identity of the CH and GAR domains combined between hG2L3 and its homologues. Note the conservation of G2L3 between species, and that its zebrafish homologue exhibits 65% amino acid identity.

Supplementary Movie 1: Deconvolved stack of NIH 3T3 cells expressing G2L3-CH. NIH3T3 cells expressing G2L3-CH (green) were fixed and stained for MTs (blue) and F-actin (red). Image stacks were taken through the z-axis every 0.2μm, and were deconvolved using Deconvolve 3D software (Applied precision, Preston, UK). Playback of the deconvolved stack is at 8 frames per second.

Supplementary Movie 2: Deconvolved stack of NIH 3T3 cells expressing G2L3-ΔC-term. NIH3T3 cells expressing G2L3-ΔC-term (green) were fixed and stained for MTs (blue) and F-actin (red). Image stacks were taken through the z-axis every 0.2μm, and were deconvolved using Deconvolve 3D software (Applied precision, Preston, UK). Playback of the deconvolved stack is at 8 frames per second.

Supplementary Figure 1: Percentage identities between other family members

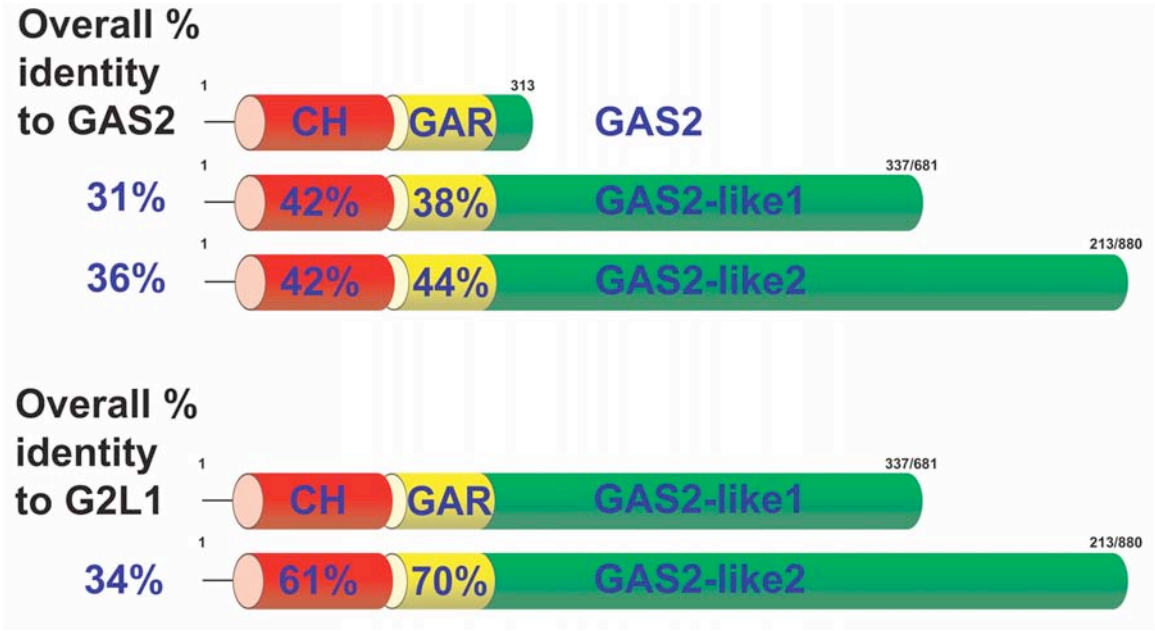

Supplementary Table 1: Listing the percentage identity of the CH and GAR domains combined between hG2L3 and its homologues.

Species	% AA identity to hG2L3
Pan troglodytes (Chimpanzee)	100
Bos taurus (Cow)	96
Mus musculus (Mouse)	93
Rattus norvegicus (Rat)	93
Gallus gallus (Chicken)	87
Danio rerio (Zebrafish)	65

5) Results chapter 3

Functional characterisation of a novel binding partner, end-binding protein 1 (EB1) to GAS2-like 3

Matthew J Stroud, Christoph Ballestrem* and Richard Kammerer*
Wellcome Trust Centre for Cell-Matrix Research, Faculty of Life Sciences, University of Manchester, M13 9PT. UK

*** Correspondence should be addressed to Chistoph Ballestrem or Richard Kammerer**
Wellcome Trust Centre for Cell Matrix Research
Faculty of Life Sciences, University of Manchester
Michael Smith Building, Oxford Road
Manchester, M13 9PT, United Kingdom
Phone: +44 (0) 161-275-1708
Fax: +44 (0) 161-275-1505

Email:
christoph.ballestrem@manchester.ac.uk
richard.kammerer@manchester.ac.uk

Abstract

Proteins involved in mediating the crosstalk between microtubule (MT) and actin cytoskeletons are fundamental to many cellular processes and play important physiological roles. We recently identified and characterised a new member of the spectraplakin superfamily, termed GAS2-like 3. GAS2-like 3 interacts with both MTs and F-actin, thus making it a good candidate to mediate communication between the two cytoskeletons. Here, we show that the MT-binding domain of GAS2-like 3 contains two binding motifs for the MT plus-end binding protein 1, a master regulator of MT dynamics, EB1. We characterise EB1 as a new and bona fide interaction partner of GAS2-like 3, which interacts with the C-terminus of G2L3 with a high binding strength *in vitro*. Furthermore, we describe a molecular mechanism in which EB1 regulates the recruitment of both full-length G2L3 and the C-terminus of G2L3 to MTs in cells. Interestingly we found that the complete C-terminus of G2L3 is required to interact with EB1, rather than the specific EB1 binding motifs themselves.

Introduction

The integrity of microtubule (MT) and actin cytoskeletons is fundamental to cellular integrity, as they provide a molecular framework for both mechanical support and an intracellular transport infrastructure (Li and Gundersen, 2008). As well as the integrity of the cytoskeleton, crosstalk between MTs and actin is essential for normal cellular function. Prominent candidates for this role are the spectraplakins, as they have the ability to crosslink MTs and actin (Kodama et al., 2003; Leung et al., 1999; Wu et al., 2008). Spectraplakins are multi-domain containing proteins with binding sites for both filamentous actin (F-actin) via their calponin homology (CH) domains and MTs via their GAS2-related (GAR) domain and/ or GSR repeats. Knockout studies performed on the mammalian spectraplakin, MT-actin crosslinking factor 1 (MACF1), in mice result in embryonic lethality. Despite this, MACF1 -/- cells can be derived and display defects in MT dynamics, guidance, cortical tethering, stability and cellular polarisation (Kodama et al., 2003). Surprisingly, the expression of a mini-version of MACF1 consisting of the CH and GAR domains is necessary and sufficient to rescue these perturbations in function, implying these are the key functional domains of spectraplakins. Various medical conditions and developmental defects arise as a result of mutations in genes encoding spectraplakins, including mental retardation, cancer and chronic skin blistering (Sonnenberg and Liem, 2007), which displays the underlying importance of proteins that link the actin and MT cytoskeletons.

Related to the spectraplakins, is the GAS2 family, which belong to the spectraplakin superfamily. The GAS2 family consists of four members, namingly; GAS2, GAS2-like 1 (G2L1), GAS2-like 2 (G2L2), and the recently described GAS2-like 3 (G2L3) (Stroud et al., 2010, manuscript submitted). GAS2 members can be thought of as mini-versions of spectraplakins, as they all contain a putative actin binding CH domain, a putative MT-binding GAR domain, however they lack the bulky plakin and spectrin repeats. Thus, members of the GAS2 family are also good candidates to mediate crosstalk between MTs and actin. A study performed on G2L1 and G2L2 (Goriounov et al., 2003), as well as our recent observations for G2L3 support this speculation. We discovered that G2L3 binds to MTs and actin via its carboxy (C)-terminus and CH domain, respectively. In a quarter of all cells analysed, G2L3 exclusively localised to MTs, and we showed that the C-terminus was the driving force behind the localisation to MTs -

(Stroud et al., 2010, manuscript submitted). Interestingly, the C-terminus of G2L3 has no predicted secondary structure, which may mediate structural interactions with MTs, nor any obvious MT-localisation signals, such as cytoskeleton associated protein-Glycine rich (CAP-GLY) domains, tumour overexpressed gene (TOG) domains or WD40-repeats as found in other MT-associated proteins (MAPs) (Akhmanova and Steinmetz, 2008). However, one noticeable factor about the C-terminus of G2L3, is the large number of basic and serine-rich stretches of amino acids. In this regard, the C-terminus of G2L3 is similar to MAPs including the MT plus-end binding proteins (+TIPS), adenopolyposis coli (APC), cytoskeletal-linker protein-associated proteins (CLASPs) and the spectraplakins (Akhmanova and Steinmetz, 2008). It has recently been shown that a stretch of basic and serine-rich residues, incorporating the amino acids Ser/Thr-Xaa-Ile/Leu-Pro, termed the MT-tip localisation signal (MtLS) is important for interactions with MT-end-binding protein 1 (EB1) (Honnappa et al., 2009).

The Drosophila spectraplakin short-stop (Shot) contains two MtLSs at its C-terminus, which interact with EB1. These interactions are hypothesised to be important when Shot is in its inactive form in the cell interior and the growing MT plus-ends are undergoing a 'search and capture' mechanism for an activation signal to engage with actin. Upon activation, Shot undergoes a conformational change to release EB1 and to engage with F-actin via its CH domains, and the MT lattice via its GAR domain. When engaged with both cytoskeletons, Shot stabilises MTs against lateral movements driven by motor proteins, and guides them along F-actin in the cell periphery (Applewhite et al., 2010). This study suggests that Shot only binds EB1 in the cell interior, however, another study suggests that the interaction between the mammalian spectraplakin, MACF1 and EB1 occurs throughout the cytoplasm from the cell interior to peripheral focal adhesions (FAs), and is necessary for the MT-actin crosslinking (Wu et al., 2008). In the latter study, an actin-dependent ATPase activity was identified in MACF1 and was found to be essential to recover defects in cell migration in MACF1 null cells. The ATPase activity of MACF1 is thought to be essential to target MTs to FAs for remodelling, which is fundamental for effective cell migration.

While the specific mechanisms of action of these proteins remain to be resolved, it is well established that both of these spectraplakins can interact with EB1

through their MtLSs. The MtLS is thought to be key in mediating the interaction between a wide variety of binding partners and the EB-homology domain of EB1 (Honnappa et al., 2009; Honnappa et al., 2005).

Further examination of the C-terminus of G2L3 revealed that similarly to spectraplakins, G2L3 also contains two MtLSs used by spectraplakins to interact with EB1. Subsequently, we found that all members of the human GAS2 family contain one or more copies of the MtLS. Using G2L3 as a model protein of the GAS2 family, we tested whether EB1 can interact with G2L3 and used this model to resolve a number of other underlying questions including: 1) Does the C-terminus of G2L3 interact with EB1 directly? 2) If so, can EB1 regulate the localisation of G2L3 to MTs, and 3) which part of the C-terminus is required for this interaction?

In this study we reveal that G2L3 contains 2 MtLSs (SKLP and TLLP) on its C-terminus, which contribute to its interaction with EB1 directly *in vitro* and in cells. We uncover a molecular mechanism in which this interaction with EB1 drives G2L3 localisation to MTs in cells, and that the C-terminus can partially tip-track at the plus ends of MTs. Furthermore we identify that the whole of the C-terminus is required for the interaction with EB1.

Results

Expression and purification of the GAS2-like 3 and End Binding Protein 1 C-termini

Sequence analysis of the G2L3-C-terminus (G2L3-C-term) revealed two MTLSs (SKLP and TLLP), as highlighted in Figure 1A. In order to verify whether G2L3-C-term interacts with EB1, we expressed both proteins recombinantly in E. coli. We expressed G2L3-C-term as a 6X-Histidine-thioredoxin fusion protein, in order to allow purification and increase the solubility of the protein, respectively (Kammerer et al., 1998). The C-terminus of EB1 was expressed as a GST-fusion protein (termed GST-EB1-C-T), containing a coiled-coil (CC) region abutted to the EB-homology domain (EBH), which is thought to bind to MtLSs (Figure 1B) (Honnappa et al., 2009).

Initial attempts to express G2L3-C-term at 37°C in JM109 (DE3) E. coli produced low amounts of full-length G2L3-C-term, and high amounts of degradation products. We accounted for the large amounts of degradation products as G2L3-C-term has no predicted secondary structure, thus can be readily cleaved by proteases (data not shown). To try and minimise the degradation products, we expressed G2L3-C-term in BL21-CodonPlus (DE3) E. coli, which are deficient in the Lon and OmpT proteases and can cleave recombinant proteins. These bacteria also contain extra copies of the argU, ileY and leuW tRNA genes, which helped to overcome the problem of expressing the rare-codon containing G2L3-C-term. This significantly increased the amount of full-length G2L3-C-term expressed, enabling us to use it for the subsequent experiments (Figure 1C).

Conversely, we were able to express GST-EB1-C-T in large amounts, owing to its high solubility. The GST fusion was subsequently cleaved at an engineered thrombin cleavage site to produce EB1-C-term. The high degree of solubility and lack of degradation imply this protein was correctly folded (Figure 1C).

The C-terminus of GAS2-like 3 interacts directly with End Binding Protein 1 *in vitro* with high binding strength

In order to test whether G2L3-C-term interacts with EB1, we performed glutathione-S-transferase (GST) pulldown assays using GST-EB1-C-T as bait. We found that GST-EB1-C-T specifically pulls down G2L3-C-term, as they co-elute in the elution fraction (Figure 2A). In contrast, G2L3-C-term is not pulled-

down when incubated with glutathione beads alone, which shows that the interaction is specific for EB1. To validate the pull-down data and obtain an estimation of the binding strength, we performed solid phase binding assays (SPBAs). When G2L3-C-term was plated, a large increase in binding of GST-EB1-C-T was observed at very low concentrations, which reached a plateau at 27nM and gave an estimate of kd of 2.1nM (Figure 2B). We also performed the reciprocal SPBA by plating EB1-C-term, and found that it also interacts with a high binding strength (estimated kd=77nM) (data not shown).

These data suggest that G2L3-C-term and EB1-C-term interact *in vitro* with a high binding strength. It is interesting to note that the estimated kd is 1000-fold higher than the levels for other EB1-interacting proteins. This may be due to the presence of two EB1-binding motifs rather than one, which aids cooperative binding.

End Binding Protein 1 enhances localisation of GAS2-like 3 to microtubules

To investigate the function of the interaction between EB1 and G2L3 in cells, we co-expressed them in cells in order to determine whether G2L3 localisation was affected. We observed a dramatically enhanced recruitment of G2L3 to MTs (Figure 3A). We found this effect was specific for EB1, as we did not observe a shift of G2L3 localisation when MTs were artificially stabilised using taxol, compared to control cells (Figure 3A). Interestingly, the varying expression levels of EB1 did not appear to affect G2L3 localisation (data not shown). To quantify the enhanced localisation, we first passed the raw image of either G2L3 or MTs through a Fast Fourier Transform Bandpass Filter, followed by subtracting the background and thresholding the image to MTs (Figure 3B). Each cell was subsequently outlined, and the area fraction was measured, which gives the percentage positive pixels for the thresholded area. The area fraction value for the G2L3 image was divided by the corresponding value for the MT image to obtain a ratio of positive pixels (Figure 3B). This ratio was significantly higher ($p<0.001$ using the student's t-test) for EB1 cotransfected cells (0.74) than G2L3 expressing control cells (0.48) or G2L3 expressing cells treated with taxol (0.49) (Figure 3C).

These data suggest that EB1 specifically governs G2L3 localisation in cells, and this spatial regulation may control G2L3 function.

The localisation of the GAS2-like 3 C-terminus is regulated by End Binding Protein 1 and shows evidence of tip-tracking

To demonstrate the interaction of G2L3 with EB1 was mediated by the G2L3-C-term in cells, we co-expressed G2L3-C-term and EB1 in cells. Similarly to the result for G2L3, we observed a dramatic enhancement of G2L3-C-term to MTs (Figure 4A). As for G2L3, this effect was specific for EB1, and the ratio of positive pixels G2L3-C-term : MTs, (0.71) was significantly enhanced compared to control (0.58) or taxol treated cells (0.56) ($p<0.001$, student's t-test) (Figure 4B).

Other proteins that interact with EB1 have been shown to tip-track at the plus ends of MTs (Applewhite et al., 2010; Wu et al., 2008). To determine whether G2L3-C-term can tip-track we performed live cell imaging on cells expressing both G2L3-C-term and EB1. We found evidence that G2L3-C-term can tip-track distal to EB1, however this was not as robust as EB1 tip-tracking (Figure 4C). This may be due to the additional direct interaction of G2L3-C-term with MTs (Stroud et al., 2010, manuscript submitted).

These data suggest that G2L3 interacts with EB1 through its C-terminus in cells, driving it to MT plus-ends where it may interact with other +TIPs.

The complete GAS2-like 3 C-terminus is required to interact with EB1

In order to elucidate the key amino acids which mediate the interaction of G2L3 with EB1, we generated two G2L3-C-term mutants in which the EB1-binding motifs were either included or excluded to perform localisation and pull-down experiments (Figure 5A). Two mutants were synthesised to encode either the first half of G2L3-C-term (termed G2L3-CT1), which contains both MtLSs, or the second half, which lacks the MtLSs (termed G2L3-CT2). As a proof of principle, G2L3-C-term localised to MTs and was pulled down from cell lysates using GST-EB1-C-T (Figures 5B and C). Conversely, neither of the truncation mutants G2L3-CT1 and G2L3-CT2 localised to MTs in cells (Figure 5B), furthermore neither were pulled down using GST-EB1-GST (Figure 5C).

These data suggest that the whole of the C-terminus of G2L3 is required in order to interact with EB1. It is plausible that an as-of-yet unidentified EB1 binding site is abrogated by splitting the C-terminus into its two constituent halves.

Discussion

Here we have characterised the MT plus-end binding protein, EB1, as a new binding partner of the MT-actin binding protein, G2L3. EB1 directly interacts with the C-terminus of G2L3 and regulates the recruitment of G2L3 to MTs. We show that the complete C-terminus is required for binding to EB1 rather than the specific EB1-binding motifs themselves.

G2L3 shares a high degree of similarity to the spectraplakins, we thereby classified it as a new member of the spectraplakin superfamily (Stroud et al., 2010, manuscript submitted). There is a notable resemblance between the C-termini of G2L3 and spectraplakins, as they all contain putative EB1 binding sites. The human, mouse, and Drosophila spectraplakins, MACF1, ACF7 and Shot, respectively, all interact with EB1 via their C-termini (Applewhite et al., 2010; Kodama et al., 2003; Slep et al., 2005). However, they display subtle differences in sub-cellular localisation to the C-terminus of G2L3.

Both the C-terminus of the Drosophila homologue, Shot, as well as full-length Shot localise to MT plus-ends and can robustly tip-track (Applewhite et al., 2010). The MtLSs in Shot are crucial for this interaction with MTs and for plus-end tracking, presumably via EB1. In contrast to Shot, we found that the two MtLSs in G2L3 were neither essential for MT localisation nor EB1-interaction. In fact G2L3 requires the entirety of its C-terminus for both MT localisation and EB1 interaction. To explain this we propose the following scenarios: The first of which could be that phosphorylation of serine or threonine residues in the vicinity of the MtLSs inhibits the interaction with EB1. In support of this, both the MtLSs on G2L3 are surrounded by putative phosphorylation sites for glycogen synthase kinase 3β (GSK3β). GSK3β is known to phosphorylate the plus-tips, APC and the CLASPs (Akhmanova and Steinmetz, 2008), which abrogates their localisation to MTs, presumably by inhibiting their interaction with EB1 (Honnappa et al., 2009). Therefore, it is possible GSK3β phosphorylated the G2L3-CT1 and G2L3-CT2 mutants at different levels, to modulate their binding strength to EB1. Alternatively, splitting the C-terminus into two halves could destroy an unidentified EB1 binding motif. Whereas the roles of MtLSs in binding to EB1 have been well documented, other uncharacterised EB1-binding motifs exist. For example, diaphanous-related formin, mDia2, binds to EB1 via an unknown mechanism (Wen et al., 2004). In concomitance with mDia2, it is

apparent that some EB1-binding motifs remain elusive and their elucidation will require further investigation.

We speculated previously that G2L3 may serve to guide MTs along actin stress fibers and target them to focal adhesions (FAs) (Stroud et al., 2010, manuscript submitted), as is observed for the spectraplakin, ACF7 (Wu et al., 2008). This guidance would be mediated by a static interaction between the F-actin and MTs via its CH domain and C-terminus, respectively. However, one caveat of this static cross-linking is the explanation of how MTs are targeted to FAs, which are constantly moving away from actin stress fibers? We now have evidence to support a dynamic interaction between G2L3 and MT plus-ends via EB1, which would enable G2L3 to target MTs to FAs and subsequently regulate their turnover. As well as a possible role in regulating FA dynamics and cell migration during interphase, the interaction with EB1 opens a plethora of possible functions, including regulation of the kinetochore during mitosis (Tirnauer et al., 2002). The high number of putative phosphorylation sites in the C-terminus suggests that phosphorylation of G2L3 may regulate its interaction with EB1. Further work will be necessary to establish whether G2L3 localisation is dependent on phosphorylation, and the functional significance of the interaction between G2L3 and EB1.

Materials and Methods

Cell Culture and Transfections

All cells were grown in DMEM (Sigma Aldrich, Dorset, UK) supplemented with 10% FBS, and 1% glutamine in a 5% CO2 in a humidified incubator, and passaged in a 1:10 dilution every 3 days. For transfections, cells were plated in 6-well dishes (for immunofluorescence) or 10cm petri dishes (for large scale) a day before transfections. For small and large-scale transient transfections, 1-1.5µg or 8µg of DNA respectively, was transfected into cells using Lipofectamine Plus (Invitrogen, Paisley, UK) in accordance with manufacturer's instructions. For immunofluorescence, cells were replated after 3-4 hours in glass-bottomed dishes (MatTek Corporation, Ashland, USA) coated with 10 µg/mL bovine fibronectin (pFN; Sigma). For treatment with taxol, cells were incubated for 30 mins with 10µM paclitaxel (Sigma). For pulldown experiments, cells were washed thrice in PBS, and once in complete DMEM, and left overnight before lysis the following day.

Fixed immunofluorescence Imaging

Cells were fixed and permeabilised with 3% paraformaldehyde (Sigma) containing 0.25% Triton X-100 (Sigma) and 0.05% glutaraldehyde (Sigma) for 15 mins, before being washed in PBS (Lonza, Verviers, Belgium). Autofluorescence from reactive amine groups was quenched using 0.01% sodium tetrahydroborate (Sigma) in PBS for 15 mins before being washed in PBS. Subsequently cells were incubated for 45 mins with anti-tubulin at 1:500 dilution (DM1A, Sigma), followed by three washes with PBS. Secondary antibodies conjugated to either Cy2, 3 or 5 (Jackson ImmunoResearch Laboratories, Suffolk, UK) were then applied for 30 mins. In the case of colabelling for actin, Texas Red or FITC-labelled phalloidin (Invitrogen) was added together with the secondary antibody). Cells were then washed three more times in PBS before being imaged using an oil-immersed 100X objective, with 1.35 numerical aperture on an inverted microscope (IX71; Olympus) controlled by a Deltavision system (Applied Precision, Washington, USA). Images were captured using a Coolsnap HQ CCD camera (Princeton Instruments, Lurgan, UK).

Live-cell Imaging

Cells were washed thrice in PBS, and DMEM was replaced with pre-warmed Ham's F12 medium supplemented with 25mM HEPES, 1% L-glutamine, 1% penicillin/ streptomycin and the pH was adjusted to 7.3 with NaOH. Cells were imaged using an oil-immersed 100X objective, with 1.35 numerical aperture (NA) on an inverted microscope (IX71; Olympus) controlled by a Deltavision system (Applied Precision, Washington, USA). Movies were captured using a Coolsnap HQ CCD camera (Princeton Instruments, Lurgan, UK).

Image Processing

Images were processed using ImageJ version 1.43R. For colocalisation studies and calculation of the ratio of G2L3 / MTs for EB1 analysis, images were background subtracted using a FFT-2D-bandpass filter, overlay images were created. From these a threshold was set to restrict analyses to MTs, and the outline of the cell was drawn followed by measuring the percentage area of positive pixels. This was repeated for G2L3 and divided by the value given for MTs to give a ratio theoretically between zero and one. Adobe Photoshop CS4 was used in the preparation of figures for this manuscript.

Sub-cloning

For immunofluorescence, G2L3 and G2L3-C-T were cloned into pEGFP-N1 or mCherry-N1 vectors (Clontech) using the restriction endonucleases NheI and HindIII at the amino acids indicated in Figure 1A. G2L3-C-T was also cloned into pEGFP-C1 vector (Clontech) using the restriction endonuclease BamHI. EB1-GFP was a kind gift from Shoichiro Tsukita's lab. For recombinant expression in E. coli, G2L3-C-T and GST-EB1-C-T were cloned into the pHisTrx and pHisGST vectors, respectively (Kammerer et al., 1998) using either the restriction endonucleases BamHI or EcoRI and BamHI, respectively. All recombinant insert DNA was verified by DNA sequencing.

Protein expression and purification

The recombinant GST-EB1-C-T and G2L3-C-T constructs were expressed in E. coli JM109 (DE3) host strain (Merck Biosciences) and BL21 CodonPlus (DE3) host strain (Stratagene, UK), respectively, as previously described (Kammerer et

al., 1995) using an autoinduction protocol (as described by (Studier, 2005)). The 6xHis-tagged G2L3-C-T was purified by immobilised metal affinity chromatography on Ni2+-Sepharose (GE Healthcare). The GST-tagged EB1-C-T was purified similarly, except using glutathione-coated Sepharose beads (GE Healthcare). Purification was performed under denaturing condition using 8 M urea as described in the pET system manual (Merck Biosciences). Removal of the GST tag by thrombin was performed as previously described (Kammerer et al., 1995). Determination of protein concentration was achieved by the absorbance of tryptophan and tyrosine residues at 280 nm (Edelhoch, 1967).

Glutathione S-Transferase pull-down assay using recombinant proteins

G2L3-C-T was incubated in a 1.5X molar excess with GST-EB1-C-T in PBS containing 40mM EDTA. Glutathione-coated Sepharose beads (GE Healthcare) were resuspended with PBS containing GST-EB1-C-T (positive control), G2L3-C-T (negative control) or their respective combination. After incubation, the beads were washed five times in PBS and the proteins eluted by being boiled in 2X SDS-loading buffer for 10 mins. These were then analysed on a 15% SDS-PAGE gel.

Solid Phase Binding Assay

Wells of Costar high binding microtitre plates (Corning Costar, UK) were coated with purified G2L3-C-T at 10µg/mL. Wells were blocked with blocking buffer [5% BSA (w/v) in PBS], followed by 3 washes with 200 µL washing buffer [0.1% BSA (w/v) in PBS]. Wells were incubated at the indicated concentrations of EB1-GST or GST (control) and washed 3X. Mouse-α-GST antibodies (500ng/mL) (GE Healthcare) were added to wells followed by 3 further washes. GST-binding proteins were detected using horseradish peroxidase (HRP)-conjugated anti-mouse antibody (Jackson Immunoresearch) diluted 1:5000 in wash buffer. Wells were washed 4 times before the addition of ABTS substrate [0.55mg/mL 2,2'-azino-bis(3-ethylbenzthiazoline-6-sulfonic acid), 0.0026% (v/v) H_2O_2 , 0.1M sodium acetate and 50mM NaH_2PO_4, pH5.0]. Absorbance readings at 405nm were measured using a Powerwave 340 multiscan plate reader (Biotek, USA). Each experimental condition was assayed in at least three replicate wells and background attachment to BSA-blocked wells subtracted from all measurements.

Means and standard error of the means were calculated for each experimental condition using Microsoft Excel 2003 (Microsoft, USA). Graphs were plotted and binding affinities estimated using the Hill equation function on Origen Pro 8 (OriginLab, Northampton, USA).

Glutathione S-Transferase pull-down assay from cell lysates

COS cells were washed with PBS and trypsinised. They were subsequently centrifuged and lysed in 500µL ice cold lysis buffer (1% NP40, 50mM Tris pH7.4, 120mM NaCl, 2.5mM EGTA pH 7.4, 10mM MgCl, supplemented with 2X protease inhibitor cocktail solution). Lysates were passed 10X through a 27G needle, and centrifuged in a precooled centrifuge at 4°C for 15mins at 800g in order to remove the insoluble fraction. An aliquot of the supernatant was taken and placed in SDS-loading buffer as the total cell lysate, the remaining supernatant was precleared with Glutathione-coated Sepharose beads (GE Healthcare) for one hour at 4°C, followed by centrifugation at 2000g and aspiration of the supernatant. During preclearing, washed Glutathione-coated Sepharose beads were incubated with either Glutathione S-Transferase (GST) conjugated-EB1 or GST alone (control) in order to attach the bait protein to the bead. After preclearing, the EB1-GST or GST coated beads were washed thrice in PBS containing 0.01% Tween 20 (PBS-T), and were resuspended in the precleared lysate, and rotated for an hour at 4°C. The samples were centrifuged at 2000g, and an aliquot of the unbound fraction was taken. The beads were subsequently washed 4 times in PBS-T and the bound proteins were eluted from the beads in 2X SDS-loading buffer at 100°C for 10 mins. The individual fractions were then separated by SDS-PAGE and analysed by immunoblotting, using an anti-GFP antibody (1:1000, Roche)

Statistical analysis

Using the ratios obtained from the image processing, Student's t-tests were performed using Microsoft Excel to compare the ratios of G2L3 expressing control cells, taxol treated G2L3 expressing cells, and EB1 with G2L3 co-expressing cells.

References

Akhmanova, A. and Steinmetz, M. O. (2008). Tracking the ends: a dynamic protein network controls the fate of microtubule tips. *Nat.Rev.Mol.Cell Biol.* **9**, 309-322.

Applewhite, D. A., Grode, K. D., Keller, D., Zadeh, A., Slep, K. C. and Rogers, S. L. (2010). The spectraplakin Short stop is an actin-microtubule cross-linker that contributes to organization of the microtubule network. *Mol Biol Cell* **21**, 1714-24.

Blose, S. H., Meltzer, D. I. and Feramisco, J. R. (1984). 10-nm filaments are induced to collapse in living cells microinjected with monoclonal and polyclonal antibodies against tubulin. *J Cell Biol* **98**, 847-58.

Edelhoch, H. (1967). Spectroscopic determination of tryptophan and tyrosine in proteins. *Biochemistry* **6**, 1948-54.

Goriounov, D., Leung, C. L. and Liem, R. K. (2003). Protein products of human Gas2-related genes on chromosomes 17 and 22 (hGAR17 and hGAR22) associate with both microfilaments and microtubules. *J.Cell Sci.* **116**, 1045-1058.

Honnappa, S., Gouveia, S. M., Weisbrich, A., Damberger, F. F., Bhavesh, N. S., Jawhari, H., Grigoriev, I., van Rijssel, F. J., Buey, R. M., Lawera, A. et al. (2009). An EB1-binding motif acts as a microtubule tip localization signal. *Cell* **138**, 366-376.

Honnappa, S., John, C. M., Kostrewa, D., Winkler, F. K. and Steinmetz, M. O. (2005). Structural insights into the EB1-APC interaction. *EMBO J* **24**, 261-269.

Kammerer, R. A., Antonsson, P., Schulthess, T., Fauser, C. and Engel, J. (1995). Selective chain recognition in the C-terminal alpha-helical coiled-coil region of laminin. *J Mol Biol* **250**, 64-73.

Kammerer, R. A., Schulthess, T., Landwehr, R., Lustig, A., Fischer, D. and Engel, J. (1998). Tenascin-C hexabrachion assembly is a sequential two-step process initiated by coiled-coil alpha-helices. *J.Biol.Chem.* **273**, 10602-10608.

Kodama, A., Karakesisoglou, I., Wong, E., Vaezi, A. and Fuchs, E. (2003). ACF7: an essential integrator of microtubule dynamics. *Cell* **115**, 343-354.

Leung, C. L., Sun, D., Zheng, M., Knowles, D. R. and Liem, R. K. (1999). Microtubule actin cross-linking factor (MACF): a hybrid of dystonin and

dystrophin that can interact with the actin and microtubule cytoskeletons. *J Cell Biol.* **147**, 1275-1286.

Li, R. and Gundersen, G. G. (2008). Beyond polymer polarity: how the cytoskeleton builds a polarized cell. *Nat.Rev.Mol.Cell Biol.* **9**, 860-873.

Slep, K. C., Rogers, S. L., Elliott, S. L., Ohkura, H., Kolodziej, P. A. and Vale, R. D. (2005). Structural determinants for EB1-mediated recruitment of APC and spectraplakins to the microtubule plus end. *J Cell Biol.* **168**, 587-598.

Sonnenberg, A. and Liem, R. K. (2007). Plakins in development and disease. *Exp.Cell Res.* **313**, 2189-2203.

Stroud, M. J., Ballestrem, C. and Kammerer, R. A. (2010). GAS2-like 3 is a new member of the spectraplakin superfamily and interacts with both microtubules and actin. *Manuscript submitted to the Journal of Cell Science*.

Studier, F. W. (2005). Protein production by auto-induction in high density shaking cultures. *Protein Expr.Purif.* **41**, 207-234.

Tirnauer, J. S., Canman, J. C., Salmon, E. D. and Mitchison, T. J. (2002). EB1 targets to kinetochores with attached, polymerizing microtubules. *Mol Biol Cell* **13**, 4308-16.

Wen, Y., Eng, C. H., Schmoranzer, J., Cabrera-Poch, N., Morris, E. J., Chen, M., Wallar, B. J., Alberts, A. S. and Gundersen, G. G. (2004). EB1 and APC bind to mDia to stabilize microtubules downstream of Rho and promote cell migration. *Nat.Cell Biol.* **6**, 820-830.

Wu, X., Kodama, A. and Fuchs, E. (2008). ACF7 regulates cytoskeletal-focal adhesion dynamics and migration and has ATPase activity. *Cell* **135**, 137-148.

Figure Legends

Figure 1: Schematic representation of GAS2-like3 (G2L3) and end-binding protein 1 (EB1). **(A)** G2L3 consists of a calponin homology (CH) domain, a GAS2-related (GAR) domain and an extended C-terminus. Note that the two MtLSs (SKLP and TLLP) are located at the C-terminus. **(B)** EB1 contains an N-terminal CH domain, which binds to MTs, followed by a coiled-coil (CC) region, which is abutted to the EB-homology (EH) domain. Note that the EH domain contains the binding sites for MtLSs and the C-terminus of EB1 was abutted to glutathione-S-transferase (GST) for expression and purification. **(C)** The recombinant proteins used for the *in vitro* binding assays in this study are the predicted molecular weight and are denoted by asterisks.

Figure 2: G2L3-C-term interacts directly with EB1 *in vitro* with high binding strength. (A) GST pulldown assay, using GST-EB1-C-T as bait and G2L3-C-term as prey; the unbound and bound fractions are denoted as I and O, respectively. Left panel: G2L3-C-term was incubated with GST-EB1-C-T, followed by incubation with glutathione-coated beads in the presence of 20mM EDTA. Note the two proteins are found in the bound fraction, indicating they interact. Middle panel: GST-EB1-C-T was incubated with glutathione-coated beads in the presence of 20mM EDTA (as a positive binding control). Right panel: G2L3-C-term was incubated with GST, followed by incubation with glutathione-coated beads in the presence of 20mM EDTA. Note that when incubated with GST alone, G2L3-C-term is not found in the bound fraction, indicating that the interaction is specific for EB1. **(B)** Solid phase binding assay, where G2L3-C-term was plated on plastic and the concentration of GST-EB1-C-T was increased. Note the rapid increase of binding at very low concentrations of GST-EB1-C-T. The values for GST-EB1-CT were normalised by subtracting the values for GST alone, and plotted. Subsequently a Hill plot was fitted to estimate a k_d of 2.1nM. The results for both experiments are indicative of more than three independent experiments.

Figure 3: EB1 enhances the localisation of G2L3 to MTs. (A) NIH3T3 cells co-expressing G2L3 with EB1 were fixed and stained using an antibody directed against α-tubulin (DM1A, (Blose et al., 1984)). NIH3T3 cells expressing G2L3

were either treated with 10μM taxol for 30 mins, or left untreated (control), before fixation and staining for α-tubulin and phalloidin to label actin. Note the dramatic enhancement of G2L3 to MTs when coexpressed with EB1, compared to control or taxol-treated cells (white arrowheads). **(B)** G2L3 and MT images were passed through a FFT-2D bandpass filter and background subtracted. The resulting image was thresholded to MTs, and the cell outline drawn. Following which, the area fraction for G2L3 positive pixels and MTs were recorded, and the ratio between G2L3: MTs was calculated. **(C)** The ratios calculated in (B) of G2L3: MTs for EB1-coexpressing cells, taxol treated cells and control cells are displayed. Note the significant enhancement of G2L3 to MTs in EB1 co-expressing cells compared to taxol-treated and control cells ($p<0.001$, student's t-test). Bars, 10μm.

Figure 4: The localisation of G2L3-C-term is regulated by EB1, and shows evidence of plus-end tip-tracking. (A) NIH3T3 cells co-expressing G2L3-C-term with EB1 were fixed and stained using an antibody directed against α-tubulin (DM1A, (Blose et al., 1984)). NIH3T3 cells expressing G2L3-C-term were either treated with 10μM taxol for 30 mins, or left untreated (control), before fixation and staining for α-tubulin and phalloidin to label actin. Note the dramatic enhancement of G2L3-C-term to MTs when coexpressed with EB1, compared to control or taxol-treated cells (white arrowheads). **(B)** The ratio of positive pixels G2L3-C-term: MTs as calculated in (Figure 4B) for EB1-coexpressing cells, taxol treated cells and control cells are displayed. Note the significant enhancement of G2L3-C-term to MTs in EB1 co-expressing cells compared to taxol-treated and control cells ($p<0.001$, student's t-test). **(C)** Still images generated from live movies of NIH3T3 cells coexpressing G2L3-C-term and EB1. Note the localisation of G2L3-C-term to the growing plus-end of MTs (white and red arrowheads). Time is indicated in seconds at the bottom right corner. Bars, 10μm.

Figure 5: The complete G2L3-C-term is required for interaction with EB1. (A) Schematic representation of the G2L3-C-term mutants expressed as GFP-fusions for localisation studies and GST pulldown assays from cell lysates. **(B)** NIH3T3 cells expressing the indicated constructs were fixed and stained for α-tubulin as in Figure 3. Note the localisation of G2L3-C-term to MTs (white

arrowheads), whereas G2L3-CT1 and G2L3-CT2 localise diffusely in the cytoplasm. **(C)** GST pulldown assays using GST-EB1-C-T as bait to pulldown the indicated G2L3-C-term mutants from cell lysates. Note that GST-EB1-C-T can pulldown G2L3-C-term, however it fails to pulldown G2L3-CT1 and G2L3-CT2.

Figure 1: Schematic representation of GAS2-like 3 and end-binding protein 1.

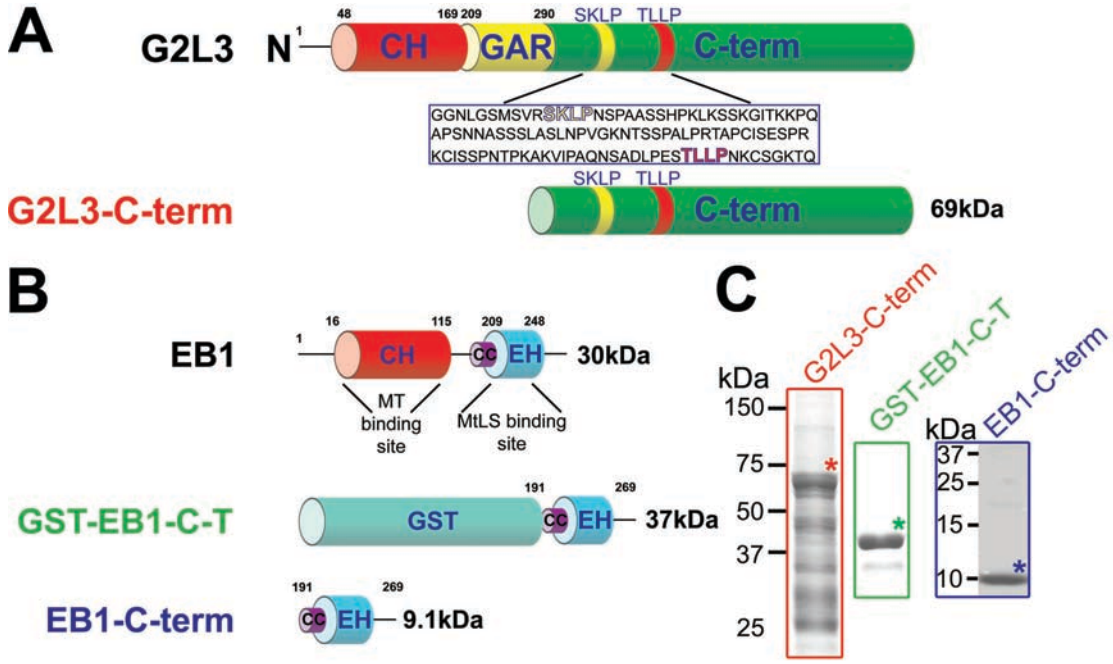

Figure 2: G2L3-C-term interacts directly with EB1 *in vitro* with high binding strength.

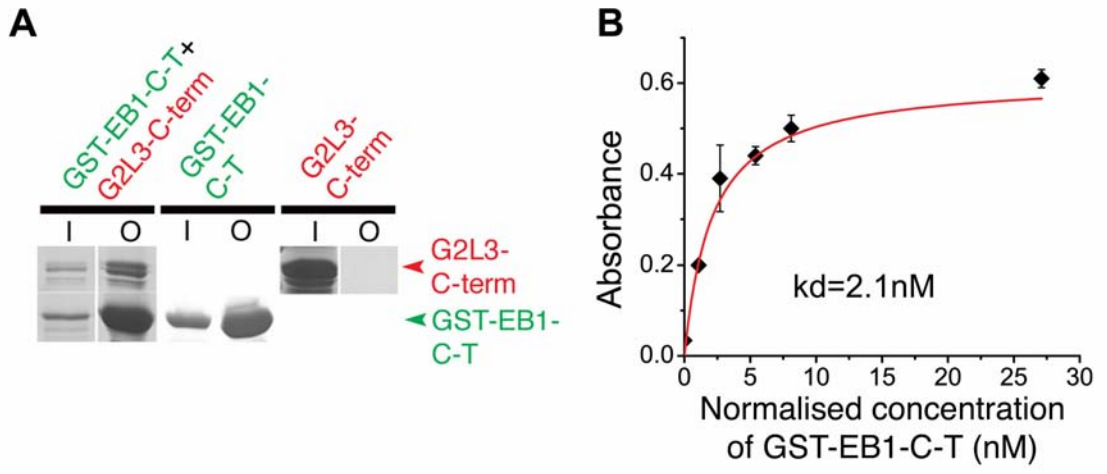

Figure 3: EB1 enhances the localisation of G2L3 to MTs.

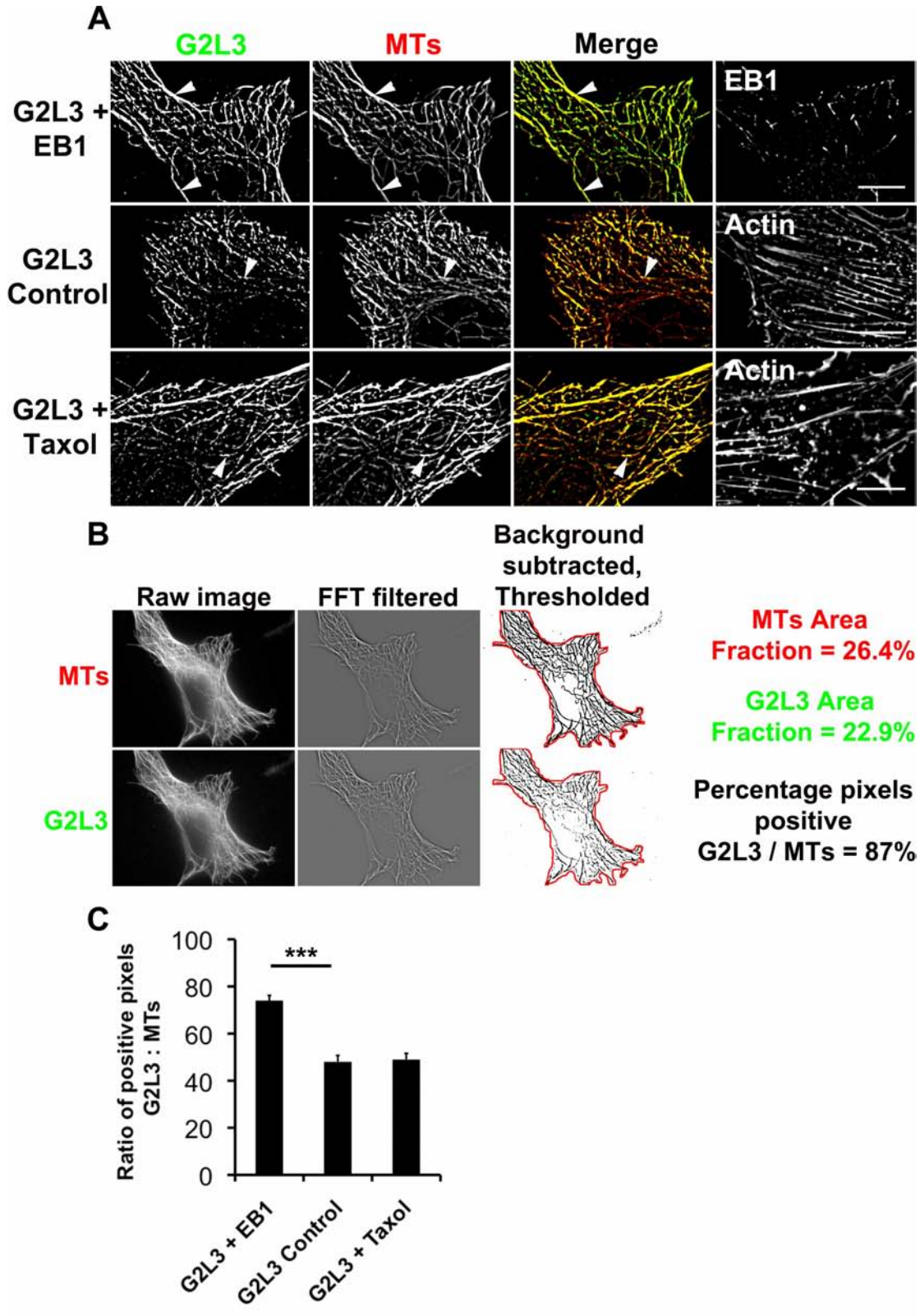

Figure 4: The localisation of G2L3-C-term is regulated by EB1, and shows evidence of plus-end tip-tracking.

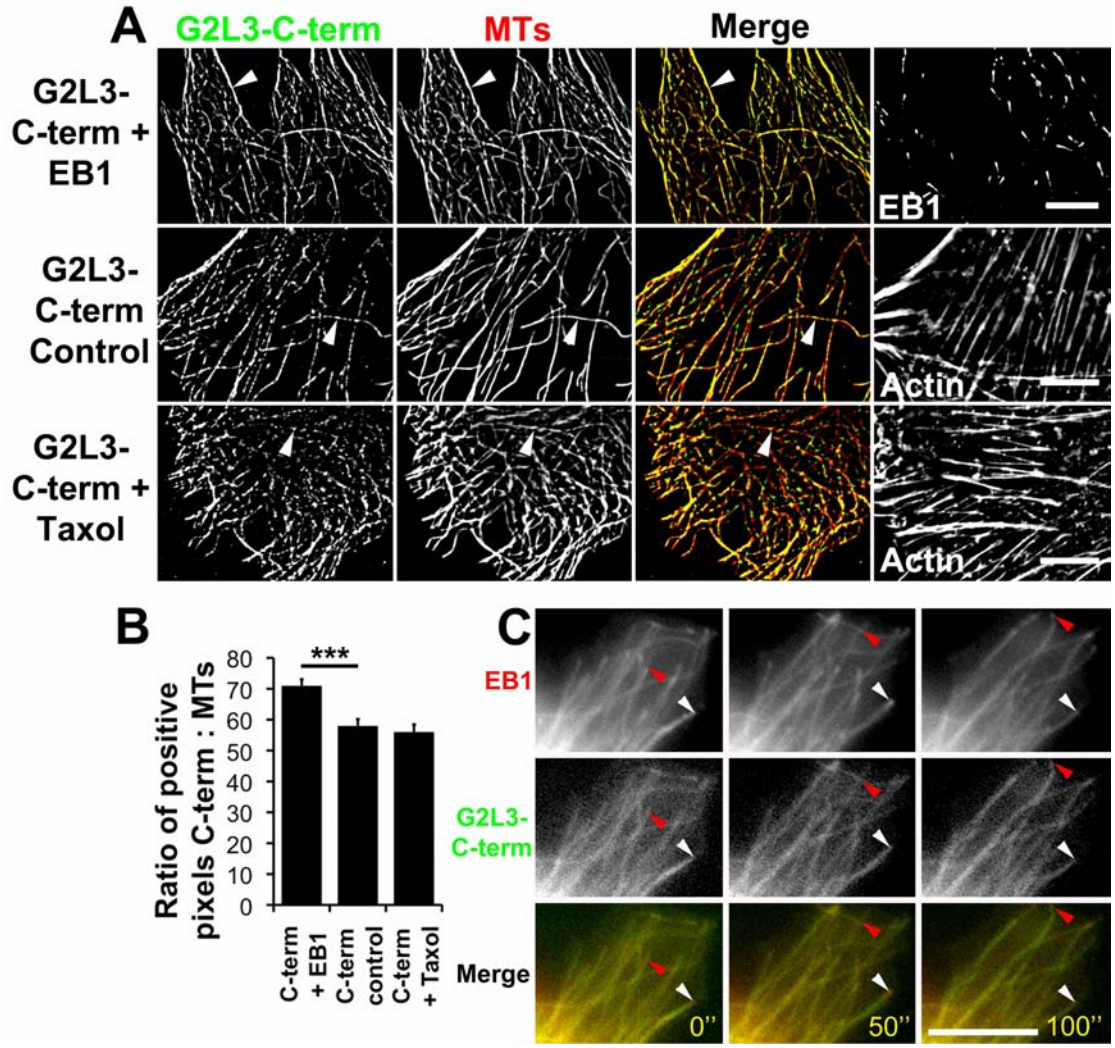

Figure 5: The complete G2L3-C-term is required for interaction with EB1.

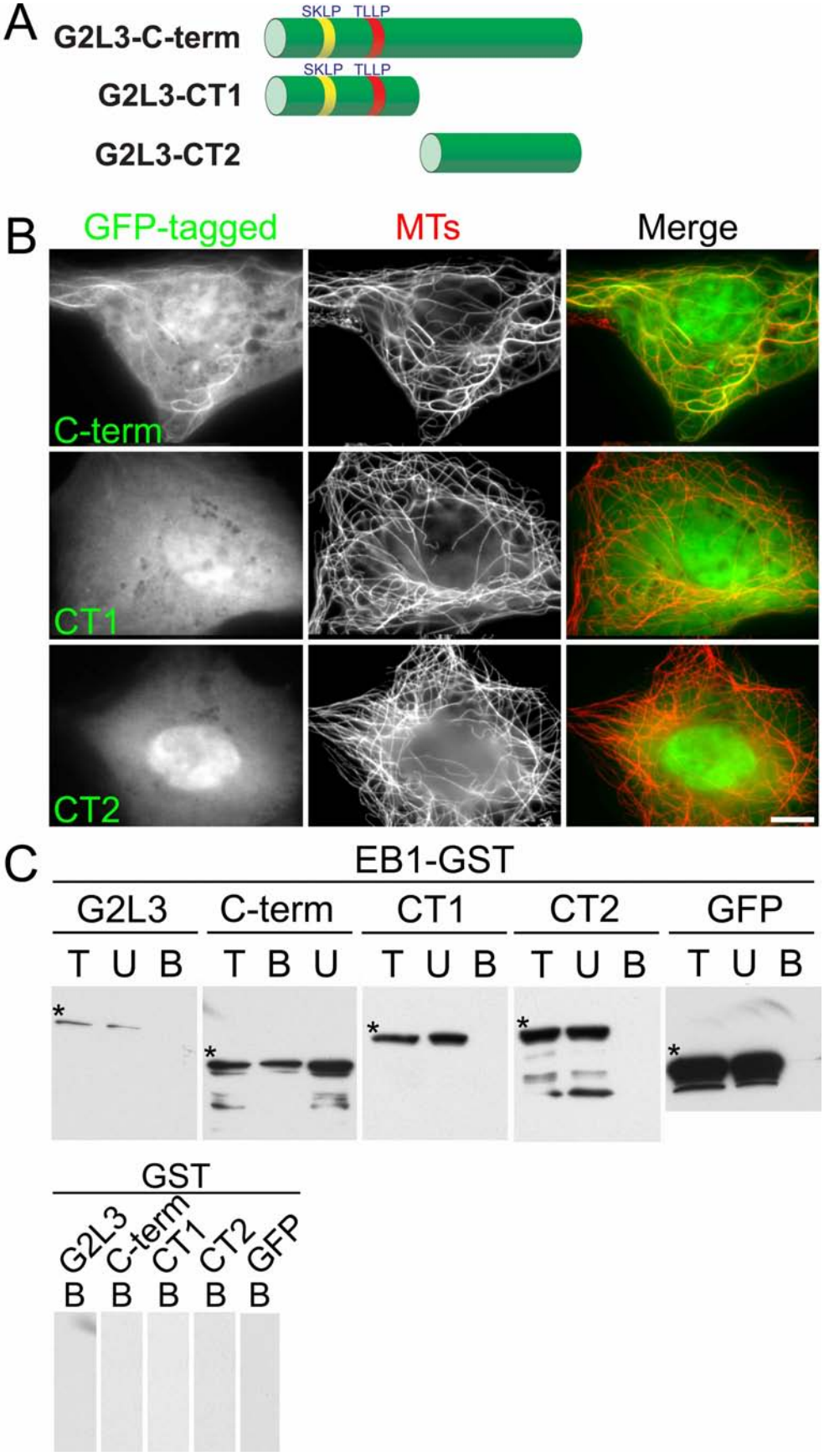

6) Final Discussion

The overall aims of this study were to characterise the new protein, G2L3, to further the understanding of how it is regulated and provide insights into its function. This study has provided valuable data on the localisation and binding of G2L3, and its regulation of localisation to MTs by EB1 and tubulin acetylation, however, its functional role remains elusive. The potential functions of G2L3 and how future experiments may help to identify and dissect these roles are considered below.

The Drosophila homologue of the GAS2 family is essential for development

The fact that members of the GAS2 family are widely conserved through evolution suggests they play an important function. Intriguingly, Drosophila only express a single homologue of the GAS2 family, termed 'Pigs', implying that studies in flies could shed light on the function of G2L3. Pigs is a direct target of Notch signalling and is thought to be essential for muscle development and the organisation of the fly ovariole (Pines et al., 2010). Interestingly, Notch-directed expression of Pigs resulted in a negative feedback mechanism in which Pigs downregulates Notch signalling. The expression of Pigs and its feedback on Notch signaling could be essential for other downstream targets of Notch, as well as Pigs expression itself. Notch signalling controls a host of developmental pathways, as well as pathways involving cancer (Artavanis-Tsakonas et al., 1999; Nickoloff et al., 2003). It has been reported that Notch signalling induces the expression of proteins, such as SNAIL-1, which are required for epithelial to mesenchymal transition (which is an essential step in the initial stages of metastasis), and for increased motility and invasiveness (Sahlgren et al., 2008). With the evidence that Pigs downregulates Notch signalling in flies, it is plausible to connect the loss of G2L3 to human cancers that are dependent on Notch signalling. Experiments to determine whether G2L3 is a downstream target of Notch would provide insight into a potential role of G2L3 in both development and cancer.

In contrast to flies, which have a single member of the GAS2 family, vertebrates contain four members of the GAS2 family. It is likely that each member of the GAS2 family plays a tissue-specific role. For example, GAS2 is found mainly in

lung tissue, G2L1 in testis and brain, G2L2 in skeletal muscle, whereas G2L3 mRNA is found in many tissues. In accordance with a tissue specific function in vertebrate development, G2L1 has been identified as a target gene for the thyroid hormone receptor in human erythroid cells, implying it could play a key role in erythroid cell development (Gamper et al., 2009).

The similarity to spectraplakins implies GAS2-like 3 may have similar roles

As discussed in the second results chapter, G2L3 shares a distinctive similarity to the spectraplakins. It is striking that despite spectraplakins containing multiple domains, only two of these (the CH and GAR domains) have apparent functional roles. Notably, G2L3 only contains these two domains, thus can be thought of as a 'mini-version' of a spectraplakin. The spectraplakin, ACF7, has been shown to govern MT dynamics, guidance, cortical tethering, stability and cellular polarisation. Many of these functions can be explained at least in part by actin-MT connections (Kodama et al., 2003). There is also evidence to suggest that ACF7 plays a role in focal adhesion dynamics, and thus cell migration (Wu et al., 2008).

To determine whether G2L3 can play similar roles to ACF7, RNA interference could be used to knockdown G2L3 expression. One potential problem with this approach could be the redundancy of the spectraplakins and the GAS2 family members. Thus the effects of knocking down G2L3 would require careful analysis, and could require the simultaneous knockdown of the other proteins that confer redundancy. A possible way to avoid knocking-down many proteins would be to use HT1080 cells, which do not contain G2L3 at the mRNA level, implying they do not express G2L3 protein. Alternatively, cells from Pigs -/- Drosophila could be used, and G2L3 could be expressed in these cells to try and the rescue the aberrant phenotypes observed in these cells.

The localisation of G2L3 to MTs and actin make it a good candidate for a role downstream of polarisation mediators, such as the Rho GTPases. IQGAP1 is an effector of the Rho GTPase, Cdc42, and has been shown to interact with the +TIP, APC (Etienne-Manneville and Hall, 2003). APC is a known binding partner of EB1 (Honnappa et al., 2005), thus it is possible that G2L3 indirectly interacts with members of the Rho GTPase family. Using HT1080 cells as a model for cells lacking G2L3, the importance of G2L3 in cell polarisation could be

determined using scratch-wound assays. It would be interesting to express G2L3 in HT1080 cells to investigate whether this effects cell polarisation. Similarly, the effect of expressing G2L3 in HT1080 cells on cell adhesion and migration could be assessed using cell-attachment and migration assays, respectively.

Owing to the interaction of G2L3 with the master regulator of MT dynamics, EB1, another plausible role of G2L3 is in regulating MT dynamics. MTs in ACF7-null endodermal cells undergo longer periods of growth and shorter periods of pausing than wild-type cells, and a subset of these MTs in ACF7-/- cells fail to grow along actin filaments (Kodama et al., 2003). Both of these defects can be rescued by expressing a version of ACF7 encoding its CH and GAR domains (the equivalent of G2L3), implying that G2L3 may be acting redundantly in ACF7 -/- cells. G2L3 knockdown experiments on ACF7 -/- cells may reveal whether the lack of G2L3 leads to more profound defects in MT dynamics and growth trajectories.

ACF7 has been shown to associate with the +TIP, EB1 (Wu et al., 2008). We identified that EB1 can recruit G2L3 to MTs, however the function of this spatial regulation is unclear. The interaction of G2L3 with EB1 may play a similar role to ACF7's interaction, in which ACF7 uses its actin-based ATPase to guide the +TIP complex along actin stress fibers towards focal adhesions. The interaction mediated by ACF7 and EB1 between actin and MTs is dynamic, as stress fibers associated with focal adhesions are constantly moving away from the focal adhesions at a rate of ~0.2-0.4 μm/ min. In contrast to ACF7, no ATPase activity of G2L3 is predicted by sequence analysis. Given the apparent lack of ATPase activity in G2L3, it is possible the C-terminus of G2L3 may provide a binding site for an actin-based motor, such as a member of the myosin family. This would enable G2L3 to dynamically guide the +TIP complex along actin stress fibers via its C-terminus in a manner similar to ACF7. G2L3 may also form a static crosslink between MTs and actin mediated via its C-terminus and CH domain, respectively, which would not require the action of a motor to move along actin filaments.

To elucidate the underlying mechanisms of how G2L3 could crosslink MTs and actin it would be important to establish new binding partners of G2L3. A possible way to isolate novel interactions would be to perform coimmunoprecipitation experiments using G2L3-GFP, followed by mass-spectrometry (MS).

Complementary to the MS-based approach yeast-two hybrid screens could be performed to identify lower-affinity binding partners.

Potential roles of GAS2-like 3 in apoptosis and regulation of mitochondrial dynamics

Communication between the cytoskeleton and mitochondria is key to the regulation of apoptosis and mitochondrial dynamics (Anesti and Scorrano, 2006; Boldogh and Pon, 2007). All neurodegenerative diseases are associated with cytoskeletal defects and/or deficiencies in the regulation of mitochondrial function. Recent data indicated that overexpression of G2L3 in cells, activated the executioner caspase, caspase 3, which suggests that G2L3 induces apoptosis (See Appendix 1, Figure 8A). Interestingly, GAS2, which is the closest relative of G2L3, has been shown to be involved in signalling pathways controlling cell growth, apoptosis and cancer (Benetti et al., 2005; Benetti et al., 2001; Brancolini et al., 1995; Lee et al., 1999). Despite the evidence of GAS2 in apoptosis (Brancolini et al., 1995; Brancolini et al., 1997), the molecular basis of how it may regulate cell death is unknown.

Classical apoptosis is usually initiated by mitochondria, which are known to host mediators of the apoptotic machinery (Karbowski and Youle, 2003; Taylor et al., 2008). As well as G2L3 localising on both F-actin and MTs, G2L3 localised to distinct foci on mitochondria in a subset of cells, suggesting G2L3 may play a very important role in apoptosis (Appendix 1, Figures 8B and 8C). The recruitment of G2L3 to mitochondria may lead to events which induce apoptosis, such as permeabilisation of the outer mitochondrial membrane by B-Cell Lymphoma 2 (BCL-2) associated X protein (Bax) and BCL-2 antagonist or killer (Bak), resulting in cytochrome C release, and subsequent caspase activation (Taylor et al., 2008). Time-lapse imaging revealed that G2L3 specifically localised to distinct foci, which undergo fusion and fission events (Appendix 1, Figure 8D).

Apoptosis may trigger fragmentation (fission) of mitochondria, showing that there is an intimate relationship between apoptosis mediating proteins (e.g. Bax and Bak), and those that regulate fusion and fission of mitochondria (Youle and Karbowski, 2005).

Several important questions arise from these data, for example, does G2L3 control the intrinsic pathway of apoptosis, or is cell death triggered as a

consequence of G2L3 perturbing mitochondrial dynamics? It would be important to investigate whether G2L3 induces classical apoptosis through Bax/Bak-mediated permeabilisation of the outer mitochondrial membrane. To test this hypothesis, G2L3 could be overexpressed in Bax/Bak -/- cells, and the levels of active caspases determined. Since G2L3 overexpression results in caspase activation, it would be necessary to use an inducible vector system allowing the rapid activation of G2L3 to follow its potential pathway of destruction in live cells. Crucially, inducible expression of G2L3 could also be used to analyse the effects on mitochondrial dynamics, and investigate whether the rates of fusion and/ or fission are perturbed. Knockdown and rescue experiments would need to be performed to elucidate the functional domains of G2L3 involved in these roles.

Physiological roles of G2L3 and working model of G2L3 function

Neurodegenerative diseases, such as Alzheimer's are known to be caused by dysfunction of both the cytoskeleton and mitochondrial dynamics. However, the molecular basis of how the two processes are interlinked remains unknown. Mutations in genes encoding spectraplakins result in various medical conditions including neurodegeneration, cancer and skin blistering (Sonnenberg and Liem, 2007). Given the similarity of G2L3 to spectraplakins, and the fact that G2L3 associates with mitochondria, as well as with MT and actin cytoskeletons, G2L3 is a promising candidate for a key mediator of communication between these cellular components. With the potential roles G2L3 may play, it could be fundamental to diseases involving mitochondria and cytoskeleton dysfunction. The working model of G2L3 function in cells is proposed below (Figure 6.1).

G2L3 could form both static and dynamic interactions with MTs and actin. In a manner that is akin to ACF7, the dynamic interaction of G2L3 with MTs is via EB1. Whereas ACF7 contains an intrinsic ATPase to guide it along actin, G2L3 apparently lacks this motor activity, thus the dynamic association with actin could be mediated indirectly using an actin-based motor, such as myosin V. This would enable the guidance of MTs along actin stress fibers to focal adhesions, which is essential for focal adhesion turnover and cell migration (Kaverina et al., 1999). The dynamic interaction may also serve to regulate MT dynamics at the plus-ends by ensuring that frequencies of MT growth, pausing and collapse are maintained. Loss of G2L3 may result in a decreased frequency of pausing and increased growing frequencies as observed for ACF7 (Kodama et al., 2003).

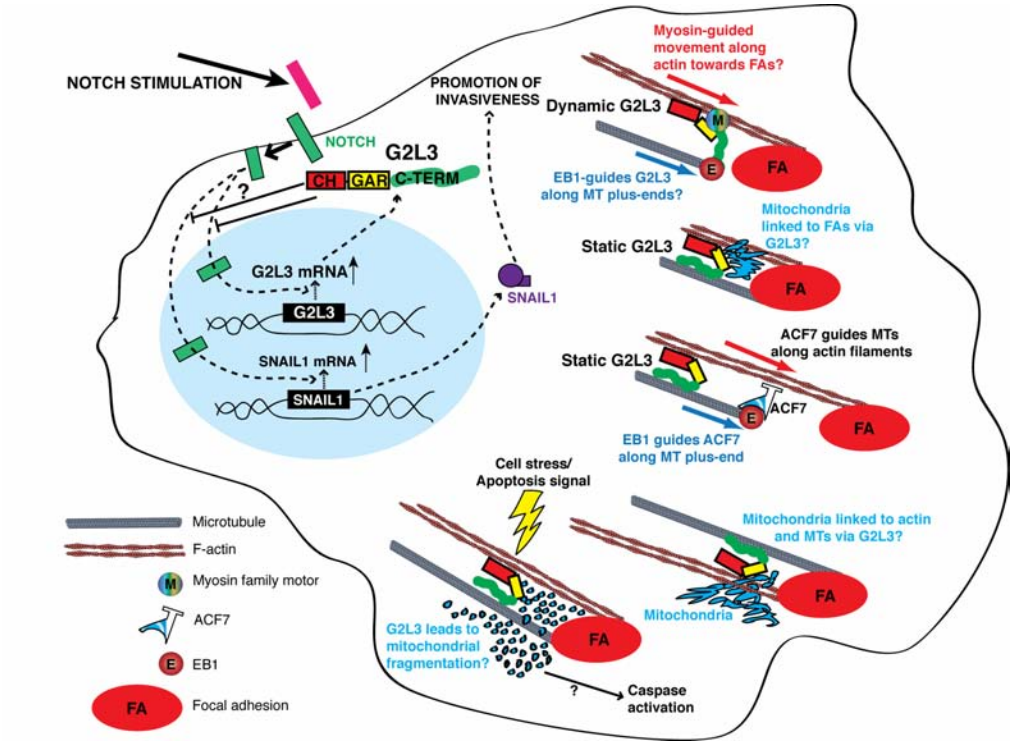

Figure 6.1: Potential roles of G2L3 in cells.

See text for description.

After nascent contacts between MTs and actin have been established via dynamic interactions, other molecules of G2L3 may be recruited to form static interactions. This additional recruitment would serve to strengthen the MT-actin crosslinking via the C-terminus and CH domain, respectively. Once the static crosslinks are established, a conformational change may expose binding sites on G2L3 for mitochondrial recruitment. This would ideally situate the mitochondria to cater for the energy-demanding processes of intracellular transport along MTs and actin and cell migration. The junctions formed by G2L3 between actin, MTs and mitochondria in cells would also be an ideal locale for sensing small changes in the cytoplasm and reacting to them. For example, in terms of energy demand, guidance cues and signals to induce apoptosis.

In terms of apoptosis, G2L3 may either act upstream or downstream of Cytochrome C release from the mitochondria. The possibility of it acting upstream is favoured, as G2L3 localises to distinct mitochondrial foci that undergo fusion and fission. Upon the cell's decision to undergo apoptosis, G2L3 may undergo a conformational change or cleavage for it to localise exclusively to mitochondria and start the apoptosis cascade. Alternatively, G2L3 may perturb mitochondrial dynamics, thus indirectly stimulate apoptosis. Currently, we have

evidence to support both of these possibilities. Clearly further work is needed to uncover the molecular mechanisms underlying G2L3-induced apoptosis.

7) References

Akhmanova, A. and Steinmetz, M. O. (2008). Tracking the ends: a dynamic protein network controls the fate of microtubule tips. Nat.Rev.Mol.Cell Biol. 9, 309-322.

Anesti, V. and Scorrano, L. (2006). The relationship between mitochondrial shape and function and the cytoskeleton. Biochim Biophys Acta 1757, 692-9.

Applewhite, D. A., Grode, K. D., Keller, D., Zadeh, A., Slep, K. C. and Rogers, S. L. (2010). The spectraplakin Short stop is an actin-microtubule cross-linker that contributes to organization of the microtubule network. Mol Biol Cell 21, 1714-24.

Artavanis-Tsakonas, S., Rand, M. D. and Lake, R. J. (1999). Notch signaling: cell fate control and signal integration in development. Science 284, 770-6.

Axelrod, D., Koppel, D. E., Schlessinger, J., Elson, E. and Webb, W. W. (1976). Mobility measurement by analysis of fluorescence photobleaching recovery kinetics. Biophys J 16, 1055-69.

Ballestrem, C., Wehrle-Haller, B., Hinz, B. and Imhof, B. A. (2000). Actin-dependent lamellipodia formation and microtubule-dependent tail retraction control-directed cell migration. Mol.Biol.Cell 11, 2999-3012.

Bartolini, F., Moseley, J. B., Schmoranzer, J., Cassimeris, L., Goode, B. L. and Gundersen, G. G. (2008). The formin mDia2 stabilizes microtubules independently of its actin nucleation activity. J.Cell Biol. 181, 523-536.

Basu, R. and Chang, F. (2007). Shaping the actin cytoskeleton using microtubule tips. Curr.Opin.Cell Biol. 19, 88-94.

Benetti, R., Copetti, T., Dell'Orso, S., Melloni, E., Brancolini, C., Monte, M. and Schneider, C. (2005). The calpain system is involved in the constitutive regulation of beta-catenin signaling functions. J Biol Chem 280, 22070-80.

Benetti, R., Del Sal, G., Monte, M., Paroni, G., Brancolini, C. and Schneider, C. (2001). The death substrate Gas2 binds m-calpain and increases susceptibility to p53-dependent apoptosis. Embo J 20, 2702-14.

Blose, S. H., Meltzer, D. I. and Feramisco, J. R. (1984). 10-nm filaments are induced to collapse in living cells microinjected with monoclonal and polyclonal antibodies against tubulin. J Cell Biol 98, 847-58.

Boldogh, I. R. and Pon, L. A. (2007). Mitochondria on the move. Trends Cell Biol 17, 502-10.

Bosher, J. M., Hahn, B. S., Legouis, R., Sookhareea, S., Weimer, R. M., Gansmuller, A., Chisholm, A. D., Rose, A. M., Bessereau, J. L. and Labouesse, M. (2003). The Caenorhabditis elegans vab-10 spectraplakin isoforms protect the epidermis against internal and external forces. J Cell Biol. 161, 757-768.

Boyault, C., Sadoul, K., Pabion, M. and Khochbin, S. (2007). HDAC6, at the crossroads between cytoskeleton and cell signaling by acetylation and ubiquitination. Oncogene 26, 5468-76.

Brancolini, C., Benedetti, M. and Schneider, C. (1995). Microfilament reorganization during apoptosis: the role of Gas2, a possible substrate for ICE-like proteases. EMBO J 14, 5179-5190.

Brancolini, C., Bottega, S. and Schneider, C. (1992). Gas2, a growth arrest-specific protein, is a component of the microfilament network system. J.Cell Biol. 117, 1251-1261.

Brancolini, C., Marzinotto, S. and Schneider, C. (1997). Susceptibility to p53 dependent apoptosis correlates with increased levels of Gas2 and Gas3 proteins. Cell Death Differ 4, 247-53.

Caviston, J. P. and Holzbaur, E. L. (2006). Microtubule motors at the intersection of trafficking and transport. Trends Cell Biol. 16, 530-537.

Clamp, M., Cuff, J., Searle, S. M. and Barton, G. J. (2004). The Jalview Java alignment editor. Bioinformatics 20, 426-427.

Dickson, R. M., Cubitt, A. B., Tsien, R. Y. and Moerner, W. E. (1997). On/off blinking and switching behaviour of single molecules of green fluorescent protein. Nature 388, 355-8.

Dompierre, J. P., Godin, J. D., Charrin, B. C., Cordelieres, F. P., King, S. J., Humbert, S. and Saudou, F. (2007). Histone deacetylase 6 inhibition compensates for the transport deficit in Huntington's disease by increasing tubulin acetylation. J Neurosci 27, 3571-83.

Edde, B., Rossier, J., Le Caer, J. P., Berwald-Netter, Y., Koulakoff, A., Gros, F. and Denoulet, P. (1991). A combination of posttranslational

modifications is responsible for the production of neuronal alpha-tubulin heterogeneity. J Cell Biochem 46, 134-42.

Edelhoch, H. (1967). Spectroscopic determination of tryptophan and tyrosine in proteins. Biochemistry 6, 1948-54.

Etienne-Manneville, S. and Hall, A. (2001). Integrin-mediated activation of Cdc42 controls cell polarity in migrating astrocytes through PKCzeta. Cell 106, 489-498.

Etienne-Manneville, S. and Hall, A. (2003). Cdc42 regulates GSK-3beta and adenomatous polyposis coli to control cell polarity. Nature 421, 753-756.

Faix, J. and Grosse, R. (2006). Staying in shape with formins. Dev.Cell 10, 693-706.

Fukata, M., Watanabe, T., Noritake, J., Nakagawa, M., Yamaga, M., Kuroda, S., Matsuura, Y., Iwamatsu, A., Perez, F. and Kaibuchi, K. (2002). Rac1 and Cdc42 capture microtubules through IQGAP1 and CLIP-170. Cell 109, 873-885.

Galjart, N. and Perez, F. (2003). A plus-end raft to control microtubule dynamics and function. Curr.Opin.Cell Biol. 15, 48-53.

Gamper, I., Koh, K. R., Ruau, D., Ullrich, K., Bartunkova, J., Piroth, D., Hacker, C., Bartunek, P. and Zenke, M. (2009). GAR22: a novel target gene of thyroid hormone receptor causes growth inhibition in human erythroid cells. Exp Hematol 37, 539-548 e4.

Giorda, R., Cerritello, A., Bonaglia, M. C., Bova, S., Lanzi, G., Repetti, E., Giglio, S., Baschirotto, C., Pramparo, T., Avolio, L. et al. (2004). Selective disruption of muscle and brain-specific BPAG1 isoforms in a girl with a 6;15 translocation, cognitive and motor delay, and tracheo-oesophageal atresia. J Med.Genet. 41, e71.

Goode, B. L., Drubin, D. G. and Barnes, G. (2000). Functional cooperation between the microtubule and actin cytoskeletons. Curr.Opin.Cell Biol. 12, 63-71.

Goriounov, D., Leung, C. L. and Liem, R. K. (2003). Protein products of human Gas2-related genes on chromosomes 17 and 22 (hGAR17 and hGAR22) associate with both microfilaments and microtubules. J.Cell Sci. 116, 1045-1058.

Honnappa, S., Gouveia, S. M., Weisbrich, A., Damberger, F. F., Bhavesh, N. S., Jawhari, H., Grigoriev, I., van Rijssel, F. J., Buey, R. M., Lawera, A. et al. (2009). An EB1-binding motif acts as a microtubule tip localization signal. Cell 138, 366-376.

Honnappa, S., John, C. M., Kostrewa, D., Winkler, F. K. and Steinmetz, M. O. (2005). Structural insights into the EB1-APC interaction. EMBO J 24, 261-269.

Ishizaki, T., Morishima, Y., Okamoto, M., Furuyashiki, T., Kato, T. and Narumiya, S. (2001). Coordination of microtubules and the actin cytoskeleton by the Rho effector mDia1. Nat.Cell Biol. 3, 8-14.

Jefferson, J. J., Leung, C. L. and Liem, R. K. (2004). Plakins: goliaths that link cell junctions and the cytoskeleton. Nat.Rev.Mol.Cell Biol. 5, 542-553.

Kammerer, R. A., Antonsson, P., Schulthess, T., Fauser, C. and Engel, J. (1995). Selective chain recognition in the C-terminal alpha-helical coiled-coil region of laminin. J Mol Biol 250, 64-73.

Kammerer, R. A., Schulthess, T., Landwehr, R., Lustig, A., Fischer, D. and Engel, J. (1998). Tenascin-C hexabrachion assembly is a sequential two-step process initiated by coiled-coil alpha-helices. J.Biol.Chem. 273, 10602-10608.

Karakesisoglou, I., Yang, Y. and Fuchs, E. (2000). An epidermal plakin that integrates actin and microtubule networks at cellular junctions. J Cell Biol. 149, 195-208.

Karbowski, M. and Youle, R. J. (2003). Dynamics of mitochondrial morphology in healthy cells and during apoptosis. Cell Death Differ 10, 870-80.

Kaverina, I., Krylyshkina, O., Beningo, K., Anderson, K., Wang, Y. L. and Small, J. V. (2002). Tensile stress stimulates microtubule outgrowth in living cells. Journal of Cell Science 115, 2283-2291.

Kaverina, I., Krylyshkina, O. and Small, J. V. (1999). Microtubule targeting of substrate contacts promotes their relaxation and dissociation. J Cell Biol 146, 1033-44.

Kirschner, M. W. and Mitchison, T. (1986). Microtubule dynamics. Nature 324, 621.

Kodama, A., Karakesisoglou, I., Wong, E., Vaezi, A. and Fuchs, E. (2003). ACF7: an essential integrator of microtubule dynamics. Cell 115, 343-354.

Lai, F. P., Szczodrak, M., Block, J., Faix, J., Breitsprecher, D., Mannherz, H. G., Stradal, T. E., Dunn, G. A., Small, J. V. and Rottner, K. (2008). Arp2/3 complex interactions and actin network turnover in lamellipodia. EMBO J. 27, 982-992.

Lansbergen, G. and Akhmanova, A. (2006). Microtubule Plus End: A Hub of Cellular Activities. Traffic 7, 499-507.

Le, C. C. and Carlier, M. F. (2008). Regulation of actin assembly associated with protrusion and adhesion in cell migration. Physiol Rev. 88, 489-513.

Lee, K. K., Tang, M. K., Yew, D. T., Chow, P. H., Yee, S. P., Schneider, C. and Brancolini, C. (1999). gas2 is a multifunctional gene involved in the regulation of apoptosis and chondrogenesis in the developing mouse limb. Dev Biol 207, 14-25.

Lee, S. and Kolodziej, P. A. (2002). Short Stop provides an essential link between F-actin and microtubules during axon extension. Development 129, 1195-1204.

Leung, C. L., Green, K. J. and Liem, R. K. (2002). Plakins: a family of versatile cytolinker proteins. Trends Cell Biol. 12, 37-45.

Li, R. and Gundersen, G. G. (2008). Beyond polymer polarity: how the cytoskeleton builds a polarized cell. Nat.Rev.Mol.Cell Biol. 9, 860-873.

Lippincott-Schwartz, J., Snapp, E. and Kenworthy, A. (2001). Studying protein dynamics in living cells. Nat Rev Mol Cell Biol 2, 444-56.

McAnaney, T. B., Zeng, W., Doe, C. F., Bhanji, N., Wakelin, S., Pearson, D. S., Abbyad, P., Shi, X., Boxer, S. G. and Bagshaw, C. R. (2005). Protonation, photobleaching, and photoactivation of yellow fluorescent protein (YFP 10C): a unifying mechanism. Biochemistry 44, 5510-24.

Nickoloff, B. J., Osborne, B. A. and Miele, L. (2003). Notch signaling as a therapeutic target in cancer: a new approach to the development of cell fate modifying agents. Oncogene 22, 6598-608.

Palazzo, A. F., Cook, T. A., Alberts, A. S. and Gundersen, G. G. (2001). mDia mediates Rho-regulated formation and orientation of stable microtubules. Nat.Cell Biol. 3, 723-729.

Pines, M. K., Housden, B. E., Bernard, F., Bray, S. J. and Roper, K. (2010). The cytolinker Pigs is a direct target and a negative regulator of Notch signalling. Development 137, 913-922.

Piruska, A., Nikcevic, I., Lee, S. H., Ahn, C., Heineman, W. R., Limbach, P. A. and Seliskar, C. J. (2005). The autofluorescence of plastic materials and chips measured under laser irradiation. Lab Chip 5, 1348-54.

Reed, N. A., Cai, D., Blasius, T. L., Jih, G. T., Meyhofer, E., Gaertig, J. and Verhey, K. J. (2006). Microtubule acetylation promotes kinesin-1 binding and transport. Curr Biol 16, 2166-72.

Romero, S., Le, C. C., Didry, D., Egile, C., Pantaloni, D. and Carlier, M. F. (2004). Formin is a processive motor that requires profilin to accelerate actin assembly and associated ATP hydrolysis. Cell 119, 419-429.

Roper, K., Gregory, S. L. and Brown, N. H. (2002). The 'spectraplakins': cytoskeletal giants with characteristics of both spectrin and plakin families. Journal of Cell Science 115, 4215-4225.

Sahlgren, C., Gustafsson, M. V., Jin, S., Poellinger, L. and Lendahl, U. (2008). Notch signaling mediates hypoxia-induced tumor cell migration and invasion. Proc Natl Acad Sci U S A 105, 6392-7.

Salmon, W. C., Adams, M. C. and Waterman-Storer, C. M. (2002). Dual-wavelength fluorescent speckle microscopy reveals coupling of microtubule and actin movements in migrating cells. J Cell Biol. 158, 31-37.

Schaefer, A. W., Kabir, N. and Forscher, P. (2002). Filopodia and actin arcs guide the assembly and transport of two populations of microtubules with unique dynamic parameters in neuronal growth cones. J Cell Biol. 158, 139-152.

Schneider, C., King, R. M. and Philipson, L. (1988). Genes specifically expressed at growth arrest of mammalian cells. Cell 54, 787-793.

Shaner, N. C., Campbell, R. E., Steinbach, P. A., Giepmans, B. N., Palmer, A. E. and Tsien, R. Y. (2004). Improved monomeric red, orange and yellow fluorescent proteins derived from Discosoma sp. red fluorescent protein. Nat Biotechnol 22, 1567-72.

Sjoblom, T., Jones, S., Wood, L. D., Parsons, D. W., Lin, J., Barber, T. D., Mandelker, D., Leary, R. J., Ptak, J., Silliman, N. et al. (2006). The consensus coding sequences of human breast and colorectal cancers. Science 314, 268-274.

Small, J. V. and Kaverina, I. (2003). Microtubules meet substrate adhesions to arrange cell polarity. Curr.Opin.Cell Biol. 15, 40-47.

Sonnenberg, A. and Liem, R. K. (2007). Plakins in development and disease. Exp.Cell Res. 313, 2189-2203.

Sprague, B. L. and McNally, J. G. (2005). FRAP analysis of binding: proper and fitting. Trends Cell Biol 15, 84-91.

Sprague, B. L., Muller, F., Pego, R. L., Bungay, P. M., Stavreva, D. A. and McNally, J. G. (2006). Analysis of binding at a single spatially localized cluster of binding sites by fluorescence recovery after photobleaching. Biophys J 91, 1169-91.

Sprague, B. L., Pego, R. L., Stavreva, D. A. and McNally, J. G. (2004). Analysis of binding reactions by fluorescence recovery after photobleaching. Biophys J 86, 3473-95.

Stroud, M. J., Ballestrem, C. and Kammerer, R. A. (2010). GAS2-like 3 is a new member of the spectraplakin superfamily and interacts with both microtubules and actin. Manuscript submitted to the Journal of Cell Science.

Studier, F. W. (2005). Protein production by auto-induction in high density shaking cultures. Protein Expr.Purif. 41, 207-234.

Subramanian, A., Prokop, A., Yamamoto, M., Sugimura, K., Uemura, T., Betschinger, J., Knoblich, J. A. and Volk, T. (2003). Shortstop recruits EB1/APC1 and promotes microtubule assembly at the muscle-tendon junction. Curr.Biol. 13, 1086-1095.

Sun, D., Leung, C. L. and Liem, R. K. (2001). Characterization of the microtubule binding domain of microtubule actin crosslinking factor (MACF): identification of a novel group of microtubule associated proteins. Journal of Cell Science 114, 161-172.

Taylor, R. C., Cullen, S. P. and Martin, S. J. (2008). Apoptosis: controlled demolition at the cellular level. Nat Rev Mol Cell Biol 9, 231-41.

Thevenaz, P., Ruttimann, U. E. and Unser, M. (1998). A pyramid approach to subpixel registration based on intensity. IEEE Trans Image Process 7, 27-41.

Tirnauer, J. S., Canman, J. C., Salmon, E. D. and Mitchison, T. J. (2002). EB1 targets to kinetochores with attached, polymerizing microtubules. Mol Biol Cell 13, 4308-16.

Tsien, R. Y. (1998). The green fluorescent protein. Annu Rev Biochem 67, 509-44.

Vasiliev, J. M. (1991). Polarization of pseudopodial activities: cytoskeletal mechanisms. J.Cell Sci. 98 (Pt 1), 1-4.

Vasiliev, J. M., Gelfand, I. M., Domnina, L. V., Ivanova, O. Y., Komm, S. G. and Olshevskaja, L. V. (1970). Effect of colcemid on the locomotory behaviour of fibroblasts. J Embryol Exp Morphol. 24, 625-640.

Wang, H. W. and Nogales, E. (2005). Nucleotide-dependent bending flexibility of tubulin regulates microtubule assembly. Nature 435, 911-915.

Wen, Y., Eng, C. H., Schmoranzer, J., Cabrera-Poch, N., Morris, E. J., Chen, M., Wallar, B. J., Alberts, A. S. and Gundersen, G. G. (2004). EB1 and APC bind to mDia to stabilize microtubules downstream of Rho and promote cell migration. Nat.Cell Biol. 6, 820-830.

Wu, X., Kodama, A. and Fuchs, E. (2008). ACF7 regulates cytoskeletal-focal adhesion dynamics and migration and has ATPase activity. Cell 135, 137-148.

Youle, R. J. and Karbowski, M. (2005). Mitochondrial fission in apoptosis. Nat Rev Mol Cell Biol 6, 657-63.

Zilberman, Y., Ballestrem, C., Carramusa, L., Mazitschek, R., Khochbin, S. and Bershadsky, A. (2009). Regulation of microtubule dynamics by inhibition of the tubulin deacetylase HDAC6. J.Cell Sci. 122, 3531-3541.

Zucman-Rossi, J., Legoix, P. and Thomas, G. (1996). Identification of new members of the Gas2 and Ras families in the 22q12 chromosome region. Genomics 38, 247-254.

8) Appendix 1: Recent data implying G2L3 is involved in apoptosis

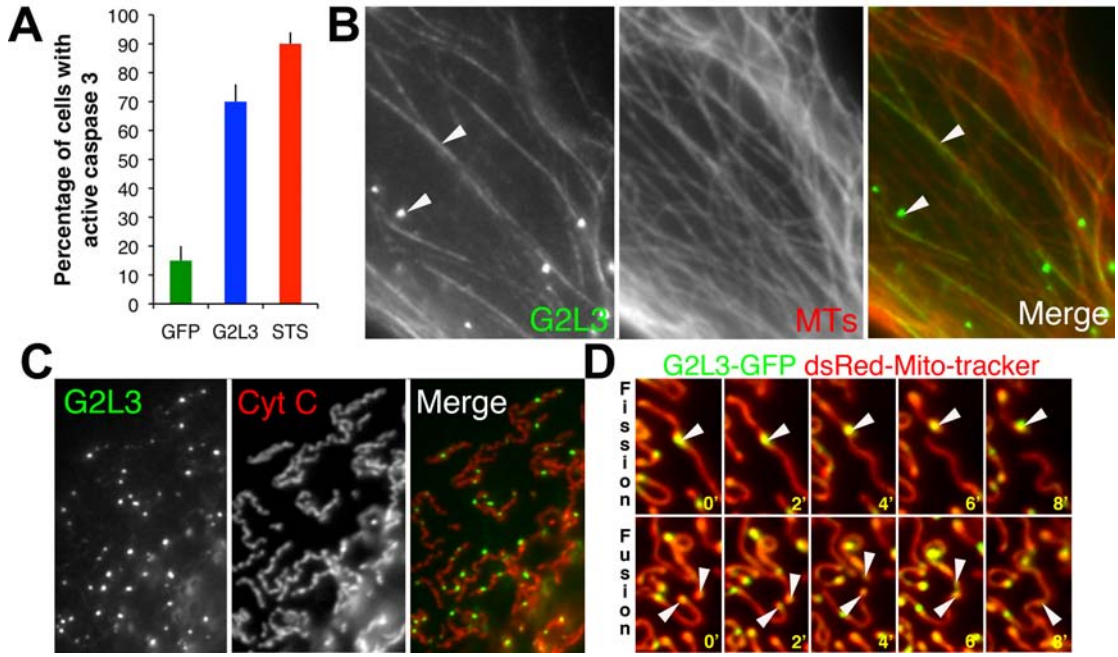

Figure 8.1: G2L3 induces caspase dependent apoptosis and localises to actin, MTs and sites of mitochondrial fusion and fission.

(A) NIH3T3 fibroblasts were transfected with GFP (control) or G2L3-GFP and the percentage of cells with active caspase 3 were analysed after 24hrs. As a positive control, untransfected cells were treated with staurosporine (STS) to artificially induce apoptosis. Note the significant increase in active caspase 3 in cells transfected with G2L3 compared to GFP ($p<0.001$), student's t-test. Error bars=standard error of the mean, results are representative of three independent experiments. **(B)** NIH3T3 cells expressing G2L3-GFP, were fixed and stained for microtubules (MTs). Note the colocalisation of G2L3 along MTs, and to discrete punctate spots. **(C)** Cytochrome C co-labelling reveals that G2L3-GFP positive punctate spots localise on discrete foci on mitochondria. **(D)** Time-lapse recordings of NIH3T3 cells expressing dsRed-Mitotracker and G2L3-GFP reveal the localisation of the latter at sites of mitochondrial division (fission; upper panel) and fusion (lower panel). G2L3 localisation is outlined by arrowheads.

9) Appendix 2: Buffers and Media

1% (w/v) Agarose gel (for DNA analysis)	1% (w/v) agarose *1 x (v/v) TAE*
Autoinduction media	*25 mM Na_2HPO_4* *25 mM KH_2PO_4* *50 mM NH_4Cl;* *5 mM Na2SO4* *2 mM MgSO4* *2.5 mM Glucose* *Ca2+ (2 mg/L)* *0.5% (v/v) Glycerol* *0.2% (w/v)Lactose* *Ampicillin (200 µg/ml)*
Binding buffer (8x)	*40mM Imidazole* *4M NaCl* *160mM Tris* *pH 7.9*
Charge buffer (8x)	*400mM Nickel sulphate*
DNA loading buffer (6x)	*0.25% (v/v) Bromophenol blue* *30% (v/v) Glycerol in water*
Elute buffer (4x)	*4M imidazole* *2M NaCl* *80mM Tis-HCl* *pH 7.9*
LB-Agar	*170mM NaCl* *1.0% (w/v) Tryptone* *0.5% (w/v) Yeast extract* *2.0% (w/v) Agar*
LB-Broth	*170mM NaCl* *0.8% (w/v) Tryptone* *1% (w/v) Yeast extract*

NP-40 Lysis Buffer	*50mM Tris-HCl, pH 7.4* *120mM NaCl* *2.5mM EDTA* *10mM $MgCl_2$* *1% (v/v) NP-40*
Phosphate Buffered Saline	*137mM NaCl* *2.7mM KCl* *4.3mM $Na_2HPO_4.7H2O$* *1.4mM KH_2PO_4*
SDS-PAGE resolving gel (7.5-15% w/v)	*7.5-15% (v/v) Acrylamide/ bisacrylamide* *375mM Tris-HC,l pH 8.8* *0.1% (w/v) SDS* *0.05% (w/v) Ammonium persulphate* *0.05 (v/v) TEMED*
SDS-PAGE stacking gel (4% w/v)	*4% (v/v) acrylamide/bisacrylamide* *125mM Tris-HCl, pH 6.8* *0.1% (w/v) SDS* *0.05% (w/v) Ammonium persulphate* *0.1% (v/v) TEMED*
SDS-PAGE gel tank buffer (10x)	*250mM Tris* *2.5M Glycine* *0.1% (w/v) SDS* *pH 8.3*
SDS-PAGE sample buffer (2x)	*100mM Tris-HCl, pH6.8* *200mM Dithiothreitol* *4% (w/v) SDS* *0.2% (w/v) Bromophenol blue* *20% Glycerol*
SDS-PAGE gel staining solution	*0.25% (w/v) Comassie brilliant blue* *7.5% (v/v) Acetic acid* *50% (v/v) Methanol*

	42.2% (v/v) Water
SDS-PAGE gel destaining solution	*45% (v/v) Methanol* *50% (v/v) Water* *5% (v/v) Acetic acid*
SPBA substrate	*100mM NaOAc* *50mM NaH_2PO_4* *40mM ABTS* *250mM H_2O_2*
Strip buffer (4x)	*400mM EDTA* *2M NaCl* *80mM Tris-HCl, pH 7.9*
Thrombin cleavage buffer	*150mM NaCl* *20mM Tris-HCl, pH 8.4*
Transfer buffer	*10mM $Na_2B_4O_7.10H_2O$*
Tricine Gel: Acrylamide A	48%Acrylamide/1.5% Bisacrylamide
Tricine Gel Buffer (1X)	*3M Tris-HCl, pH 8.4* *0.3% (w/v) SDS*
Tricine Gel Lower Reservoir (1X)	*200mM Tris-HCl, pH 8.9*
Tricine Gel Upper Reservoir (1X)	*100mM Tris-HCL, pH 8.25* *100mM Tricine* *0.1% (w/v) SDS*
Tris-acetate buffer (TAE) (50x)	*2M Tris Base* *1M Glacial acetic acid* *0.5M EDTA, pH 8*
Wash buffer (8x)	*480mM Imidazole* *4M NaCl* *160mM Tris-HCl, pH 7.9*

10) Appendix 3: Vector Maps

pHisTrx

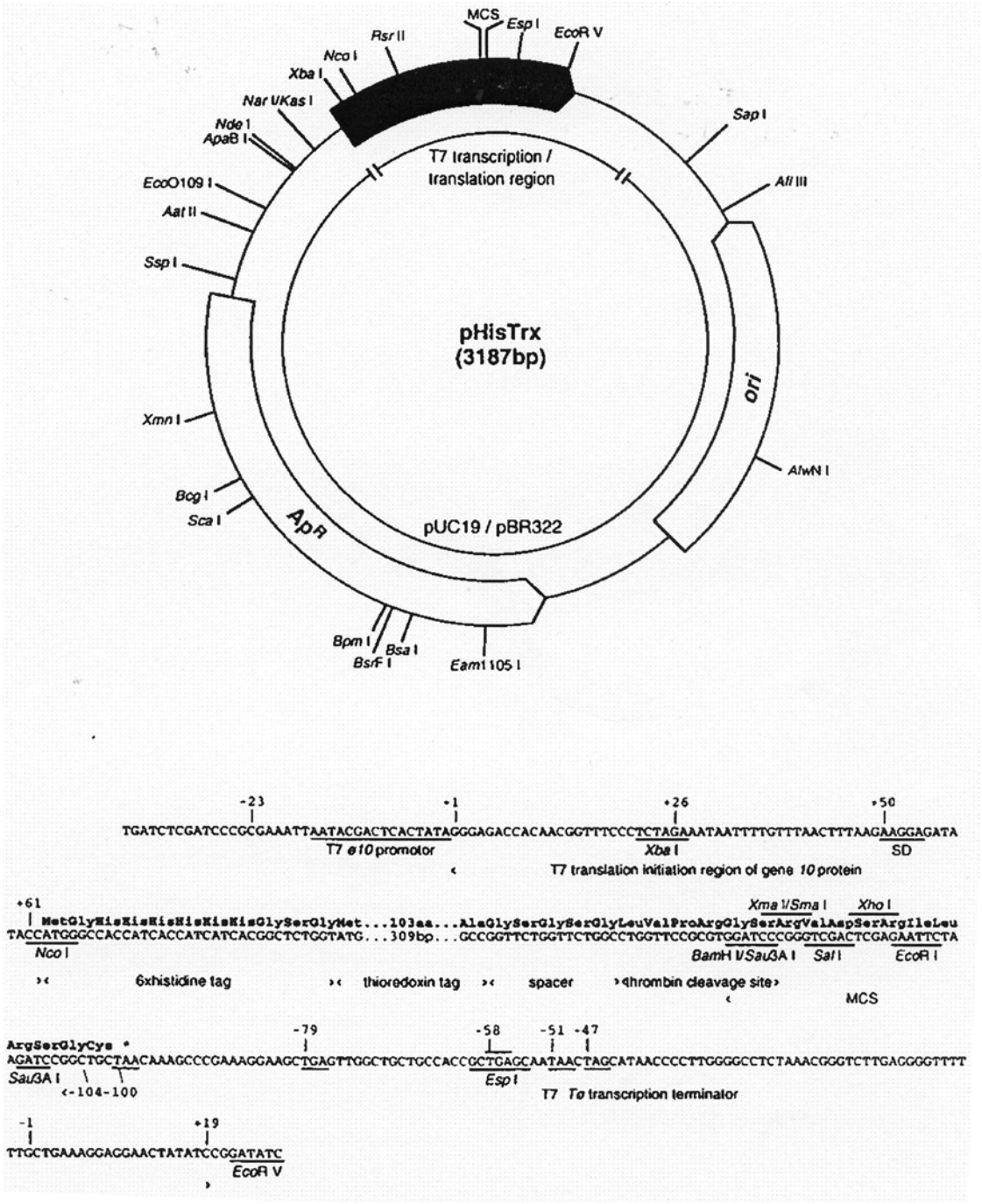

pEGFP-N1

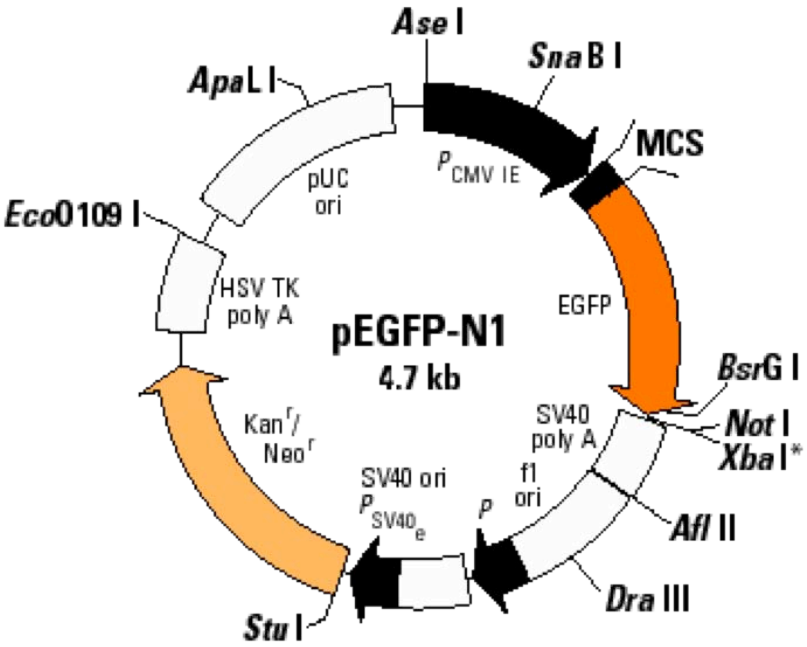

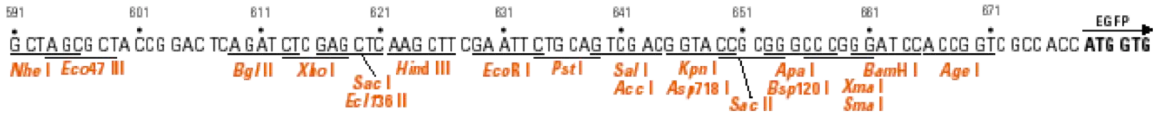

pEGFP-C1

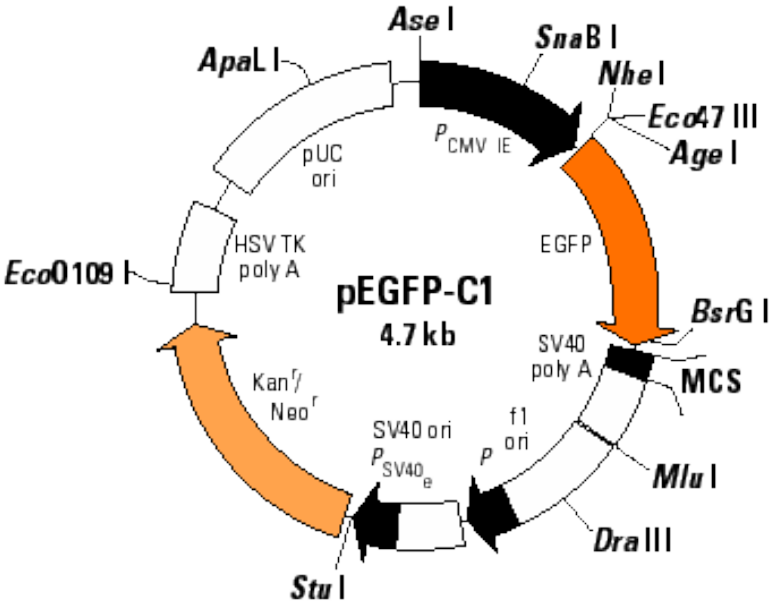

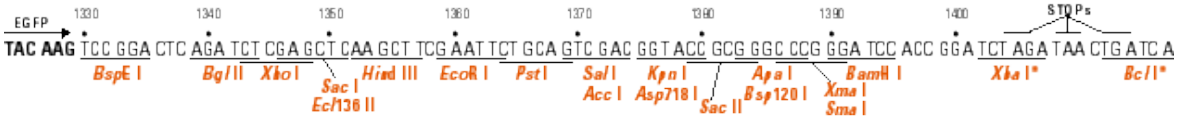

11) Appendix 4:

A Novel Receptor-induced Activation Site in the Nipah Virus Attachment Glycoprotein (G) Involved in Triggering the Fusion Glycoprotein (F)

Hector C. Aguilar‡1, Zeynep Akyol Ataman‡2, Vanessa Aspericueta‡2, Angela Q. Fang‡, Matthew Stroud§, Oscar A. Negrete‡, Richard A. Kammerer§, and Benhur Lee‡¶ 3

From the ‡Department of Microbiology, Immunology, and Molecular Genetics, ¶Department of Pathology and Laboratory Medicine, AIDS institute, David Geffen School of Medicine at UCLA, Los Angeles, California 90095 and the §Wellcome Trust Centre for Cell-Matrix Research, Faculty of Life Sciences, University of Manchester, Michael Smith Bldg., Oxford Rd., Manchester M13 9PT, United Kingdom

THE JOURNAL OF BIOLOGICAL CHEMISTRY
VOL.284, NO.3,pp.1628–1635, January 16, 2009

THE JOURNAL OF BIOLOGICAL CHEMISTRY VOL. 284, NO. 3, pp. 1628–1635, January 16, 2009

A Novel Receptor-induced Activation Site in the Nipah Virus Attachment Glycoprotein (G) Involved in Triggering the Fusion Glycoprotein (F)*[S]

Received for publication, September 26, 2008, and in revised form, October 25, 2008 Published, JBC Papers in Press, November 19, 2008, DOI 10.1074/jbc.M807469200

Hector C. Aguilar[‡1], Zeynep Akyol Ataman[‡2], Vanessa Aspericueta[‡2], Angela Q. Fang[‡], Matthew Stroud[§], Oscar A. Negrete[‡], Richard A. Kammerer[§], and Benhur Lee[‡¶‖3]

From the [‡]Department of Microbiology, Immunology, and Molecular Genetics, [¶]Department of Pathology and Laboratory Medicine, [‖]AIDS institute, David Geffen School of Medicine at UCLA, Los Angeles, California 90095 and the [§]Wellcome Trust Centre for Cell-Matrix Research, Faculty of Life Sciences, University of Manchester, Michael Smith Bldg., Oxford Rd., Manchester M13 9PT, United Kingdom

Cellular entry of paramyxoviruses requires the coordinated action of both the attachment (G/H/HN) and fusion (F) glycoproteins, but how receptor binding activates G to trigger F-mediated fusion during viral entry is not known. Here, we identify a receptor (ephrinB2)-induced allosteric activation site in Nipah virus (NiV) G involved in triggering F-mediated fusion. We first generated a conformational monoclonal antibody (monoclonal antibody 45 (Mab45)) whose binding to NiV-G was enhanced upon NiV-G-ephrinB2 binding. However, Mab45 also inhibited viral entry, and its receptor binding-enhanced (RBE) epitope was temperature-dependent, suggesting that the Mab45 RBE epitope on G may be involved in triggering F. The Mab45 RBE epitope was mapped to the base of the globular domain (β6S4/β1H1). Alanine scan mutants within this region that did not exhibit this RBE epitope were also non-fusogenic despite their ability to bind ephrinB2, oligomerize, and associate with F at wild-type (WT) levels. Although circular dichroism revealed conformational changes in the soluble ectodomain of WT NiV-G upon ephrinB2 addition, no such changes were detected with soluble RBE epitope mutants or short-stalk G mutants. Additionally, WT G, but not a RBE epitope mutant, could dissociate from F upon ephrinB2 engagement. Finally, using a biotinylated HR2 peptide to detect pre-hairpin intermediate formation, a cardinal feature of F-triggering, we showed that ephrinB2 binding to WT G, but not the RBE-epitope mutants, could trigger F. In sum, we implicate the coordinated interaction between the base of NiV-G globular head domain and the stalk domain in mediating receptor-induced F triggering during viral entry.

The paramyxoviruses comprise a group of important human pathogens, such as measles, mumps, human parainfluenza viruses, and the highly pathogenic Nipah (NiV)[4] and Hendra (HeV) viruses. NiV infections have a mortality rate in humans of up to 75%, and NiV is classified as a BSL4 pathogen because of its bio- or agro-terrorism potential (1). The efficacy of entry inhibitors targeted against HIV suggests that a better understanding of *Paramyxovirus* entry and fusion will facilitate similarly efficacious antiviral therapeutics.

Although past studies have identified regions in either the fusion (F) or attachment (G/H/HN) glycoproteins that are important for membrane fusion or F-G/H/HN association (2–10), the region(s) in G important for receptor-activated triggering of F-mediated fusion remains unknown. Current models of *Paramyxovirus* membrane fusion posit that receptor binding to the attachment glycoprotein (G, H, or HN) triggers a conformational cascade in the fusion protein (F). Such F-triggering results in fusion peptide (FP) exposure, which involves formation of a pre-hairpin intermediate and subsequent six-helix bundle formation (11). The energy released upon refolding into the stable six-helix bundle ground state is what drives the fusion of the viral and host-cell membranes. These are common functional and structural features responsible for membrane fusion for all enveloped viruses regardless of whether the fusion protein has predominantly trimeric α-helical coiled-coil (Class I), β (Class II), or a combination of α and β (Class III) core structures (12). Important human pathogens such as the HIV, influenza, and various paramyxoviruses have Class I fusion proteins, and their similar structural features point to similar membrane fusion mechanisms (11, 12). Besides sharing trimeric coiled-coil structures, they are synthesized as precursors that are cleaved into a metastable conformation; cleavage generates a new hydrophobic N terminus FP that gets released and inserted into the target cell membrane upon triggering (11, 12). Class I fusion proteins have two heptad repeat regions, HR1 and HR2, at their N and C termini, respectively, that fold up onto each other during six-helix bundle formation to bring about merging

* This work was supported, in whole or in part, by National Institutes of Health Grants AI070495, AI060694, and AI069317 (to B. L.). Additional support was provided by a Charles E. Culpepper Medical Scholarship from the Rockefeller Brothers Fund and a Burroughs Welcome Fund Career Development Award. The costs of publication of this article were defrayed in part by the payment of page charges. This article must therefore be hereby marked "*advertisement*" in accordance with 18 U.S.C. Section 1734 solely to indicate this fact.

[S] The on-line version of this article (available at http://www.jbc.org) contains supplemental Figs. 1–5.

[1] To whom correspondence may be addressed: Dept. of MIMG, 257 BSRB, 615 Charles E. Young Dr. East, UCLA, Los Angeles, CA 90095. Tel.: 310-206-8792; Fax: 310-267-2580; E-mail: haguilar@ucla.edu.

[2] These authors contributed equally.

[3] To whom correspondence may be addressed: Dept. of MIMG, 257 BSRB, 615 Charles E. Young Dr. East, UCLA, Los Angeles, CA 90095. Tel.: 310-206-8792; Fax: 310-267-2580; E-mail: bleebhL@ucla.edu.

[4] The abbreviations used are: NiV, Nipah virus; G/H/HN, attachment glycoprotein; F, and fusion glycoprotein; RBE, receptor binding-enhanced; CD, circular Dichroism; HR, heptad repeat region; MFI, mean fluorescence intensity; HA, hemagglutinin; CHO, Chinese hamster ovary; WT, wild type; Mab45, monoclonal antibody 45; FP, fusion peptide.

of target cell and viral membranes (12). For *Paramyxovirus* F proteins, the C-terminal HR2 region is generally thought to be pre-formed, but the N-terminal HR1 region is formed only upon F-triggering and FP insertion (11, 13). The formation of this trimeric HR1 core just before six-helix bundle formation, is known as the pre-hairpin intermediate.

Despite their common features, viral fusion proteins vary in their detailed structures, triggering factors, and number of viral surface proteins involved. For paramyxoviruses, receptor binding and fusion functions are carried out by two distinct transmembrane proteins (attachment (G, H, or HN) and fusion (F) proteins, respectively), and with few exceptions both are required for membrane fusion. The underlying mechanism of fusion triggering by the attachment protein may vary depending on their use of protein *versus* carbohydrate receptors (14). For example, we and others have observed an inverse correlation between fusogenicity of the F protein and the avidity of the F/G or F/H interactions for NiV and measles virus (2, 3, 5, 15, 16), both of which use protein-based receptors; however, for Newcastle disease virus, a glycan-using *Paramyxovirus*, there seems to be a direct correlation between fusogenicity and the avidity of F/HN interactions (8).

For the paramyxoviruses, the early steps in the fusion cascade, particularly how H/HN "triggers" F, are not well understood, and the region(s) in H/HN responsible for F triggering remains unclear, although the stalk domain of H/HN appears to be important for F triggering or for interaction with F (5–8). For NiV, the G attachment glycoprotein binds either the ephrinB2 (B2) or ephrinB3 (B3) protein receptors (17–19), but it is not known how receptor engagement induces G to undergo the allosteric changes involved in triggering F. However, by homology to H or HN, it is likely that the stalk domain in NiV-G is also involved in F-triggering (20). Here we analyze the early steps in the fusion cascade for NiV and identify a specific region in NiV-G distinct from the receptor binding site that is involved in 1) B2-induced changes that trigger FP exposure in F, 2) modulating the avidity of F/G interactions resulting in displacement of F from G, and 3) transducing receptor-induced membrane fusion. Our results offer testable hypotheses as to whether this model of fusion cascade holds true for other paramyxoviruses that use protein-based receptors.

EXPERIMENTAL PROCEDURES

Expression Plasmids—HA and AU1 tagged codon-optimized (CO) NiV-G (G) and NiV-F (F) expression plasmids, respectively (21), and G deletion mutants 1, 2, 3, 4, 9, 11, and 14 (17), were previously described. Deletion mutants Δ4 and Δ9 and triple Ala site mutants 4-1, 4-2, 4-3, 4-4, and 4-5 were made by site-directed mutagenesis of the CO wild-type (WT) G plasmid using the QuikChange™ kit (Stratagene). All mutations were confirmed by sequencing the entire open reading frame.

Cell Culture—The growth conditions for CHO-pgsA745 (CHO), CHOB2-pgsA745 (CHOB2), Vero, and 293T cells have been previously described (2, 17).

Antibody Production and Quantification of Cell Surface Expression and Antibody Binding Levels by Flow Cytometry—Production of rabbit anti-G and anti-F antisera from CO G and F plasmids was previously described (2, 3, 17), and production of rabbit monoclonal anti-G antibodies was essentially as described for anti-F monoclonal antibodies (3). Sera or hybridoma supernatants containing anti-F- or anti-G-specific activities were used at 1:1000 dilution for flow cytometry on NiV-F/G-transfected cells, and bound antibody was detected as previously described (2, 3). For ephrinB2 (B2) binding assays, soluble B2-humanFc protein (R&D) was added at 10 nM and detected using anti-human Fc secondary antibodies (Caltag) as indicated previously (17).

Quantitation of Cell-Cell Fusion—CO WT or mutant G and CO WT F expression plasmids (1:1 ratio, 1 μg of total) were transfected into 293T cells grown in 12-well plates at 70% confluency. 12–18 h post-transfection, cells were 4′,6-diamidino-2-phenylindole-stained, and syncytia formation was quantified as indicated previously (2, 3, 21).

Circular Dichroism (CD)—Changes in the secondary structure of NiV-G were monitored by CD spectroscopy in a Jasco-715 spectrometer. Data were collected between 200 and 240 nm, keeping the high voltage below noise levels at all times. Experiments were repeated three times, and each trial was the average of three scans at 20 nm/min and 0.2 nm of resolution. PBS+ buffer (phosphate-buffered saline supplemented with 500 μM Mg_2Cl and 900 μM $CaCl_2$) (22) was used in a 300-μl cuvette at room temperature. CD spectra of ephrinB2 (B2) (2.5 μM), soluble G (1.2 μM), and B2:G mixture were collected. Data were corrected by subtracting the buffer signal. The theoretical spectrum of the B2:G mixture, assuming no interprotein interaction, was calculated by the linear addition of the individual B2 and G scans, and the changes in the ellipticity were calculated by subtracting the experimental B2:G data from the theoretical spectrum. The change in ellipticity magnitude was calculated by averaging the ellipticity values between 223 and 208 nm in both theoretical and experimental data.

NiV-F/NiV-G Co-immunoprecipitation—NiV-F/G vesicular stomatitis virus pseudotyped virions were allowed to mix with CHO cells (negative control) or CHOB2 cells for 2 h at 4 °C then triggered at 37 °C for 0, 15, or 60 min and lysed in 1% Triton-X100. G was immunoprecipitated under each condition using rabbit anti-G polyclonal antibodies as previously described (2, 3, 21). Co-immunoprecipitated F was detected by Western blotting using the primary anti-AU1 tag antibodies, and signals were quantified by densitometry as previously described (2, 3).

Triggering of NiV-F—CHO cells were transfected with WT F and WT or mutant G expression plasmids as well as a green fluorescent protein expression plasmid at a 10:10:1 ratio, respectively. 18 h post-transfection, a 1:1 ratio of the transfected cells and either CHO (negative control) or CHOB2 cells were mixed and incubated for 45 min at 4 °C or 37 °C in the presence of excess (500 μM) biotinylated HR2 peptide (biotin-KVDISSQISSMNQSLQQSKDYIKEAQRLLDTVNPSL). Subsequently, the cells were washed with wash buffer (1% FBS in phosphate-buffered saline), fixed in 0.5% paraformaldehyde in wash buffer, and washed again 2X with wash buffer. The biotinylated HR2 peptide bound to F was detected using streptavidin-allophycocyanin and quantified by flow cytometric analysis. To enhance our signal:noise ratio and to focus only on F-expressing cells, green fluorescent protein (GFP++) cells

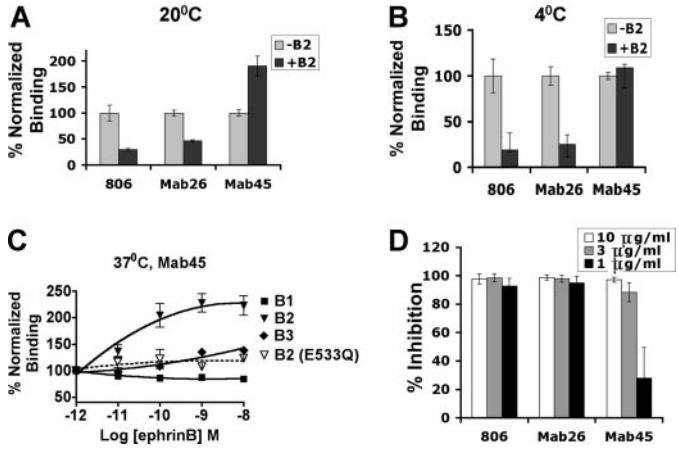

FIGURE 1. **Enhanced binding of Mab45 to NiV-G (G) induced by ephrinB2 (B2) receptor binding.** *A*, polyclonal (*806*) and monoclonal (*Mab26* and *Mab45*) anti-NiV-G antibodies binding to full-length NiV-G expressed in CHOpgsA745 (CHO) cells in the presence or absence of soluble B2 protein at room temperature (~20 °C) as detected by flow cytometry. % normalized binding indicates MFI values normalized to the MFI values obtained in the absence of soluble B2 (set at 100% for each antibody examined). Average ± S.E. are shown, $n = 3$. *B*, similar experiment to *A*, except performed at 4 °C. *C*, binding of Mab45 to CHO cells expressing G or mutant E533Q at 37 °C when increasing concentrations of soluble ephrinB1 (*B1*), ephrinB2 (*B2*), or ephrinB3 (*B3*) were used. Logarithm of the molar concentration of the soluble ephrinBs used was plotted against % normalized binding, calculated as in *A*. Average ± S.E. are shown, $n = 4$. *D*, the inhibitory properties of 806, Mab26, or Mab45 antibodies were measured by mixing the indicated concentrations with NiV/vesicular stomatitis virus renilla luciferase pseudotyped particles immediately before infection of Vero cells. Data are shown as % inhibition normalized to luciferase activity in the absence of any antibodies. Average ± S.E. are shown; $n = 3$.

were gated and analyzed for their allophycocyanin (HR2-biotin binding) signals.

RESULTS

Enhanced Binding of Monoclonal Antibody 45 (Mab45) to NiV-G (G) Induced by EphrinB2 Receptor Binding—Receptor-induced conformational epitopes can be suggestive of conformational changes in viral envelopes that eventually lead to membrane fusion and viral entry. This is exemplified by CD4-induced coreceptor binding epitopes in HIV gp120. Binding to coreceptor after CD4-induced conformational changes in HIV gp120 triggers fusion peptide exposure in gp41 and the subsequent six-helix bundle formation that eventually leads to membrane fusion (23, 24). NiV also uses a protein-based receptor and a type I fusion protein, although in this *Paramyxovirus*, the receptor-interacting attachment glycoprotein (G) is physically distinct from the fusion (F) protein. To determine whether receptor engagement of G also results in conformational changes that lead to F triggering and fusion peptide exposure, we first sought to develop conformational antibodies against NiV-G that exhibit a receptor-induced epitope. Fig. 1*A* shows a representative set of NiV-G-specific rabbit polyclonal (806) and monoclonal antibodies (Mab26 and Mab45) obtained via genetic immunization with expression plasmids for codon-optimized Nipah matrix M, F, and G (see "Experimental Procedures"). Note that both Mab26 and the polyclonal anti-NiV-G antiserum (806) showed a relative decrease in NiV-G binding in the presence of soluble ephrinB2 (B2), the cognate receptor for henipaviruses, suggesting that B2 may compete for the binding epitopes of these antibodies. In contrast, Mab45 bound better to G in the presence of soluble B2 (Fig. 1*A*). CHO cells expressing full-length G were used in these assays because they do not express endogenous henipavirus receptors (17, 18), and thus, we could control for receptor engagement by adding exogenous soluble B2. The enhancement of Mab45 binding to G upon B2 engagement was observed at 20 and 37 °C (Fig. 1, *A* and *C*) but not at 4 °C (Fig. 1*B*), suggesting that the receptor-induced enhancement of Mab45 binding to NiV-G was a temperature/energy-dependent process.

To further examine the specificity of this phenomenon, increasing amounts of soluble ephrinB1 (B1), ephrinB2 (B2), or ephrinB3 (B3) were added to CHO cells expressing NiV-G and were allowed to incubate at 37 °C for 15 min in the presence of a constant amount of Mab45 (0.2 μg/ml). Fig. 1*C* shows that there was a dose-dependent enhancement of Mab45 binding to G when titrating in B2 and to a much lesser extent, B3, and not at all for B1. This was consistent with the much higher affinity of B2 than B3 for NiV-G (18). Indeed, the EC_{50} of the dose-response curve for B2-enhanced Mab45 binding was remarkably close to the established K_d of ephrinB2 for NiV-G (~0.1 nM). Additionally, a receptor binding-deficient NiV-G mutant, E533Q, which is expressed and can be bound by Mab45 at WT levels (25), displayed no enhancement of Mab45 binding upon the addition of B2, underscoring that receptor binding to NiV-G was necessary for the enhancement of Mab45 binding (Fig. 1*C*). Altogether, these results suggested that upon B2 binding, a structural change occurred in NiV-G that allowed Mab45 to bind more efficiently and that such a change(s) was energy-dependent.

Mapping of the Mab45 Conformational Epitope in NiV-G—Because Mab45 binding to NiV-G was enhanced upon receptor binding and yet Mab45 was still able to block NiV entry (Fig. 1*D*), we hypothesized that Mab45 receptor binding-enhanced (RBE) epitope may be important for the receptor-induced changes in G that lead to F triggering and membrane fusion. Thus, we first sought to map the Mab45 epitope on NiV-G. The Mab45 epitope was conformational, as Mab45 did not Western blot, and screening of overlapping 22-mer peptides spanning the entire ectodomain of NiV-G did not result in any positive hits (supplemental Fig. 1). Next, we utilized a series of well expressed, previously described soluble NiV-G deletion mutants (17) in a pre-absorption/competition assay to show that region 4 and 9 (Fig. 2*A* and supplemental Fig. 2) were important for Mab45 and Mab26 binding, respectively. Then, we confirmed these results in the context of the full-length NiV-G protein by deleting the regions 4 or 9 and measuring the direct binding of Mab45 and Mab26 to these deletion mutants expressed on CHO cells. Fig. 2*B* shows that although the Δ4 mutant bound monoclonal anti-HA tag or Mab26 antibodies, it did not bind Mab45. Conversely, although expressed at lower levels at the cell surface, Δ9 bound anti-HA or Mab45 antibodies but not Mab26 (Fig. 2*B*). Thus, we confirmed that region 4 in G, located at the β6S4/β1H1 region (amino acids 195–211) at the base of the head domain, is important for Mab45 binding, whereas region 9, within the β3H1/β3H2 region (amino acids 371–392) at the top of the head domain near the receptor bind-

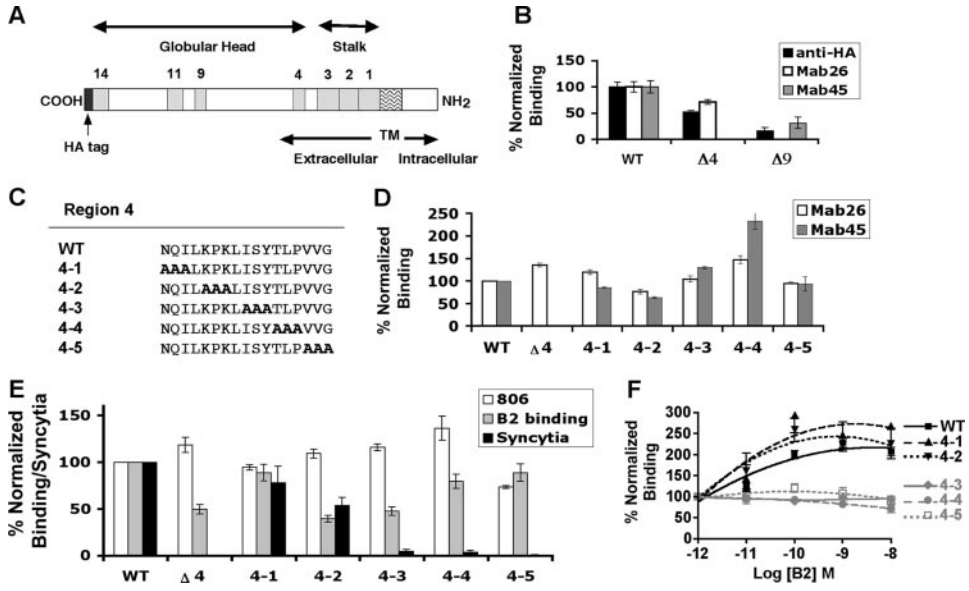

FIGURE 2. **Role of the β6S4/β1H1 region of G in membrane fusion and Mab45 binding enhancement.** *A*, schematic of NiV-G showing the various domains. Deletion sites 1, 2, 3, 4, 9, 11, and 14 are depicted, and their sequences are shown in supplemental Table 1. *B*, binding of anti-HA, Mab26, and Mab45 to CHO cells expressing WT or deletion mutant G constructs Δ4 and Δ9, as measured by flow cytometry. Average ± S.E. are shown, $n = 3$. Both Mab45 and Mab26 are conformational antibodies, as they do not Western blot. *C*, sequence of region 4 of G showing the location of the triple Ala mutations 4-1, 4-2, 4-3, 4-4, and 4-5 constructed in the context of full-length G. *D*, binding of the full-length WT and the indicated mutant G proteins to Mab26 and Mab45 by flow cytometry, normalized to their anti-HA antibody binding levels. Average ± S.E. are shown, $n = 3$. *E*, levels of binding of region 4 mutants to polyclonal anti-NiV-G antiserum 806 or to soluble ephrinB2 (B2) in CHO cells and levels of syncytia formation in 293T cells normalized to anti-HA antibody binding to correct for any discrepancies in cell surface expression levels. Average ± S.E. values are shown, $n = 3$. *F*, levels of binding of WT and region 4 mutant proteins to Mab45 at various concentrations of B2, normalized to Mab45 binding in the absence of B2 (set at 100%) as in Fig. 1*C*. Data were plotted using Prism, and average ± S.E. values are shown, $n = 3$.

ing site, is important for Mab26 binding (supplemental Fig. 3*A*) (26, 27).

To further map the putative Mab45 epitope, we constructed a series of triple alanine scan mutants within region 4 (mutants 4-1 through 4-5, Fig. 2*C*). We determined the relative levels of binding of these mutant proteins to anti-HA, Mab45, and Mab26 by flow cytometry using CHO cells expressing the full-length WT or mutant G proteins in the absence of any ephrinB2. Fig. 2*D* shows the levels of Mab45 and Mab26 binding normalized to the anti-HA levels to correct for any cell surface expression differences. Surprisingly, although deletion of the entire region 4 (Δ4) abolished Mab45 binding to NiV-G, none of the triple alanine mutants showed a significant decrease in Mab45 binding. These results may imply that the Mab45 epitope was complex and was not determined by any short primary linear sequence, even within region 4. Alternatively, because Mab45 was a conformational antibody as mentioned above, deletion of region 4 may have resulted in a gross perturbation of NiV-G that abrogated Mab45 binding as an indirect effect. Thus, region 4, which we posited as being part of the putative Mab45 epitope, may have no direct but only an indirect involvement with the RBE epitope that we hypothesized as being involved in the receptor-induced changes in G that lead to membrane fusion.

Role of the Region of G in Membrane Fusion—To further clarify whether region 4 (β6S4/β1H1) or the putative Mab45 epitope plays an active role in the receptor-induced conformational cascade that leads to Nipah virus fusion, we analyzed the receptor binding and fusogenic capabilities of the region 4 mutants when coexpressed with F. The Δ4 mutant itself was relatively well expressed and bound to B2 at 50% that of wild-type levels but was completely defective in a syncytia formation assay (Fig. 2*E*). Interestingly, although WT G and mutant proteins 4-1 and 4-2 formed syncytia with an efficiency that paralleled their ability to bind B2, almost no syncytia formation was observed for the 4-3, 4-4, and 4-5 mutant proteins despite them being 1) expressed at significant levels at the cell surface (Fig. 2*D*), 2) able to bind soluble B2 (Fig. 2*E*), 3) able to associate with F (supplemental Fig. 4*A*), and 4) able to form G oligomers (supplemental Fig. 4*B*).

Because there were no obvious differences between the fusion-competent (4-1, 4-2) and fusion-defective (4-3, 4-4, 4-5) mutants in terms of the four above-mentioned criteria for the conformational integrity of NiV-G, we asked whether the fusion-competent and fusion-defective mutants were able to undergo the receptor-induced changes that potentially lead to fusion. Thus, we determined whether Mab45 RBE epitope was associated with the fusogenic capacities of the region 4 mutant proteins. We subjected all region 4 mutants to the B2-enhanced Mab45 binding assay described in Fig. 1*C*. Remarkably, the fusion-competent mutants 4-1 and 4-2 displayed WT levels of Mab45 binding enhancement with similar EC_{50} values for the amount of B2 used (~0.1 nM), whereas the fusion-defective 4-3, 4-4, and 4-5 mutants did not show any Mab45 binding enhancement regardless of how much B2 was added (Fig. 2*F*). These results suggest a role for the involvement of the RBE Mab45 epitope in the receptor-induced changes in NiV-G that lead to membrane fusion. In particular, the region demarcated by the alanine scan mutants 4-3 to 4-5 of NiV-G (ISYTLPVVG) may play a role in membrane fusion by mediating the receptor-induced conformational changes that lead to F triggering.

EphrinB2 Binding to NiV-G Induces Secondary Structure Changes in NiV-G That Are Correlated with Fusogenicity—Based on the above results, we hypothesized that the non-fusogenic region 4 mutants of G (*e.g.* 4-5) will not undergo the post receptor-binding structural changes that lead to F triggering and membrane fusion. In addition to the receptor-induced enhancement of Mab45 binding, we sought to obtain independent biophysical evidence of conformational changes in NiV-G induced by B2 binding. We performed CD studies on the entire soluble ectodomain of WT NiV-G (amino acids 71–602) and the equivalent soluble 4-5 mutant protein when mixed individually with soluble B2. We took advantage of the linear characteristics of the CD

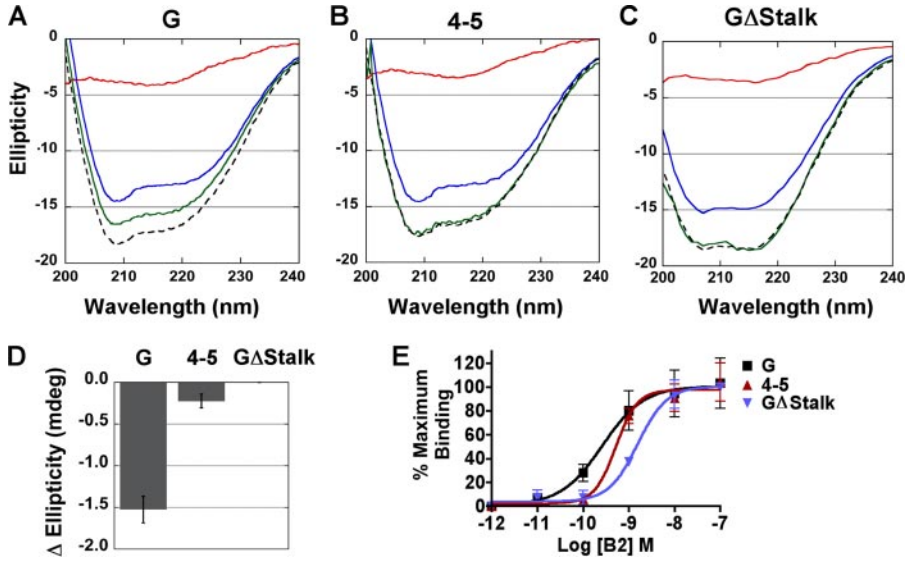

FIGURE 3. **EphrinB2 binding to NiV-G induces secondary structure changes in NiV-G that are correlated with fusogenicity.** *A*, changes in the secondary structure of soluble G (*blue*) at 1.2 μM were monitored using CD spectroscopy upon the addition of B2 (*red*) at 2.5 μM. A theoretical spectrum is shown using a *black dashed line*, and the experimental G:B2 scan is shown in *green*. The difference between the latter two lines reflects differences in secondary structure. *B* and *C*, same experiment as in *A*, except replacing WT G for soluble 4-5 and GΔstalk proteins, respectively. The GΔStalk protein lacked amino acids 71–154 of the stalk domain. *D*, the difference between experimental and theoretical data (Δ [θ]) were generated by averaging the CD signals between 223 and 208 nm and subtracting the experimental signal (*green line*) coming from the indicated G and B2 mixture from the theoretical signal (*black dashed line*). Data are the average ± S.E., $n = 3$. *E*, soluble WT G, 4-5, or GΔStalk mutant proteins coating a maxisorb plate bound soluble B2 similarly in an ELISA enzyme-linked immunosorbent assay format assay. A sigmoidal dose response curve is shown (data are the average ± S.D., performed in triplicate).

signals. The combined CD spectra of two proteins in a solution is the linear addition of the individual CD signals coming from each individual protein when there are no interprotein interactions that lead to conformational changes (28). Only when there is a conformational change do the experimental CD spectra of the protein mixture deviate from the linear sum of the individual proteins. Interestingly, we detected a deviation from the theoretical CD spectra upon B2 binding to NiV-G but not to the 4-5 mutant (compare Fig. 3, *A* with *B*, *green lines* and *dotted black lines* represent the experimental and theoretical spectra, respectively), indicating a conformational change in the secondary structure of at least one of these two proteins. Because the identical soluble B2 protein was used to bind both NiV-G and 4-5 proteins, Fig. 3, *A* and *B*, and the soluble NiV-G proteins gave a much more pronounced CD signal than that of B2 (Fig. 3 *A* and *B*, *blue* and *red lines*, respectively), these data strongly suggest that the conformational change that resulted in the change in CD spectra came from NiV-G. Note that the 4-5 mutant G protein was expressed well and bound B2 at WT levels in both the full-length and soluble versions (Figs. 2*E* and 3*E*) but was fusion-defective (Fig. 2*E*), implicating a link between fusogenicity and the B2-induced a conformational change in G.

As an additional control, we tested another soluble NiV-G with a truncated stalk domain (GΔStalk), as the stalk domain of paramyxoviral attachment proteins is also critically involved in F-triggering (5–8). Fig. 3*C* shows that B2 binding to GΔStalk did not induce any secondary structural changes, as evidenced by the lack of deviation between the observed and theoretical CD spectra even though GΔStalk was clearly able to bind B2 (Fig. 3*E*). Fig. 3*D* quantifies the relative changes in the CD spectra (Δ[θ]) upon B2 binding to NiV-G, the 4-5 mutant, and the GΔStalk construct. The change in CD spectra differences observed for NiV-G was modest but highly significant ($p < 0.002$ and $p < 0.008$, Student's t test) when compared with the GΔStalk or the 4-5 mutant, respectively, suggesting an interactive role between the base of the globular head and the stalk domain of NiV-G in B2-induced conformational changes. Because the identical soluble B2 was added in all cases, the secondary structural changes likely come from G and not B2. Remarkably, the recently solved structures of NiV-G complexed with B2 or B3 indicate that the region demarcated by the 4-4 and 4-5 mutants is highly flexible and, indeed, comprises the only few residues that cannot be resolved in the B2-NiVG complex (26, 27).

Lack of G "Activation" Correlates with a Lack of F Dissociation from G—For paramyxoviruses that use protein-based receptors, we and others have shown an inverse correlation between fusogenicity and the avidity of F/H or F/G interactions (2, 3, 5, 15, 16), suggesting that dissociation of F from G after receptor engagement is the rate-limiting parameter in the fusion cascade. Thus, we hypothesized that B2-induced activation of G, as measured by the temperature-dependent enhancement of Mab45 binding and changes in CD spectra, will result in a relative dissociation of F from G. To test this hypothesis, we mixed NiV F/G pseudotyped vesicular stomatitis virus virions with CHO cells that constitutively expressed B2 (CHOB2) (18) or not (CHO), and allowed them to bind for 2 h at 4 °C to synchronize the infection process. Thereafter, we moved the cell/virus mixtures to 37 °C for 0, 15, or 60 min. At the indicated time points, the cell/virus mixture was lysed, immunoprecipitated with anti-G specific antibodies, and Western-blotted for the amount of F that was co-immunoprecipitated. Fig. 4*A* shows that in the absence of B2, the amount of F_0/F_1 on virions that was co-immunoprecipitated with G did not change over time, whereas in the presence of B2 (Fig. 4*B*) there was a clear reduction of F_1 and, to a lesser extent F_0, which was co-immunoprecipitated with G over time. Densitometric data show that co-immunoprecipitated F_1 was reduced by 50 and 80% at 15 and 60 min, respectively, after shifting to 37 °C (Fig. 4*D*). Strikingly, the non-fusogenic 4-5 mutant G protein, which did not exhibit B2-induced activation, also did not show a dissociation of F_0/F_1 from G over time (Fig. 4, *C* and *D*) in the presence of B2. These results suggest that the region roughly demarcated by the 4-5 mutant may be involved in the conformational cascade that leads to receptor-induced F/G dissociation and perhaps the downstream triggering of F.

Lack of G Activation Results in the Inability to Trigger F—To further study whether the inability to undergo receptor-induced activation in the non-fusogenic (region 4) mutant G proteins was related to the inability to trigger F, we developed a triggering assay for the NiV-F protein. Current models of paramyxoviral membrane fusion suggest that F triggering involves formation and exposure of the HR1 (13) that is coincident with fusion peptide insertion into the target cell membrane (10). The HR1 and HR2 in this pre-hairpin intermediate then fold together to form the 6-helix bundle that drives membrane fusion. HR2 peptides in NiV-F are thought to inhibit membrane fusion by binding to the exposed HR1 region (2, 3, 29), and thus, we assayed whether we could detect F-triggering by HR2 peptide binding to the exposed HR1 region during the pre-hairpin intermediate stage under permissive conditions. First, we constructed a biotinylated peptide that contained the sequence of the HR2 region of NiV-F previously determined to inhibit NiV infection and fusion (HR2-biotin) (2, 29). This peptide was able to inhibit viral entry efficiently at an IC_{50} of 10 nM (supplemental Fig. 5*A*). Next, we showed that HR2-biotin preferentially bound to an artificially trimerized HR1 core designed to mimic the inner HR1 core of the six-helix bundle (supplemental Fig. 5, *B–D*). To detect F triggering, CHOB2 cells were first mixed with CHO cells expressing the NiV-F and G glycoproteins for 2 h at 4 °C to synchronize receptor binding. The HR2-biotin peptide was then added to the cell mixture, and the fusion process was induced or not by incubating them at 37 or 4 °C, respectively, for another 45 min. HR2-biotin binding as a surrogate marker for F triggering or pre-hairpin intermediate formation was detected by fluorescence-activated cell sorter analysis using allophycocyanin-conjugated streptavidin. To focus only on F-expressing cells, NiV-F/G was co-transfected with a fluorescent protein expression (GFP) expression plasmid, and GFP++ cells were gated and analyzed for their allophycocyanin (HR2-biotin binding) signals. For WT F/G, we were able to detect a significant increase in HR2-biotin binding over background levels at 37 °C, but not at 4 °C, and in the presence of B2 but not in its absence (Fig. 5, *A* and *B*), indicating that binding of biotinylated HR2 peptide was a sensitive and specific assay for detecting F triggering.

We then applied this assay to some of the (region 4) G mutants that were unable to undergo B2-induced conformational changes described above. Compared with WT G, the 4-4

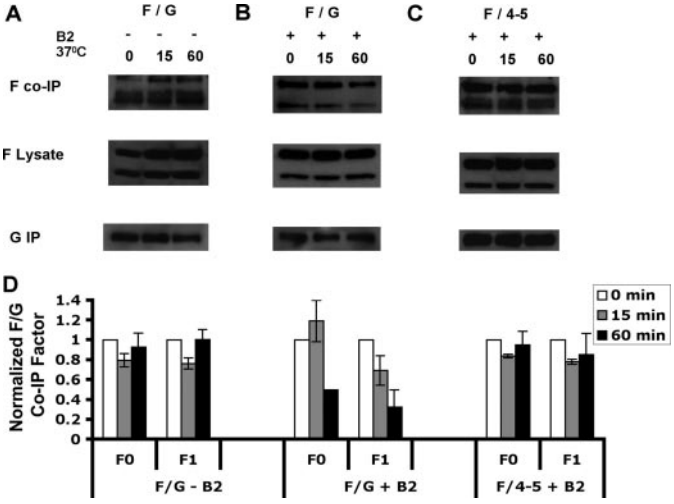

FIGURE 4. **Lack of G activation correlates with lack of F dissociation from G.** *A*, co-immunoprecipitation of NiV-F using anti-NiV-G antibodies (*top*) from F/G/vesicular stomatitis virus pseudotyped virions allowed to mix with CHO cells (negative control) for 2 h at 4 °C then triggered at 37 °C for 0, 15, or 60 min, and lysed in 1% Triton X-100. Amounts of NiV-F in the viral/cell lysate (*middle*) and amounts of immunoprecipitated G under each condition (*bottom*) are shown. *Co-IP*, co-immunoprecipitation. *B*, same experiment as in *A* but using CHOB2 instead of CHO cells. *C*, same experiment as in *B* except using the 4-5 mutant G protein instead of the WT G protein. One representative experiment of three is shown. *D*, quantification of the effects of ephrinB2 binding on F/G interactions. The bands in *A–C* were quantified by densitometry using a VersaDoc Imaging System (Bio-Rad). For each time point and experimental condition, the normalized co-immunoprecipitation (*Co-IP*) F ratio was calculated as the ratio of co-immunoprecipitated F_0 or F_1 signals (from *A–C*, *top panels*) over the total F_0 or F_1 signals in the cell lysates (*A–C*, *middle panels*) (to normalize for F expression levels) divided by the total amount of immunoprecipitated G (*A–C*, *bottom panels*), as shown in the formulas below. For each experimental condition, the normalized co-immunoprecipitation F ratio at various time points was normalized to the ratio obtained at time 0, which was set at 1 unit. Note that F_1 dissociated from WT G more than F_0 in the presence of B2. Data are the average ± S.E. are shown, $n = 3$. Normalized co-immunoprecipitation (Co-IP) F_0 ratio = (Co-IP F_0/(F_0 in cell lysates))/(G IP); normalized co-IP F_1 ratio = (Co-IP F_1/(F_1 in cell lysates))/(G IP).

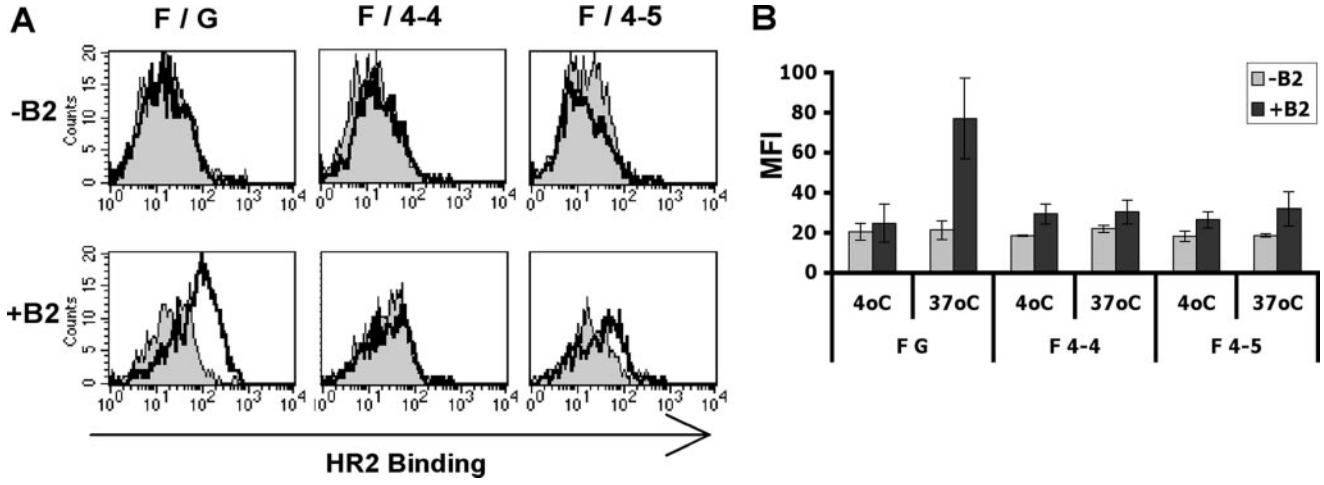

FIGURE 5. **Lack of G activation results in inability to trigger F.** *A*, CHO cells expressing F and G were mixed with either CHO cells (negative control) or CHOB2 cells for 2 h at 4 °C. Cell mixtures were brought to 37 °C or kept at 4 °C for 45 more min to allow for triggering of F or not in the presence of 500 nM biotinylated HR2 peptide. *B*, the MFI values are summarized for 4 or 37 °C and in the absence (−*B2*) or presence (+*B2*) of B2 for the F/G (WT), F/4-4, and F/4-5 protein pairs. Data are the average ± S.E. are shown, $n = 3$. The *p* value for the MFI of the (+*B2*) *versus* (−*B2*) conditions at 37 °C for WT F/G was 0.02.

and 4-5 mutants were unable to trigger F as shown by their relative lack of HR2 peptide binding (Fig. 5*A*). The mean channel fluorescence values from this fluorescence-activated cell sorter-based assay are summarized in Fig. 5*B*. The 4-4 mutant displayed a complete lack of HR2 peptide binding under permissive conditions, whereas the 4-5 mutant showed only a small amount of HR2 peptide binding in the presence of B2 at 37 °C (~30% increase in mean fluorescence intensity (MFI) compared with >300% increase in MFI for WT G).

DISCUSSION

Here we identified a region (ISYTLPVVG) at the base of the globular head domain of NiV-G (β6S4/β1H1) to be involved in B2-induced changes in G that trigger FP exposure in F. This region is likely critical for transducing the receptor-induced signals that result in virus-cell membrane fusion. Mutations within this region in NiV-G (mutants 4-4 and 4-5) abrogated or greatly decreased 1) membrane fusion (Fig. 2*E*), 2) temperature-dependent enhancement of Mab45 binding (Fig. 2*F*), 3) secondary structural changes detected by CD (Fig. 3*B*), 4) receptor-induced F dissociation from G (Fig. 4*C*), and 5) pre-hairpin formation during F triggering (Fig. 5). These five phenotypes were all induced in WT G upon B2 engagement. The β6S4/β1H1 region demarcated by the 4-4 and 4-5 mutants were involved in all the above phenotypes related to the fusion cascade, and yet the 4-4 and 4-5 mutants do not seem to affect the overall structure nor the receptor binding ability of the attachment protein (Fig. 2*E* and supplemental Fig. 4). The explosion of recent structural data on paramyxoviral attachment and fusion proteins have added greatly to our understanding of the paramyxoviral fusion cascade, and recent reviews have emphasized the importance of understanding the mechanisms by which G triggers F and of identifying regions in G involved in F triggering as future significant goals (11–14, 20). Mutations have been described in other paramyxoviral attachment proteins (primarily in their stalk region) that do not affect receptor binding but are nevertheless fusion-defective, perhaps due to defect in F and G/H/HN association or a defect in triggering (7, 30–39). However, our results indicate the identification at least in part of a long sought receptor-induced activation site in G that triggers F and, importantly, implicates both this region and the stalk domain in mediating the receptor-induced allosteric signal during the fusion cascade.

For paramyxoviruses that use glycan-based receptors, strong data exist that argue against conformational changes in the globular head of HN upon receptor binding (40–44), although there seems to be a consensus that some change must occur, perhaps in the stalk domain, and at the level of the quaternary structure of the attachment protein (43, 45) upon receptor binding in order for F-triggering to proceed. In the recently published structures of henipavirus G, there do not appear to be significant conformational differences between the receptor bound or unbound state (26, 27). However, none of the published paramyxoviral attachment protein structures include the stalk domain, and thus, it is not clear whether the issue of receptor-induced conformational changes can be resolved in studies without the stalk domain, as clearly, some sort of allosteric transfer of receptor-induced signals need to occur for the fusion cascade to proceed (14, 20). Here, we provide evidence for receptor-induced allosteric changes in G by both temperature-dependent Mab45 binding enhancement and changes in CD spectra (Fig. 1 and 3). Notably, the lack of the stalk domain in G (mutant GΔStalk) prevented CD spectra changes upon B2 binding (Fig. 3*C*). Thus, it is possible that to observe changes in the G protein upon receptor binding, either the full-length protein (as in the case of our cell surface Mab45 binding assay) or at least the whole soluble ectodomain (as in our stalk-domain containing G for our CD experiments) is necessary. The β6S4/β1H1 region and stalk domain regions may act in concert in the fusion process; this notion is supported by their close spatial proximity (supplemental Fig. 3) and previous *Paramyxovirus* studies that implicate the stalk domain in membrane fusion (5–8).

Our results present evidence for Mab45 ability to enhance its recognition of WT G upon its binding to B2 at 37 or 20 °C but not at 4 °C. The temperature dependence of this phenomenon is noteworthy as membrane fusion has been clearly shown to be an energy-dependent process, as only pre-hairpin intermediates of fusion which undergo FP exposure and insertion into the target membranes, but not complete fusion, have been observed at temperatures lower than 37 °C but higher than 4 °C (10, 12, 13). Thus, the enhancement of Mab45 binding to G upon B2 engagement at 20 or 37 °C, but not at 4 °C, is consistent with previous membrane fusion studies and can be used as a tool to detect receptor-induced activation of G.

In the recently solved structures of henipavirus-G proteins, the β6S4/β1H1 region, especially residues PVV, either failed to give resolvable electron density maps or were specifically mentioned as a highly flexible region (26, 27). Remarkably, this region, demarcated by our 4-4 and 4-5 mutants and part of the Mab45 RBE epitope, plays a role in the receptor-induced triggering of F. Altogether, these results suggest that the flexibility of this region is important for the fusion process. Moreover, when we modeled NiV-G as a dimer after the hPIV3 crystal structure (supplemental Fig. 3*B*) (42), this region was situated partially at the dimer interface, suggesting that the flexibility of this interdimeric interface is important for the fusion process. We speculate this flexibility reflects that NiV-G may exist in multiple conformations, some of which are accessible for Mab45 binding. EphrinB2 binding may collapse these conformations to a common stable ground state that exposes the RBE epitope, perhaps by re-orienting the globular head domains in a way that allows for better Mab45 binding. The Mab45 RBE is, therefore, a surrogate marker for a receptor-induced stabilization of the metastable NiV-G. In addition, we observed a relative dissociation of the G/F proteins upon receptor binding, and such dissociation was abrogated for the 4-5 mutant. Although it is unlikely that the PVV region directly interacts with F, because mutations in this region (4-4 and 4-5) did not significantly affect the F/G interactions *per se* (supplemental Fig. 4*A*) but only B2-induced F/G dissociation, it suggests that this hyperflexible PVV region in G interacts with the stalk domain in a manner required to trigger F. Interestingly, Broder and co-workers (4) also implicated the stalk domain of Hendra virus-G in the receptor-induced changes that mediate fusion. In addition, we have a panel of cysteine mutants in the stalk

domain with similar phenotypes to those observed for the mutants in this hyperflexible β6S4/β1H1 region.[5]

In summary, our results identify a receptor-induced allosteric activator in NiV-G that is critical for triggering the pre-hairpin intermediate formation in F and eventual membrane fusion. NiV-G activation involves a RBE-epitope at the base of the globular head domain that likely works in conjunction with the stalk domain in mediating the allosteric transfer of B2-induced signals that propagate the NiV fusion cascade. Whether this model is generalizable for other paramyxoviruses that use protein-based receptors remains to be determined.

Acknowledgments—We acknowledge support from the UCLA AIDS Institute and the Centers for AIDS Research flow cytometry core supported by National Institutes of Health Grants CA16042 and AI28697. We thank Y-nhi H. Phan and Michael Cerrato for technical support.

REFERENCES

1. Wild, T. F. (2008) *Pathol. Biol.* (*Paris*), in press
2. Aguilar, H. C., Matreyek, K. A., Filone, C. M., Hashimi, S. T., Levroney, E. L., Negrete, O. A., Bertolotti-Ciarlet, A., Choi, D. Y., McHardy, I., Fulcher, J. A., Su, S. V., Wolf, M. C., Kohatsu, L., Baum, L. G., and Lee, B. (2006) *J. Virol.* **80,** 4878–4889
3. Aguilar, H. C., Matreyek, K. A., Choi, D. Y., Filone, C. M., Young, S., and Lee, B. (2007) *J. Virol.* **81,** 4520–4532
4. Bishop, K. A., Hickey, A. C., Khetawat, D., Patch, J. R., Bossart, K. N., Zhu, Z., Wang, L. F., Dimitrov, D. S., and Broder, C. C. (2008) *J. Virol.* **82,** 11398–11409
5. Corey, E. A., and Iorio, R. M. (2007) *J. Virol.* **81,** 9900–9910
6. Lee, J. K., Prussia, A., Paal, T., White, L. K., Snyder, J. P., and Plemper, R. K. (2008) *J. Biol. Chem.* **283,** 16561–16572
7. Melanson, V. R., and Iorio, R. M. (2006) *J. Virol.* **80,** 623–633
8. Melanson, V. R., and Iorio, R. M. (2004) *J. Virol.* **78,** 13053–13061
9. Russell, C. J., Kantor, K. L., Jardetzky, T. S., and Lamb, R. A. (2003) *J. Cell Biol.* **163,** 363–374
10. Russell, C. J., Jardetzky, T. S., and Lamb, R. A. (2001) *EMBO J.* **20,** 4024–4034
11. Lamb, R. A., and Jardetzky, T. S. (2007) *Curr. Opin. Struct. Biol.* **17,** 427–436
12. White, J. M., Delos, S. E., Brecher, M., and Schornberg, K. (2008) *Crit. Rev. Biochem. Mol. Biol.* **43,** 189–219
13. Yin, H. S., Wen, X., Paterson, R. G., Lamb, R. A., and Jardetzky, T. S. (2006) *Nature* **439,** 38–44
14. Iorio, R. M., and Mahon, P. J. (2008) *Trends Microbiol.* **16,** 135–137
15. Bishop, K. A., Stantchev, T. S., Hickey, A. C., Khetawat, D., Bossart, K. N., Krasnoperov, V., Gill, P., Feng, Y. R., Wang, L., Eaton, B. T., Wang, L. F., and Broder, C. C. (2007) *J. Virol.* **81,** 5893–5901
16. Plemper, R. K., Hammond, A. L., Gerlier, D., Fielding, A. K., and Cattaneo, R. (2002) *J. Virol.* **76,** 5051–5061
17. Negrete, O. A., Levroney, E. L., Aguilar, H. C., Bertolotti-Ciarlet, A., Nazarian, R., Tajyar, S., and Lee, B. (2005) *Nature* **436,** 401–405
18. Negrete, O. A., Wolf, M. C., Aguilar, H. C., Enterlein, S., Wang, W., Muhlberger, E., Su, S. V., Bertolotti-Ciarlet, A., Flick, R., and Lee, B. (2006) *PLoS Pathog.* **2,** e7
19. Bonaparte, M. I., Dimitrov, A. S., Bossart, K. N., Crameri, G., Mungall, B. A., Bishop, K. A., Choudhry, V., Dimitrov, D. S., Wang, L. F., Eaton, B. T., and Broder, C. C. (2005) *Proc. Natl. Acad. Sci. U. S. A.* **102,** 10652–10657
20. Lee, B., Ataman, Z. A., and Jin, L. (2008) *Nat. Struct. Mol. Biol.* **15,** 540–542
21. Levroney, E. L., Aguilar, H. C., Fulcher, J. A., Kohatsu, L., Pace, K. E., Pang, M., Gurney, K. B., Baum, L. G., and Lee, B. (2005) *J. Immunol.* **175,** 413–420
22. Connolly, S. A., and Lamb, R. A. (2006) *Virology* **355,** 203–212
23. Finnegan, C., and Blumenthal, R. (2006) *Infect. Disord. Drug Targets* **6,** 355–367
24. Gallo, S. A., Finnegan, C. M., Viard, M., Raviv, Y., Dimitrov, A., Rawat, S. S., Puri, A., Durell, S., and Blumenthal, R. (2003) *Biochim. Biophys. Acta* **1614,** 36–50
25. Negrete, O. A., Chu, D., Aguilar, H. C., and Lee, B. (2007) *J. Virol.* **81,** 10804–10814
26. Bowden, T. A., Aricescu, A. R., Gilbert, R. J., Grimes, J. M., Jones, E. Y., and Stuart, D. I. (2008) *Nat. Struct. Mol. Biol.* **15,** 567–572
27. Xu, K., Rajashankar, K. R., Chan, Y. P., Himanen, J. P., Broder, C. C., and Nikolov, D. B. (2008) *Proc. Natl. Acad. Sci. U. S. A.* **105,** 9953–9958
28. McCubbin, W. D., Mani, R. S., and Kay, C. M. (1974) *Biochemistry* **13,** 2689–2694
29. Bossart, K. N., Mungall, B. A., Crameri, G., Wang, L. F., Eaton, B. T., and Broder, C. C. (2005) *Virol. J.* **2,** 57–71
30. Deng, R., Wang, Z., Glickman, R. L., and Iorio, R. M. (1994) *Virology* **204,** 17–26
31. Deng, R., Wang, Z., Mirza, A. M., and Iorio, R. M. (1995) *Virology* **209,** 457–469
32. Bousse, T., Takimoto, T., Gorman, W. L., Takahashi, T., and Portner, A. (1994) *Virology* **204,** 506–514
33. McGinnes, L., Sergel, T., and Morrison, T. (1993) *Virology* **196,** 101–110
34. Mirza, A. M., Deng, R., and Iorio, R. M. (1994) *J. Virol.* **68,** 5093–5099
35. Porotto, M., Murrell, M., Greengard, O., and Moscona, A. (2003) *J. Virol.* **77,** 3647–3654
36. Sergel, T., McGinnes, L. W., Peeples, M. E., and Morrison, T. G. (1993) *Virology* **193,** 717–726
37. Stone-Hulslander, J., and Morrison, T. G. (1999) *J. Virol.* **73,** 3630–3637
38. Tsurudome, M., Kawano, M., Yuasa, T., Tabata, N., Nishio, M., Komada, H., and Ito, Y. (1995) *Virology* **213,** 190–203
39. Yuasa, T., Kawano, M., Tabata, N., Nishio, M., Kusagawa, S., Komada, H., Matsumura, H., Ito, Y., and Tsurudome, M. (1995) *Virology* **206,** 1117–1125
40. Porotto, M., Fornabaio, M., Kellogg, G. E., and Moscona, A. (2007) *J. Virol.* **81,** 3216–3228
41. Crennell, S., Takimoto, T., Portner, A., and Taylor, G. (2000) *Nat. Struct. Biol.* **7,** 1068–1074
42. Lawrence, M. C., Borg, N. A., Streltsov, V. A., Pilling, P. A., Epa, V. C., Varghese, J. N., McKimm-Breschkin, J. L., and Colman, P. M. (2004) *J. Mol. Biol.* **335,** 1343–1357
43. Yuan, P., Thompson, T. B., Wurzburg, B. A., Paterson, R. G., Lamb, R. A., and Jardetzky, T. S. (2005) *Structure* **13,** 803–815
44. Zaitsev, V., von Itzstein, M., Groves, D., Kiefel, M., Takimoto, T., Portner, A., and Taylor, G. (2004) *J. Virol.* **78,** 3733–3741
45. Russell, C. J., and Luque, L. E. (2006) *Trends Microbiol.* **14,** 243–246

[5] O. A. Negrete, D. Chu, B. Schulz, H. C. Aguilar, and B. Lee. Manuscript in preparation.